

Reduced Density Matrices Through Machine Learning

Awwab A. Azam,^{1,*} Lexu Zhao,^{2,*} and Jiabin Yu^{2,3,†}

¹*Department of Electrical and Computer Engineering, University of Florida, Gainesville, USA*

²*Department of Physics, University of Florida, Gainesville, Florida 32611, USA*

³*Quantum Theory Project, University of Florida, Gainesville, FL, USA*

n -particle reduced density matrices (n -RDMs) play a central role in understanding correlated phases of matter, but their calculation is often computationally inefficient for strongly-correlated states at large system sizes. In this work, we use neural network (NN) architectures to accelerate and even predict n -RDMs for large systems. Our underlying intuition is that, for gapped states, n -RDMs are often smooth functions over the Brillouin zone (BZ) and are therefore interpolable, allowing NNs trained on small-size systems to predict large-size ones. Building on this, we devise two NNs: (i) a self-attention NN that maps random RDMs to physical ones, and (ii) a Sinusoidal Representation Network (SIREN) that directly maps momentum-space coordinates to RDM values. We test the NNs on RDMs in three 2D models: the pair-pair correlation functions of the Richardson model of superconductivity, the translationally-invariant Hartree-Fock (HF) 1-RDM in a four-band repulsive model, and the translation-breaking HF 1-RDM in the half-filled Hubbard model. We find that a SIREN trained on a 6×6 momentum mesh and a SIREN trained on 4 tilted meshes (each of which has 12 momentum points) can predict the 18×18 pair-pair correlation function with a relative accuracy of 94.29% and 93.77%, respectively. NNs trained on 6×6 and 8×8 meshes provide high-quality initial guesses for 50×50 translation-invariant HF and 30×30 fully translation-breaking-allowed HF, reducing the required number of iterations by up to 91.63% and 92.78%, respectively, compared to random initializations. Our results illustrate the potential of NN-based methods for interpolable n -RDMs, which might open a new avenue for future research on strongly correlated phases.

Introduction Understanding strongly correlated phases of matter is a central topic in condensed matter physics. The rapid progress of neural-network (NN) methods has created new opportunities for studying strongly correlated quantum phases via NN-based wavefunction ansatzes [1–51], which have been applied to various systems including Hubbard model [2, 4, 6, 50, 52–54]. One notable type of such NN ansatzes uses the self-attention mechanism [55] to construct correlated orbitals from single-particle orbitals, expressing the many-body wavefunction as a linear combination of a small number of Slater determinants formed from these correlated orbitals [8, 34, 35, 44, 56]. In this work, we propose a different way of using machine learning (or NNs) to understand strongly-correlated states—by focusing on their reduced density matrices.

Given a many-body Hamiltonian, the zero-temperature n -particle reduced density matrix (n -RDM) is defined as

$$O_{\mathbf{k}_1\alpha_1, \mathbf{k}_2\alpha_2, \dots, \mathbf{k}_n\alpha_n, \mathbf{k}'_1\alpha'_1, \mathbf{k}'_2\alpha'_2, \dots, \mathbf{k}'_n\alpha'_n} = \left\langle c_{\mathbf{k}_1\alpha_1}^\dagger c_{\mathbf{k}_2\alpha_2}^\dagger \dots c_{\mathbf{k}_n\alpha_n}^\dagger c_{\mathbf{k}'_1\alpha'_1} c_{\mathbf{k}'_2\alpha'_2} \dots c_{\mathbf{k}'_n\alpha'_n} \right\rangle, \quad (1)$$

where $\langle \dots \rangle$ represents the average with respect to the ground state(s), and $c_{\mathbf{k}\alpha}^\dagger$ creates a particle with Bloch momentum \mathbf{k} and intra-unit-cell degree of freedom α (which labels sub-lattice, orbital, spin, etc).

The n -RDM plays a vital role in understanding strongly correlated states [57–79]. First, the Hamiltonians of realistic condensed matter systems almost always involve only one-body and two-body terms, implying that the 1-RDM and 2-RDM are sufficient to evaluate the many-body ground-state energy [57, 80–85]. This observation lies at the heart of semidefinite programming approaches [61, 63, 86–94], which iteratively compute the 2-RDM. Second, the order parameters that characterize spontaneous symmetry breaking—such as charge-density waves and magnetism—often depend only on the 1-RDM [95], which explains the effectiveness of the Hartree-Fock (HF) method [96].

Given the importance of the n -RDMs, it would be transformative to design an NN that predicts n -RDMs for a given Hamiltonian, particularly for large systems where existing algorithms become computationally inefficient. Because semidefinite programming and the HF algorithm compute n -RDMs iteratively, the NN predictions (even if they are not exactly precise) can serve as an initial guess which is already very close to the converged state, thereby dramatically reducing the number of iterations required for convergence. Furthermore, 2-RDM methods (e.g. semidefinite programming) are inherently susceptible to converging to non-physical solutions, but comparing the converged solution to the NN predictions may help determine whether the converged solution is physical, since the NNs are trained on physical 2-RDMs and thus their predictions are likely to be physical.

In this work, we develop two such NNs: (i) a self-attention NN that maps random initial 1-RDMs to the predicted final 1-RDMs, and (ii) a Sinusoidal Represent-

* These authors contributed equally to this work.

† yujiabin@ufl.edu

tation Network (SIREN) [97] that learns n -RDMs and interpolates them to denser \mathbf{k} meshes (Sec. A). The underlying reason for the existence of such NNs lies in the interpolable nature of n -RDMs. These NNs are trained on small system sizes, where the n -RDMs can be efficiently computed using existing methods, and are then used to predict the n -RDMs of much larger systems. We first benchmark SIREN on the pair-pair correlation functions of the superconducting ground states of the exactly-solvable Richardson model, and find that a SIREN trained only on the 6×6 mesh can achieve a relative accuracy of 94.29% for predictions on 18×18 . Additionally, a SIREN trained on four tilted meshes, each of which has 12 \mathbf{k} points, achieves a relative accuracy of 93.77% on 18×18 (Sec. B).

We then benchmark the self-attention NN on the translationally-invariant HF calculations for a four-band model with short-range repulsion. Our results show that an NN trained only on 6×6 and 8×8 meshes can maintain a relatively low mean squared error (MSE, below 5×10^{-3}) for up to 50×50 . Furthermore, for momentum mesh sizes from $10 \times 10, 12 \times 12, \dots, 50 \times 50$, using the NN predictions as the initial 1-RDM for HF calculations results in a 91.61%–94.24% reduction in the number of HF iterations required for convergence compared to the HF calculations with random initialization (Sec. C).

We finally benchmark both NNs on the HF calculations that allow translation breaking in half-filled Hubbard model. We again compare the HF iteration numbers between using the NN-predicted final 1-RDM as initial 1-RDMs and using the random initial 1-RDMs. We find a significant (60.79%–92.78%) reduction in the number of HF iterations for up to 30×30 using SIRENs trained only on the 8×8 mesh, and a self-attention NN trained only on 8×8 and 10×10 meshes (Sec. D). The remarkable reduction in iteration numbers for HF calculations—that forbid or allow translational breaking—demonstrates the potential of NNs for speeding up the calculation of or even the precise prediction of RDMs of large-size systems.

We note that our work is the first to construct NNs that predict large-size n -RDMs for strongly correlated phases, exploiting the interpolable structure of n -RDMs in momentum space. In contrast to our work, previous developments of NNs that involve RDMs either focus on real-space 1-RDM in ab initio calculations (such as density functional theory) to establish maps between 1-RDM and other quantities [20, 98–101] or 2-RDM for chemical molecules [102, 103]. Our general idea of using NNs for interpolable n -RDMs, exemplified by our implementations for pair-pair correlation functions and 1-RDMs, might open a new avenue for studying strongly correlated states.

Interpolability of n -RDM In this section, we discuss the interpolability of the n -RDM in the BZ. As shown in Eq. (1), the n -RDM is a function of $2n$ Bloch momenta; for a finite 2D system with $L \times L$ unit cells and periodic boundary conditions these momenta lie on an

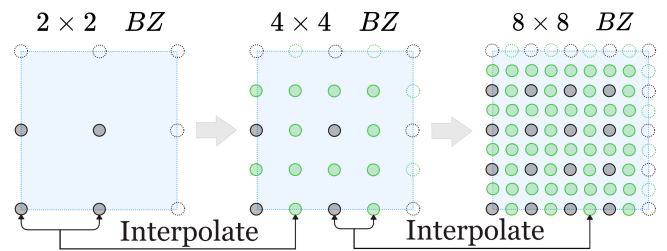


FIG. 1. **Interpolability of n -RDMs in the BZ.** Momentum meshes for large systems can be generated by inserting new \mathbf{k} points between those of the small momentum meshes. Therefore, n -RDMs in momentum space are often interpolable.

$L \times L$ mesh in the BZ, and increasing the system size to a commensurate L' simply inserts additional momentum points between those of the original mesh (Fig. 1) while the Bloch momenta always occupy the same convex hull—the BZ.

If n -RDM is a smooth function of $2n$ Bloch momenta in the thermodynamic limit, then its values on extra momentum points can be interpolated from those on the original $L \times L$ grid. Namely, although the n -RDMs are extrapolated from small to large real-space system sizes, they are in fact interpolated in momentum space. This smoothness condition is naturally satisfied for gapped ground states, and even for gapless states certain combinations of n -RDMs (e.g., the pair-pair correlator in the Richardson model [104–106]) can remain smooth functions of the Bloch momenta. Thus, smooth n -RDMs (or smooth combinations thereof) are ubiquitous in condensed-matter systems.

These properties are crucial for NNs to function effectively. Our goal is to train a NN on small system sizes and use it to predict n -RDMs for large systems. As large size RDM always lie within the fixed convex hull of the training distribution, predicting smooth n -RDMs for large systems from the training data on small systems is an interpolation (as opposed to extrapolation) task. Furthermore, smooth n -RDMs are continuous functions, so they can be well approximated by NNs (in principle with an arbitrary degree of precision [107–109], given no restrictions on the number of parameters). Therefore, our task here is analogous to image-resolution enhancement, where extra pixel points are inserted to enhance the resolution—a problem where NNs already perform well [110], implying the feasibility of our approach.

NN Architectures We now discuss the NN architectures used in this work. We will focus on the 1-RDM ($O_{\mathbf{k}\alpha, \mathbf{k}'\alpha'} = \langle c_{\mathbf{k}\alpha}^\dagger c_{\mathbf{k}'\alpha'} \rangle$), with $\alpha = 1, 2, \dots, \xi$) in momentum space and discuss the generalization at the end. Particularly, we focus on fixed momentum transfer $\mathbf{k} - \mathbf{k}' = \mathbf{q}$, where $\mathbf{q} = 0$ means translation-invariance and we will include more than one \mathbf{q} for spontaneous translation-symmetry breaking cases.

The two NNs described in this section can be trained on small-size $O^{\mathbf{q}}$ (generated via HF calculations) to pre-

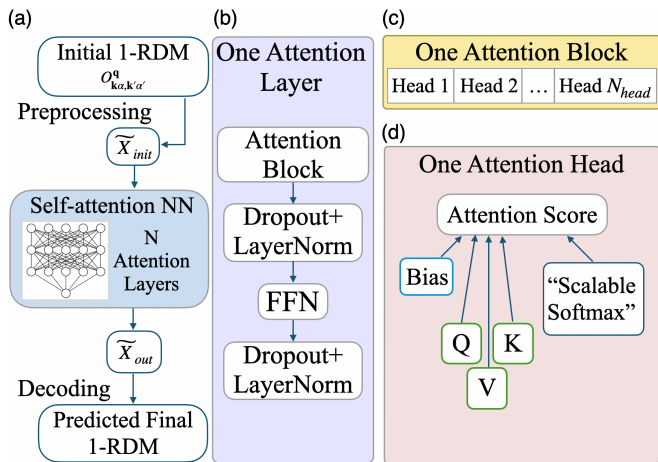


FIG. 2. **Schematics of our self-attention NN.** (a) An initial 1-RDM on an $L \times L$ BZ is preprocessed to \tilde{X}_{init} , transformed by the network to \tilde{X}_{out} , and decoded to the predicted final 1-RDM. (b) Each layer applies an attention block and a FFN with Dropout and LayerNorm. (c) The attention block includes N_{head} parallel heads. (d) Each head uses Q, K, V with a learned periodic relative-position bias and a scalable softmax temperature (e.g., $\propto \log L^2$).

dict large-size O^q . We will only outline the key steps here, and leave details to Sec. A. The first NN architecture that we construct is a self-attention NN (Fig. 2) that maps a random initial 1-RDM O_{init}^q to a predicted final 1-RDM O_{out}^q . It is trained on small $L \times L$ using numerically generated pairs $\{O_{\text{init}}^q(\mathbf{k})\}, \{O_{\text{tgt}}^q(\mathbf{k})\}$, where L denotes the number of lattice sites along each side, and O_{tgt}^q denotes the true final 1-RDM from the HF calculation. The overall structure is shown in Fig. 2(a). We first preprocess the 1-RDM $O_{k,\alpha\alpha'}^q$ into a set of standardized [111, 112] $2\xi^2$ -dimensional real vectors \tilde{x}_i at the i^{th} Bloch momentum, which is then fed into the self-attention NN consisting of N attention layers. All the \tilde{x}_i are linearly transformed and stacked into the input matrix $H^{(0)}$ of size $L^2 \times D$ for the first attention layer. Subsequently, the ℓ^{th} attention layer maps $H^{(\ell-1)} \mapsto H^{(\ell)}$ with $l = 1, 2, \dots, N$, after which $H^{(N)}$ is decoded back to $O_{\text{out}}^q(\mathbf{k})$, which is the predicted final 1-RDM. Within the ℓ^{th} attention layer (Fig. 2(b)), we have an attention block, a feedforward network (FFN), Dropout, and LayerNorm, where the last two (Dropout and LayerNorm) are common NN layers to prevent overfitting and improve optimization stability [113, 114]. Each attention block uses N_{head} parallel heads (Fig. 2(c)); in head h , the per-head width is $d_k \equiv D/N_{\text{head}}$. We form $\alpha^{(h)} = H^{(\ell-1)} W_{\alpha}^{(h)}$, where $\alpha \in \{Q, K, V\}$ for the “query”, “key”, and “value” matrices respectively, and each $W_{\alpha}^{(h)} \in \mathbb{R}^{D \times d_k}$ is learnable.

Our construction modifies the original self-attention mechanism [55] in two major ways. First, to encode the momentum information, we introduce a novel positional encoding scheme that uses a learnable bias B_{ij} to increase

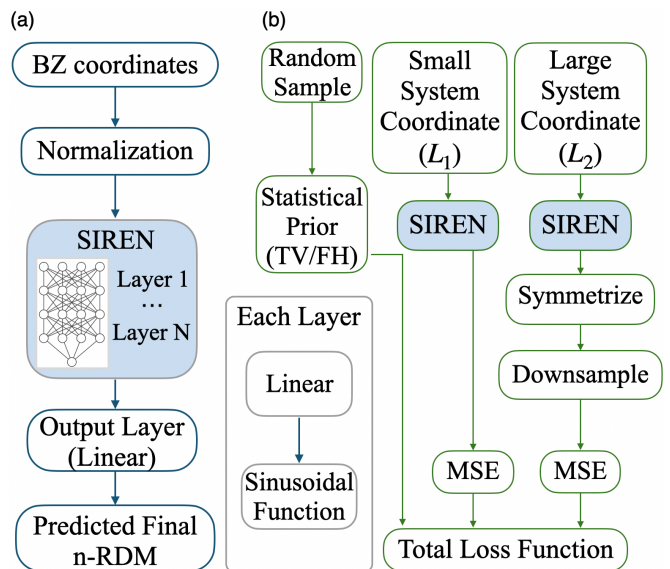


FIG. 3. **Schematic of our SIREN.** (a) Normalize BZ coordinates to $\mathbf{v}(\mathbf{k}) \in [-1, 1]^2$, then pass \mathbf{v} through layers of linear and sine functions to predict one component of the final n -RDM (e.g., a specific α, α' component for 1-RDM); aggregating components reconstructs the predicted final n -RDM. (b) We train the NN using a total loss consisting of: (i) the MSE on a small $L_1 \times L_1$ mesh, (ii) a loss term computed by evaluating the SIREN on a larger $L_2 \times L_2$ mesh, symmetrizing, downsampling back to $L_1 \times L_1$ and taking the MSE with the true final RDM for the $L_1 \times L_1$ mesh, and (iii) an optional statistical prior (TV or FH) on randomly chosen coordinates $\mathbf{u}_i \in [-1, 1]^2$ for regularization. Therefore, only true final RDMs for the small $L_1 \times L_1$ mesh are used as training data.

or decrease the attention scores based on the momentum-space separation between \mathbf{k}_i and \mathbf{k}_j (Fig. 2(d)). Second, we also use a learnable scalar s [115] to avoid “attention fading” and better enable the NN to handle variable-size inputs.

The second NN architecture we use is SIREN [97], which represents the 1-RDM as a set of smooth, periodic functions of \mathbf{k} coordinates, thereby enabling interpolation to denser \mathbf{k} meshes. The overall structure is shown in Fig. 3(a). We first map BZ \mathbf{k} points to normalized coordinates $\mathbf{v}(\mathbf{k}) \in [-1, 1]^2$. Then, for each fixed (α, α') , the real and imaginary parts of $O_{k,\alpha\alpha'}^q$ are a function of \mathbf{v} , and we train a scalar function Φ_{θ} such that $\Phi_{\theta}(\mathbf{v}) \approx \text{Re}[O_{\alpha\alpha'}^q(\mathbf{k})]$ or $\text{Im}[O_{\alpha\alpha'}^q(\mathbf{k})]$. Specifically, we construct each Φ_{θ} using 4 hidden layers of sinusoidal functions followed by a linear function, and finally assemble Φ_{θ} for different (α, α') to give the final predicted $O^q(\mathbf{k}_i)$. To train the SIREN on a $L_1 \times L_1$ mesh, we introduce a custom loss function with three parts (Fig. 3(b)): (i) the mean-squared error (MSE) on the smaller system of size L_1 , (ii) a novel consistency term that evaluates Φ_{θ} on a denser mesh of size L_2 , averages over a chosen symmetry subgroup G , downsamples back to size L_1 , and then computes the MSE with the true final $L_1 \times L_1$ 1-RDM, and (iii) a statistical prior consist-

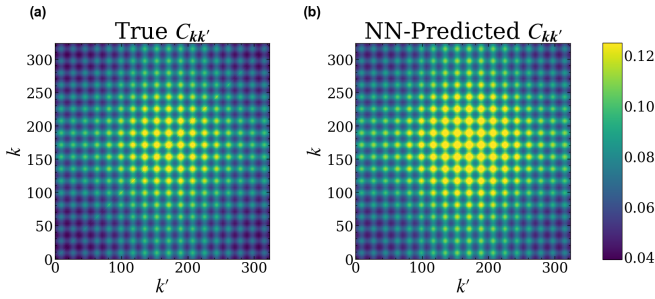


FIG. 4. Comparison between (a) the true final $C_{\mathbf{k}\mathbf{k}'}$ for $L = 18$ and (b) the predicted final $L = 18$ $C_{\mathbf{k}\mathbf{k}'}$ given by a SIREN trained on $L = 6$. Here the indices $k, k' \in \{0, \dots, L^2 - 1\}$ enumerate the $L \times L$ BZ points by flattening (ℓ_1, ℓ_2) with $\ell_{1,2} \in \{0, \dots, L - 1\}$ via $k = \ell_1 + L\ell_2$; the corresponding momentum vector is \mathbf{k} , and similarly for \mathbf{k}' .

ing of TV/Hessian regularization at a randomly sampled set of points [97]. It is straightforward to generalize our NN architectures to any special combination of n -RDM (with $n > 1$) that only depends on one Bloch momentum (with other momenta fixed just like $O_{\mathbf{k}, \alpha\alpha'}^q$). Beyond one-momentum quantities, the SIREN can be applied to the pair-pair correlation function (a special 2-RDM) for superconductors, which depends on two momenta, as we show in the subsequent section. In general, we expect the SIREN can naturally be extended to quantities that are a smooth function of more than two momenta.

Pair-Pair Correlation Functions In this section, we benchmark the SIREN on the pair-pairing correlation function for superconductivity. As a benchmark, we consider the exactly-solvable Richardson model [104–106] in 2 dimensions on an $L \times L$ \mathbf{k} mesh

$$H = \sum_{\mathbf{k}, s} \varepsilon_{\mathbf{k}} c_{\mathbf{k}s}^\dagger c_{\mathbf{k}s} + \frac{u}{L^2} \sum_{\mathbf{k}} A_{\mathbf{k}}^\dagger \sum_{\mathbf{k}'} A_{\mathbf{k}'}, \quad (2)$$

where L^2 is the number of lattice sites, $\varepsilon_{\mathbf{k}} = t(\cos k_x + \cos k_y)$ with $t = 0.1$, $u = -1$, and $c_{\mathbf{k}s}^\dagger$ creates an electron with Bloch momentum \mathbf{k} and spin s . We work in the number-conserving case, where the pair-pair correlation function is just the Cooper-channel matrix channel of 2-RDM $C_{\mathbf{k}\mathbf{k}'} = O_{\mathbf{k}\uparrow, -\mathbf{k}\downarrow, \mathbf{k}'\uparrow, -\mathbf{k}'\downarrow} = \langle A_{\mathbf{k}}^\dagger A_{\mathbf{k}'} \rangle$, as $\langle A_{\mathbf{k}} \rangle = \langle c_{\mathbf{k}\uparrow}^\dagger c_{-\mathbf{k}\downarrow}^\dagger \rangle = 0$. The model is exactly solved for electron filling $1/6$ for $L = 6$, $L = 12$, and $L = 18$ (see details in Sec. B). We then trained a SIREN on the obtained $C_{\mathbf{k}\mathbf{k}'}$ for $L = 6$, and tested the precision of the prediction on larger sizes up to $L = 18$ by evaluating the relative accuracy $r_n = \left(1 - \frac{\sqrt{\text{MSE}}}{\max(C) - \min(C)}\right)$. (Here “MSE” stands for the mean squared error between the NN-predicted final and the true final correlation function, as discussed in Sec. B.) Remarkably, the SIREN trained only on $L = 6$ can predict $C_{\mathbf{k}\mathbf{k}'}$ for a larger size ($L = 18$) with a rather high accuracy of $r_n = 94.29\%$ (see Fig. 4 for comparison), verifying the validity of our method.

To further demonstrate the efficiency of our method, we consider smaller training meshes. Because the dimen-

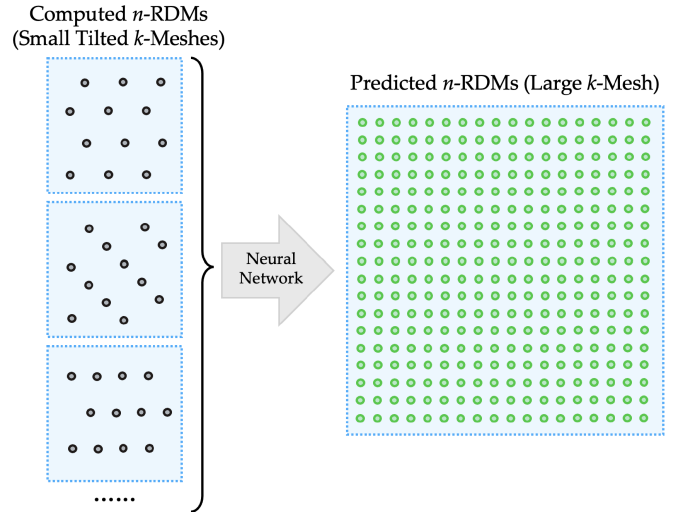


FIG. 5. Instead of training on the pair-pair correlation function for a single square lattice (e.g. $L \times L$ for $L = 6$), for efficiency we can train a NN (implemented by a SIREN in our case) on $C_{\mathbf{k}\mathbf{k}'}$ for multiple tilted meshes, each of which has a smaller number (e.g. 12) of \mathbf{k} points, and use it to predict $C_{\mathbf{k}\mathbf{k}'}$ for a much larger size (e.g. 18×18) without a significant drop in accuracy.

sion of the Hilbert space scales exponentially with system size, it is often computationally much cheaper to calculate RDMs for several smaller momentum meshes rather than for a single larger mesh. Building on this insight, we trained an additional SIREN on $C_{\mathbf{k}\mathbf{k}'}$ for 4 tilted meshes (see Sec. B), each of which has 12 \mathbf{k} points, as depicted in Fig. 5. The trained SIREN is then able to predict $C_{\mathbf{k}\mathbf{k}'}$ for the 18×18 mesh with a relative accuracy of 93.77%, which further underscores the efficiency of our method.

Translationally-Invariant HF We further benchmark our self-attention NN on translationally-invariant HF for the 1-RDM. The final true 1-RDM is calculated via the HF algorithm starting from a random initial 1-RDM. The model we consider is a $L \times L$ square lattice with a four-component spinor per unit cell, short-range hopping terms, and repulsive interaction.

We choose the hopping such that the lower two single-particle bands have a nontrivial time-reversal-invariant Z_2 topology [116]. We perform the translationally-invariant HF calculations at filling $\nu = 1$ for $L = 6, 8, 10, 12, \dots, 50$. Using this data, we train a self-attention NN on 10,000 (initial 1-RDM, true final 1-RDM) pairs for each of $L = 6, 8$ (see Sec. C). In order to evaluate its effectiveness, we feed 1,000 random initial 1-RDMs for each of $L = 10, 12, \dots, 50$ into the trained NN to obtain the corresponding predicted final 1-RDMs. We then use those predicted final 1-RDMs as initial conditions for the HF calculation and record the number of iterations to converge, and compare it with HF started from a random initialization. Particularly, we find that it takes an average of 8.057 iteration steps to converge when using the predicted final 1-RDMs for $L = 50$ as the ini-

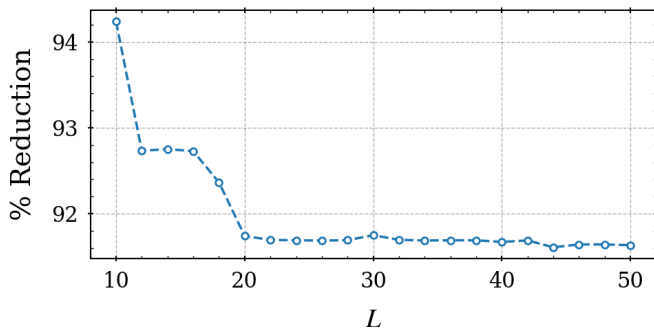


FIG. 6. **NN for translation-invariant HF.** Here, “% Reduction” is the percent difference between the number of HF iterations using a predicted final 1-RDM from the self-attention NN as the initial 1-RDM as compared to using a random initial 1-RDM, and is plotted as a function of the system size L for the four-band model. See Sec. C for the exact values. The HF calculation is forced to preserve the lattice translation symmetry.

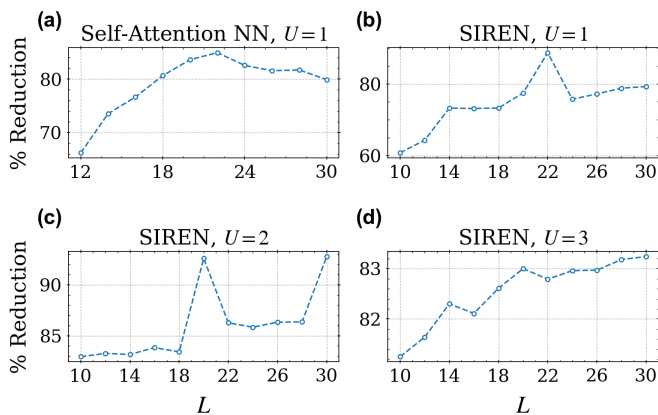


FIG. 7. **NN for the Hubbard model.** Summary of results for the Hubbard model using a self-attention NN ($U = 1$) and SIRENs ($U = 1, 2, 3$) showing the percent reduction in the number of HF iterations as a function of the system size L . See Sec. D for the exact values. The HF calculations here allow any kind of breaking of lattice translation symmetries that are compatible with the momentum mesh.

tial 1-RDMs for HF, as compared to an average of 96.301 iterations with random initial 1-RDMs. Thus, our NN, when trained on $L = 6, 8$, results in a 91.63% reduction

in the number of iterations required for HF convergence for $L = 50$. The percent reduction for other system sizes is shown in Fig. 6. Notably, they are all above 90%. (see Sec. C for details).

HF Allowing Translational Breaking Finally, we benchmark both NNs for HF calculations that allow any kind of translation breaking that is compatible with the momentum meshes. We focus on the Hubbard model on a 2D square lattice [117, 118] with onsite U and hopping $t = 1$. We consider the half filling and assume that a spin $U(1)$ is conserved. Then, the 1-RDM that serves as the order parameters is spin-resolved: $[O_\sigma]_{\mathbf{k}\mathbf{k}'} = \langle c_{\mathbf{k}'\sigma}^\dagger c_{\mathbf{k}\sigma} \rangle$, $\sigma \in \{\uparrow, \downarrow\}$. We perform zero-total-spin HF calculations for $L = 8, 10, \dots, 20$ and $U = 1, 2, 3$, allowing all translation breaking that is compatible with the momentum mesh. The lowest-energy converged $[O_\sigma]_{\mathbf{k}\mathbf{k}'}$ are not zero only when $\mathbf{k}' - \mathbf{k}$ is (π, π) and $(0, 0)$, which is consistent with the (π, π) -antiferromagnetism at half filling [119]. We train both a self-attention NN and a SIREN. The self-attention NN was trained on $L = 8$ and $L = 10$ for $U = 1$ only (due to limited training data), and tested on $L = 12, \dots, 30$. The SIRENs were trained on $L = 8$ for $U = 1, 2, 3$, and tested on $L = 10, \dots, 30$. For evaluation, we again compute the percent reduction in the number of HF iterations using the predicted final 1-RDM as the initial guess versus using a random initial 1-RDM, and observe a dramatic reduction (73.27%—92.78%) at larger sizes (*i.e.*, $L \geq 18$). Fig. 7 shows the percent reduction plotted as a function of L for different values of U .

Conclusion and Discussion: In summary, we showed that large-size n -RDMs can be predicted by NNs trained on small-size n -RDMs, with benchmarks on the pair-pair correlation function and translationally-invariant/breaking HF. One immediate future step is to use these NNs to help predict new correlated states in other systems. Certainly, the development of NNs for general 2-RDMs (or n -RDM with $n > 2$) is an important future direction. The application of our NNs to strongly correlated systems, such as moiré materials, is also expected to yield useful results.

Acknowledgments: J.Y.’s work is supported by startup funds at University of Florida. A.A.A.’s work is supported by the AI Scholars program at the University of Florida and by the UF CCMS Undergraduate Fellowship. The authors acknowledge UFIT Research Computing for providing computational resources and support.

-
- [1] G. Carleo and M. Troyer, *Science* **355**, 602–606 (2017).
 - [2] Y. Nomura, A. S. Darmawan, Y. Yamaji, and M. Imada, *Physical Review B* **96**, 10.1103/physrevb.96.205152 (2017).
 - [3] I. Glasser, N. Pancotti, M. August, I. D. Rodriguez, and J. I. Cirac, *Physical Review X* **8**, 10.1103/physrevx.8.011006 (2018).
 - [4] D. Luo and B. K. Clark, *Phys. Rev. Lett.* **122**, 226401 (2019).
 - [5] K. Choo, T. Neupert, and G. Carleo, *Physical Review B* **100**, 10.1103/physrevb.100.125124 (2019).
 - [6] N. Irikura and H. Saito, *Physical Review Research* **2**, 10.1103/physrevresearch.2.013284 (2020).
 - [7] M. Hibat-Allah, M. Ganahl, L. E. Hayward, R. G. Melko, and J. Carrasquilla, *Physical Review Research* **2**, 10.1103/physrevresearch.2.023358 (2020).
 - [8] D. Pfau, J. S. Spencer, A. G. D. G. Matthews, and W. M. C. Foulkes, *Phys. Rev. Res.* **2**, 033429 (2020).

- [9] O. Sharir, Y. Levine, N. Wies, G. Carleo, and A. Shashua, *Physical Review Letters* **124**, [10.1103/physrevlett.124.020503](https://doi.org/10.1103/physrevlett.124.020503) (2020).
- [10] J. Hermann, Z. Schätzle, and F. Noé, *Nature Chemistry* **12**, 891–897 (2020).
- [11] K. Inui, Y. Kato, and Y. Motome, *Phys. Rev. Res.* **3**, [043126](https://doi.org/10.1103/PhysRevRes.3.043126) (2021).
- [12] X. Li, C. Fan, W. Ren, and J. Chen, *Fermionic neural network with effective core potential* (2021), [arXiv:2108.11661](https://arxiv.org/abs/2108.11661) [physics.chem-ph].
- [13] D. Luo, G. Carleo, B. K. Clark, and J. Stokes, *Physical Review Letters* **127**, [10.1103/physrevlett.127.276402](https://doi.org/10.1103/physrevlett.127.276402) (2021).
- [14] C. K. Lee, P. Patil, S. Zhang, and C. Y. Hsieh, *Physical Review Research* **3**, [10.1103/physrevresearch.3.023095](https://doi.org/10.1103/physrevresearch.3.023095) (2021).
- [15] C. Adams, G. Carleo, A. Lovato, and N. Rocco, *Physical Review Letters* **127**, [10.1103/physrevlett.127.022502](https://doi.org/10.1103/physrevlett.127.022502) (2021).
- [16] C. Roth and A. H. MacDonald, *Group convolutional neural networks improve quantum state accuracy* (2021), [arXiv:2104.05085](https://arxiv.org/abs/2104.05085) [quant-ph].
- [17] M. Scherbela, R. Reisenhofer, L. Gerard, P. Marquetand, and P. Grohs, *Solving the electronic schrödinger equation for multiple nuclear geometries with weight-sharing deep neural networks* (2021), [arXiv:2105.08351](https://arxiv.org/abs/2105.08351) [physics.comp-ph].
- [18] J. Robledo Moreno, G. Carleo, A. Georges, and J. Stokes, *Proceedings of the National Academy of Sciences* **119**, [10.1073/pnas.2122059119](https://doi.org/10.1073/pnas.2122059119) (2022).
- [19] G. Pescia, J. Han, A. Lovato, J. Lu, and G. Carleo, *Physical Review Research* **4**, [10.1103/physrevresearch.4.023138](https://doi.org/10.1103/physrevresearch.4.023138) (2022).
- [20] H. Li, Z. Wang, N. Zou, M. Ye, R. Xu, X. Gong, W. Duan, and Y. Xu, *Nature Computational Science* **2**, 367–377 (2022).
- [21] X. Li, Z. Li, and J. Chen, *Nature Communications* **13**, 7895 (2022).
- [22] I. L. Gutiérrez and C. B. Mendl, *Quantum* **6**, 627 (2022).
- [23] D. R. Vivas, J. Madroñero, V. Bucheli, L. O. Gómez, and J. H. Reina, *Neural-network quantum states: A systematic review* (2022), [arXiv:2204.12966](https://arxiv.org/abs/2204.12966) [quant-ph].
- [24] D. Luo, S. Yuan, J. Stokes, and B. K. Clark, *Gauge equivariant neural networks for 2+1d u(1) gauge theory simulations in hamiltonian formulation* (2022), [arXiv:2211.03198](https://arxiv.org/abs/2211.03198) [hep-lat].
- [25] Z. Chen, D. Luo, K. Hu, and B. K. Clark, *Simulating 2+1d lattice quantum electrodynamics at finite density with neural flow wavefunctions* (2022), [arXiv:2212.06835](https://arxiv.org/abs/2212.06835) [hep-lat].
- [26] J. M. Martyn, K. Najafi, and D. Luo, *Physical Review Letters* **131**, [10.1103/physrevlett.131.081601](https://doi.org/10.1103/physrevlett.131.081601) (2023).
- [27] G. Cassella, H. Sutterud, S. Azadi, N. Drummond, D. Pfau, J. S. Spencer, and W. Foulkes, *Physical Review Letters* **130**, [10.1103/physrevlett.130.036401](https://doi.org/10.1103/physrevlett.130.036401) (2023).
- [28] M. Wilson, S. Moroni, M. Holzmann, N. Gao, F. Wudarski, T. Vegge, and A. Bhowmik, *Physical Review B* **107**, [10.1103/physrevb.107.235139](https://doi.org/10.1103/physrevb.107.235139) (2023).
- [29] W. Ren, W. Fu, X. Wu, and J. Chen, *Nature Communications* **14**, [10.1038/s41467-023-37609-3](https://doi.org/10.1038/s41467-023-37609-3) (2023).
- [30] C. Roth, A. Szabó, and A. H. MacDonald, *Physical Review B* **108**, [10.1103/physrevb.108.054410](https://doi.org/10.1103/physrevb.108.054410) (2023).
- [31] R. Li, H. Ye, D. Jiang, X. Wen, C. Wang, Z. Li, X. Li, D. He, J. Chen, W. Ren, and L. Wang, *Forward laplacian: A new computational framework for neural network-based variational monte carlo* (2023), [arXiv:2307.08214](https://arxiv.org/abs/2307.08214) [physics.comp-ph].
- [32] D. Luo, D. D. Dai, and L. Fu, *Pairing-based graph neural network for simulating quantum materials* (2023), [arXiv:2311.02143](https://arxiv.org/abs/2311.02143) [cond-mat.str-el].
- [33] J. Kim, G. Pescia, B. Fore, J. Nys, G. Carleo, S. Gandolfi, M. Hjorth-Jensen, and A. Lovato, *Neural-network quantum states for ultra-cold fermi gases* (2023), [arXiv:2305.08831](https://arxiv.org/abs/2305.08831) [cond-mat.quant-gas].
- [34] I. von Glehn, J. S. Spencer, and D. Pfau, *A self-attention ansatz for ab-initio quantum chemistry* (2023), [arXiv:2211.13672](https://arxiv.org/abs/2211.13672) [physics.chem-ph].
- [35] Y. Teng, D. D. Dai, and L. Fu, *Solving and visualizing fractional quantum hall wavefunctions with neural network* (2024), [arXiv:2412.00618](https://arxiv.org/abs/2412.00618) [cond-mat.str-el].
- [36] G. Pescia, J. Nys, J. Kim, A. Lovato, and G. Carleo, *Physical Review B* **110**, [10.1103/physrevb.110.035108](https://doi.org/10.1103/physrevb.110.035108) (2024).
- [37] Y. Qian, T. Zhao, J. Zhang, T. Xiang, X. Li, and J. Chen, *Physical Review Letters* **134**, [10.1103/physrevlett.134.176503](https://doi.org/10.1103/physrevlett.134.176503) (2025).
- [38] G. Goldshlager, N. Abrahamsen, and L. Lin, *Journal of Computational Physics* **516**, 113351 (2024).
- [39] W. T. Lou, H. Sutterud, G. Cassella, W. Foulkes, J. Knolle, D. Pfau, and J. S. Spencer, *Physical Review X* **14**, [10.1103/physrevx.14.021030](https://doi.org/10.1103/physrevx.14.021030) (2024).
- [40] Z. Chen, L. Newhouse, E. Chen, D. Luo, and M. Soljačić, *Antn: Bridging autoregressive neural networks and tensor networks for quantum many-body simulation* (2024), [arXiv:2304.01996](https://arxiv.org/abs/2304.01996) [quant-ph].
- [41] Z. Chen and J. Lu, *Exact and efficient representation of totally anti-symmetric functions* (2025), [arXiv:2311.05064](https://arxiv.org/abs/2311.05064) [math.CA].
- [42] X. Li, Y. Chen, B. Li, H. Chen, F. Wu, J. Chen, and W. Ren, *Deep learning sheds light on integer and fractional topological insulators* (2025), [arXiv:2503.11756](https://arxiv.org/abs/2503.11756) [cond-mat.str-el].
- [43] I. Romero, J. Nys, and G. Carleo, *Communications Physics* **8**, [10.1038/s42005-025-01955-z](https://doi.org/10.1038/s42005-025-01955-z) (2025).
- [44] M. Geier, K. Nazaryan, T. Zaklama, and L. Fu, *Is attention all you need to solve the correlated electron problem?* (2025), [arXiv:2502.05383](https://arxiv.org/abs/2502.05383) [cond-mat.str-el].
- [45] D. Luo, T. Zaklama, and L. Fu, *Solving fractional electron states in twisted mote₂ with deep neural network* (2025), [arXiv:2503.13585](https://arxiv.org/abs/2503.13585) [cond-mat.str-el].
- [46] Y. Gu, W. Li, H. Lin, B. Zhan, R. Li, Y. Huang, D. He, Y. Wu, T. Xiang, M. Qin, L. Wang, and D. Lv, *Solving the hubbard model with neural quantum states* (2025), [arXiv:2507.02644](https://arxiv.org/abs/2507.02644) [cond-mat.str-el].
- [47] A. Chen, Z.-Q. Wan, A. Sengupta, A. Georges, and C. Roth, *Neural network-augmented pfaffian wavefunctions for scalable simulations of interacting fermions* (2025), [arXiv:2507.10705](https://arxiv.org/abs/2507.10705) [cond-mat.str-el].
- [48] H. Lange, A. Böhrer, C. Roth, and A. Bohrdt, *Phys. Rev. Lett.* **135**, 136504 (2025).
- [49] L. Fu, *A minimal and universal representation of fermionic wavefunctions (fermions = bosons + one)* (2025), [arXiv:2510.11431](https://arxiv.org/abs/2510.11431) [cond-mat.str-el].
- [50] C. Roth, A. Chen, A. Sengupta, and A. Georges, *Superconductivity in the two-dimensional hubbard model revealed by neural quantum states* (2025), [arXiv:2511.07566](https://arxiv.org/abs/2511.07566) [cond-mat.supr-con].
- [51] H. Lange, A. Chen, A. Georges, F. Grusdt, A. Bohrdt,

- and C. Roth, *Simulating superconductivity in mixed-dimensional $t_{\parallel}\text{-}J_{\parallel}\text{-}J_{\perp}$ bilayers with neural quantum states* (2026), [arXiv:2602.10091](https://arxiv.org/abs/2602.10091) [cond-mat.str-el].
- [52] K. Ch'ng, J. Carrasquilla, R. G. Melko, and E. Khatami, *Phys. Rev. X* **7**, 031038 (2017).
- [53] E. Ibarra-García-Padilla, H. Lange, R. G. Melko, R. T. Scalettar, J. Carrasquilla, A. Bohrdt, and E. Khatami, *Physical Review Research* **7**, 10.1103/physrevresearch.7.013122 (2025).
- [54] K. Choo, G. Carleo, N. Regnault, and T. Neupert, *Phys. Rev. Lett.* **121**, 167204 (2018).
- [55] A. Vaswani, N. Shazeer, N. Parmar, J. Uszkoreit, L. Jones, A. N. Gomez, L. u. Kaiser, and I. Polosukhin, in *Advances in Neural Information Processing Systems*, Vol. 30, edited by I. Guyon, U. V. Luxburg, S. Bengio, H. Wallach, R. Fergus, S. Vishwanathan, and R. Garnett (Curran Associates, Inc., 2017).
- [56] H. Ma, B. Kan, H. Shang, and J. Yang, *Transformer-based neural networks backflow for strongly correlated electronic structure* (2025), [arXiv:2509.25720](https://arxiv.org/abs/2509.25720) [quant-ph].
- [57] A. J. Coleman, *Rev. Mod. Phys.* **35**, 668 (1963).
- [58] H. Kummer, *Journal of Mathematical Physics* **8**, 2063 (1967).
- [59] R. Erdahl, *Reports on Mathematical Physics* **15**, 147 (1979).
- [60] A. J. Coleman and V. I. Yukalov, *Reduced Density Matrices: Coulson's Challenge* (Springer, Berlin, Heidelberg, 2000).
- [61] Z. Zhao, B. J. Braams, M. Fukuda, M. L. Overton, and J. K. Percus, *The Journal of Chemical Physics* **120**, 2095 (2004).
- [62] G. Gidofalvi and D. A. Mazziotti, *Phys. Rev. A* **69**, 042511 (2004).
- [63] D. A. Mazziotti, *Accounts of Chemical Research* **39**, 207 (2006).
- [64] G. Gidofalvi and D. A. Mazziotti, *Phys. Rev. A* **74**, 012501 (2006).
- [65] D. A. Mazziotti, ed., *Reduced-Density-Matrix Mechanics: With Application to Many-Electron Atoms and Molecules*, *Advances in Chemical Physics*, Vol. 134 (John Wiley & Sons, Inc., New York, 2007).
- [66] C. A. Schwerdtfeger and D. A. Mazziotti, *The Journal of Chemical Physics* **130**, 224102 (2009).
- [67] N. Shenvi and A. F. Izmaylov, *Phys. Rev. Lett.* **105**, 213003 (2010).
- [68] D. A. Mazziotti, *Chemical Reviews* **112**, 244 (2012).
- [69] B. Verstichel, H. van Aggelen, W. Poelmans, and D. Van Neck, *Physical Review Letters* **108**, 213001 (2012).
- [70] D. A. Mazziotti, *Phys. Rev. Lett.* **108**, 263002 (2012).
- [71] C. Schilling and R. Schilling, *Phys. Rev. Lett.* **122**, 013001 (2019).
- [72] A. Rubio-García, J. Dukelsky, D. R. Alcoba, P. Capuzzi, O. B. Oña, E. Ríos, A. Torre, and L. Lain, *The Journal of Chemical Physics* **151**, 154104 (2019).
- [73] C. L. Benavides-Riveros, J. Wolff, M. A. L. Marques, and C. Schilling, *Phys. Rev. Lett.* **124**, 180603 (2020).
- [74] K. Head-Marsden and D. A. Mazziotti, *The Journal of Physical Chemistry A* **124**, 4848 (2020), PMID: 32469523, <https://doi.org/10.1021/acs.jpca.0c01937>.
- [75] F. Castillo, J.-P. Labbé, J. Liebert, A. Padrol, E. Philippe, and C. Schilling, *An effective solution to convex 1-body n -representability* (2021), [arXiv:2105.06459](https://arxiv.org/abs/2105.06459) [quant-ph].
- [76] C. Schilling and S. Pittalis, *Phys. Rev. Lett.* **127**, 023001 (2021).
- [77] R. R. Li, M. D. Liebenthal, and A. E. DePrince, *The Journal of Chemical Physics* **155**, 174110 (2021).
- [78] M. J. Knight, H. M. Quiney, and A. M. Martin, *New Journal of Physics* **24**, 053004 (2022).
- [79] A. E. I. DePrince, *WIREs: Computational Molecular Science* **14**, e1702 (2024).
- [80] C. Garrod and J. K. Percus, *Journal of Mathematical Physics* **5**, 1756 (1964).
- [81] D. A. Mazziotti, *Phys. Rev. A* **57**, 4219 (1998).
- [82] D. A. Mazziotti, *Phys. Rev. A* **65**, 062511 (2002).
- [83] E. Cancès, G. Stoltz, and M. Lewin, *The Journal of Chemical Physics* **125**, 064101 (2006).
- [84] D. A. Mazziotti, *Phys. Rev. Lett.* **117**, 153001 (2016).
- [85] A. E. D. III, *Variational determination of the two-electron reduced density matrix: A tutorial review* (2023), [arXiv:2310.10746](https://arxiv.org/abs/2310.10746) [physics.chem-ph].
- [86] L. Vandenberghe and S. Boyd, *SIAM Review* **38**, 49 (1996), <https://doi.org/10.1137/1038003>.
- [87] M. Nakata, H. Nakatsuji, M. Ehara, M. Fukuda, K. Nakata, and K. Fujisawa, *The Journal of Chemical Physics* **114**, 8282 (2001).
- [88] D. A. Mazziotti, *Phys. Rev. Lett.* **93**, 213001 (2004).
- [89] D. A. Mazziotti, *Phys. Rev. A* **72**, 032510 (2005).
- [90] R. M. Erdahl, in *Reduced-Density-Matrix Mechanics: With Application to Many-Electron Atoms and Molecules*, edited by D. A. Mazziotti (John Wiley & Sons, Inc., New York, 2007) pp. 61–91.
- [91] D. A. Mazziotti, *Phys. Rev. Lett.* **106**, 083001 (2011).
- [92] D. A. Mazziotti, *Phys. Rev. A* **102**, 052819 (2020).
- [93] D. A. Mazziotti, *Phys. Rev. Lett.* **130**, 153001 (2023).
- [94] M. G. Scheer, *Hamiltonian bootstrap* (2024), [arXiv:2410.00810](https://arxiv.org/abs/2410.00810) [cond-mat.str-el].
- [95] K. J. Giesbertz and M. Ruggenthaler, *Physics Reports* **806**, 1–47 (2019).
- [96] A. Szabo and N. S. Ostlund, *Modern Quantum Chemistry: Introduction to Advanced Electronic Structure Theory* (Dover Publications, 1989).
- [97] V. Sitzmann, J. N. P. Martel, A. W. Bergman, D. B. Lindell, and G. Wetzstein, *Implicit neural representations with periodic activation functions* (2020), [arXiv:2006.09661](https://arxiv.org/abs/2006.09661) [cs.CV].
- [98] X. Shao, L. Paetow, M. E. Tuckerman, and M. Pavanello, *Machine learning electronic structure methods based on the one-electron reduced density matrix* (2023), [arXiv:2302.10741](https://arxiv.org/abs/2302.10741) [physics.chem-ph].
- [99] K. Ma, C. Yang, J. Zhang, Y. Li, G. Jiang, and J. Chai, *Entropy* **26** (2024).
- [100] S. Hazra, U. Patil, and S. Sanvito, *Journal of Chemical Theory and Computation* **20**, 4569–4578 (2024).
- [101] X. Gong, H. Li, N. Zou, R. Xu, W. Duan, and Y. Xu, *Nature Communications* **14**, 10.1038/s41467-023-38468-8 (2023).
- [102] J.-N. Boyn, A. E. DePrince, and K. D. Vogiatzis, *The Journal of Physical Chemistry Letters* **14**, 6413 (2023).
- [103] L. H. Delgado-Granados, L. M. Sager-Smith, K. Trifonova, and D. A. Mazziotti, *The Journal of Physical Chemistry Letters* **16**, 2231 (2025).
- [104] R. W. Richardson, *Physics Letters* **3**, 277 (1963).
- [105] R. W. Richardson and N. Sherman, *Nuclear Physics* **52**, 221 (1964).
- [106] J. Dukelsky, S. Pittel, and G. Sierra, *Rev. Mod. Phys.* **76**, 643 (2004).

- [107] G. Cybenko, *Mathematics of Control, Signals, and Systems* **2**, 303–314 (1989).
- [108] K. Hornik, M. Stinchcombe, and H. White, *Neural Networks* **2**, 359–366 (1989).
- [109] A. Pinkus, *Acta Numerica* **8**, 143–195 (1999).
- [110] J. Kim, J. K. Lee, and K. M. Lee, in *Proceedings of the IEEE Conference on Computer Vision and Pattern Recognition (CVPR)* (2016) pp. 1646–1654.
- [111] I. Goodfellow, Y. Bengio, and A. Courville, *Deep Learning* (MIT Press, 2016) <http://www.deeplearningbook.org>.
- [112] Y. LeCun, L. Bottou, G. B. Orr, and K.-R. Müller, in *Neural Networks: Tricks of the Trade*, Lecture Notes in Computer Science, Vol. 1524, edited by G. B. Orr and K.-R. Müller (Springer, Berlin, Heidelberg, 1998) pp. 9–50.
- [113] N. Srivastava, G. Hinton, A. Krizhevsky, I. Sutskever, and R. Salakhutdinov, *Journal of Machine Learning Research* **15**, 1929 (2014).
- [114] J. L. Ba, J. R. Kiros, and G. E. Hinton, *Layer normalization* (2016), [arXiv:1607.06450](https://arxiv.org/abs/1607.06450) [stat.ML].
- [115] K. M. Nakanishi, *Scalable-softmax is superior for attention* (2025), [arXiv:2501.19399](https://arxiv.org/abs/2501.19399) [cs.CL].
- [116] C. L. Kane and E. J. Mele, *Phys. Rev. Lett.* **95**, 146802 (2005).
- [117] J. Hubbard, *Proceedings of the Royal Society of London Series A* **276**, 238 (1963).
- [118] J. Hubbard, *Proceedings of the Royal Society of London Series A* **277**, 237 (1964).
- [119] J. E. Hirsch and S. Tang, *Phys. Rev. Lett.* **62**, 591 (1989).
- [120] J. Bergstra, D. Yamins, and D. Cox, in *Proceedings of the 30th International Conference on Machine Learning*, Proceedings of Machine Learning Research, Vol. 28, edited by S. Dasgupta and D. McAllester (PMLR, Atlanta, Georgia, USA, 2013) pp. 115–123.
- [121] I. Loshchilov and F. Hutter, in *International Conference on Learning Representations* (2017).
- [122] X. Glorot and Y. Bengio, in *Proceedings of the Thirteenth International Conference on Artificial Intelligence and Statistics*, Proceedings of Machine Learning Research, Vol. 9, edited by Y. W. Teh and M. Titterton (PMLR, Chia Laguna Resort, Sardinia, Italy, 2010) pp. 249–256.
- [123] K. He, X. Zhang, S. Ren, and J. Sun, in *2015 IEEE International Conference on Computer Vision (ICCV)* (2015) pp. 1026–1034.
- [124] D. Bahdanau, K. Cho, and Y. Bengio, *Neural machine translation by jointly learning to align and translate* (2016), [arXiv:1409.0473](https://arxiv.org/abs/1409.0473) [cs.CL].
- [125] P. Shaw, J. Uszkoreit, and A. Vaswani, *Self-attention with relative position representations* (2018), [arXiv:1803.02155](https://arxiv.org/abs/1803.02155) [cs.CL].
- [126] B. Mildenhall, P. P. Srinivasan, M. Tancik, J. T. Barron, R. Ramamoorthi, and R. Ng, in *Computer Vision – ECCV 2020: 16th European Conference, Glasgow, UK, August 23–28, 2020, Proceedings, Part I* (Springer-Verlag, Berlin, Heidelberg, 2020) p. 405–421.
- [127] I. Loshchilov and F. Hutter, *Decoupled weight decay regularization* (2019), [arXiv:1711.05101](https://arxiv.org/abs/1711.05101) [cs.LG].
- [128] C. E. Rasmussen and C. K. I. Williams, *Gaussian Processes for Machine Learning* (MIT Press, Cambridge, MA, 2006).
- [129] T. Gneiting, *Journal of Multivariate Analysis* **83**, 493 (2002).
- [130] M. D. Buhmann, *Radial Basis Functions: Theory and Implementations*, Cambridge Monographs on Applied and Computational Mathematics, Vol. 12 (Cambridge University Press, Cambridge, 2003).
- [131] S. Li, C. You, G. Guruganesh, J. Ainslie, S. Ontanon, M. Zaheer, S. Sanghai, Y. Yang, S. Kumar, and S. Bhojanapalli, *arXiv preprint arXiv:2310.04418* (2023).
- [132] Y. Zhou, U. Alon, X. Chen, X. Wang, R. Agarwal, and D. Zhou, *Transformers can achieve length generalization but not robustly* (2024), [arXiv:2402.09371](https://arxiv.org/abs/2402.09371) [cs.LG].
- [133] O. Press, N. A. Smith, and M. Lewis, *Train short, test long: Attention with linear biases enables input length extrapolation* (2022), [arXiv:2108.12409](https://arxiv.org/abs/2108.12409) [cs.CL].
- [134] J. S. Bridle, in *NATO Neurocomputing* (1989).
- [135] D. Hendrycks and K. Gimpel, *Gaussian error linear units (gelus)* (2023), [arXiv:1606.08415](https://arxiv.org/abs/1606.08415) [cs.LG].
- [136] R. G. Keys, *IEEE Transactions on Acoustics, Speech, and Signal Processing* **29**, 1153 (1981).
- [137] D. P. Mitchell and A. N. Netravali, in *Proceedings of the 15th Annual Conference on Computer Graphics and Interactive Techniques (SIGGRAPH '88)* (ACM, Atlanta, Georgia, USA, 1988) pp. 221–228.
- [138] D. P. Kingma and J. Ba, *Adam: A method for stochastic optimization* (2017), [arXiv:1412.6980](https://arxiv.org/abs/1412.6980) [cs.LG].
- [139] J. Bardeen, L. N. Cooper, and J. R. Schrieffer, *Phys. Rev.* **108**, 1175 (1957).
- [140] N. A. Slavnov, *Theoretical and Mathematical Physics* **79**, 502 (1989).
- [141] H.-Q. Zhou, J. Links, R. H. McKenzie, and M. D. Gould, *Physical Review B* **65**, [10.1103/physrevb.65.060502](https://doi.org/10.1103/physrevb.65.060502) (2002).
- [142] A. Faribault, P. Calabrese, and J.-S. Caux, *Physical Review B* **77**, [10.1103/physrevb.77.064503](https://doi.org/10.1103/physrevb.77.064503) (2008).
- [143] G. Gorohovskiy and E. Bettelheim, *Physical Review B* **84**, [10.1103/physrevb.84.224503](https://doi.org/10.1103/physrevb.84.224503) (2011).
- [144] R. P. Feynman, *Phys. Rev.* **56**, 340 (1939).

SUPPLEMENTARY INFORMATION

Appendix A: NN Architecture

We train NNs on n -RDMs computed on small $L \times L$ lattices and use them to predict n -RDMs for larger systems, exploiting their smooth, periodic structure over the BZ. We use two complementary architectures: (i) a self-attention NN that treats momenta as tokens and learns n -RDMs via self-attention [55, 124, 125], and (ii) an implicit neural representation (INR) in the style of NeRF/SIREN that models n -RDMs as a continuous periodic function evaluable at arbitrary system sizes [97, 126].

1. Self-Attention NN Architecture for the 1-RDM

We start with the self-attention NN for 1-RDM.

a. physical set-up

The self-attention NN is applied on a 1-RDM in two spatial dimensions (2D) for the examples in Sec. C and Sec. D. Therefore, in this part, we will first discuss 1-RDM that will be fed into the NN. The 1-RDM has the general form

$$O_{\mathbf{k}\alpha, \mathbf{k}'\alpha'} = \langle c_{\mathbf{k}\alpha}^\dagger c_{\mathbf{k}'\alpha'} \rangle \quad (\text{A1})$$

where \mathbf{k} and \mathbf{k}' ranges over the first BZ, α represents intra-unit-cell degrees of freedom (sublattice, orbital, spin, etc.), taking ξ different values of them per \mathbf{k} . $c_{\mathbf{k}\alpha}^\dagger$ is the creation operator for a state with Bloch momentum \mathbf{k} and index α , and $\langle \dots \rangle$ is the ground state average. \mathbf{k} takes $L \times L$ different values:

$$\mathbf{k} = (l_1/L)\mathbf{b}_1 + (l_2/L)\mathbf{b}_2, \quad (\text{A2})$$

where $l_1, l_2 = 0, 1, 2, \dots, L-1$, and \mathbf{b}_1 and \mathbf{b}_2 are two primitive reciprocal lattice vectors. When the translation symmetry is not spontaneously broken, the 1-RDM is reduced to

$$O_{\mathbf{k}, \alpha\alpha'} = \langle c_{\mathbf{k}\alpha}^\dagger c_{\mathbf{k}\alpha'} \rangle, \quad O_{\mathbf{k}} \in \mathbb{C}^{\xi \times \xi}, \quad (\text{A3})$$

so the tensor has shape $L \times L \times \xi \times \xi$. This is the case for Sec. C. When the translation symmetry is spontaneously broken, we will look at $O_{\mathbf{k}\alpha, \mathbf{k}'\alpha'}$ with fixed $\mathbf{q} \equiv \mathbf{k}' - \mathbf{k}$, *i.e.*,

$$O_{\mathbf{k}, \alpha\alpha'}^{\mathbf{q}} = O_{\mathbf{k}\alpha, \mathbf{k}+\mathbf{q}\alpha'} \quad (\text{A4})$$

For a fixed \mathbf{q} , $O^{\mathbf{q}}$ is also a tensor of dimension $L \times L \times \xi \times \xi$. In the notation of $O_{\mathbf{k}, \alpha\alpha'}^{\mathbf{q}}$, the translational invariant case is just to focus on $O_{\mathbf{k}, \alpha\alpha'}^{\mathbf{q}=0}$. Therefore, regardless of the translation symmetry, $O_{\mathbf{k}, \alpha\alpha'}^{\mathbf{q}}$ has dimension $L \times L \times \xi \times \xi$.

b. Preprocessing (transform 1-RDM to NN input)

With the 1-RDM $O^{\mathbf{q}}$ defined above, we now show how they are transformed into fixed-length vectors and standardized to form the input for our self-attention NN, which is preprocessing part of Fig. 2(a). From Eq. (A2), the BZ grid has $L \times L$ momenta with the i th momentum labelled as \mathbf{k}_i ($i = 1, 2, \dots, L^2$).

For each \mathbf{k}_i , we consider the corresponding 1-RDM block, $O^{\mathbf{q}}(\mathbf{k}_i)$. We transform (flatten) this matrix into a real vector $\mathbf{x}(\mathbf{k}_i) \in \mathbb{R}^{2\xi^2}$ in the following way. For the translation-invariant case, $O^{\mathbf{q}}(\mathbf{k}_i) \in \mathbb{C}^{\xi \times \xi}$ and $\mathbf{q} = 0$ (Sec. C),

$$\mathbf{x}(\mathbf{k}_i) \equiv \begin{bmatrix} \text{vec}(\text{Re } O^{\mathbf{q}}(\mathbf{k}_i)) \\ \text{vec}(\text{Im } O^{\mathbf{q}}(\mathbf{k}_i)) \end{bmatrix} \in \mathbb{R}^{2\xi^2}. \quad (\text{A5})$$

Here the operation $\text{vec}(\dots)$ simply turns a matrix into a long column vector by transposing and then stacking its rows from top to bottom. Namely,

$$[\text{vec}(M)]_{(\alpha-1)\xi+\alpha'} \equiv M_{\alpha\alpha'}, \quad \alpha, \alpha' = 1, \dots, \xi. \quad (\text{A6})$$

For the specific translational-symmetry-breaking case in Hubbard model discussed in Sec. D, we have $O^{\mathbf{q}}(\mathbf{k}_i)$ real. Furthermore, \mathbf{q} only takes two values, $\mathbf{q} \in \{0, \mathbf{Q}\}$ with $\mathbf{Q} = (\pi, \pi)$. Thus, in this case, we do not split the 1-RDM into real/imaginary parts; instead we stack the two q -blocks:

$$\mathbf{x}(\mathbf{k}_i) \equiv \begin{bmatrix} \text{vec}(O^0(\mathbf{k}_i)) \\ \text{vec}(O^{\mathbf{Q}}(\mathbf{k}_i)) \end{bmatrix} \in \mathbb{R}^{2\xi^2}. \quad (\text{A7})$$

Therefore, both cases (Eqs. (A5) and (A7)) leads to $\mathbf{x}(\mathbf{k}_i)$ with the same shape, thus the components of $\mathbf{x}(\mathbf{k}_i)$ can be labeled by $f \in \{1, \dots, 2\xi^2\}$. See Sec. C and Sec. D for more details about the preprocessing steps for each model. For one BZ mesh, stack the L^2 vectors $\mathbf{x}(\mathbf{k}_i)$ row-wise to form

$$X \equiv \begin{bmatrix} \mathbf{x}(\mathbf{k}_1)^\top \\ \vdots \\ \mathbf{x}(\mathbf{k}_{L^2})^\top \end{bmatrix} \in \mathbb{R}^{L^2 \times 2\xi^2}. \quad (\text{A8})$$

A single training sample consists of two 1-RDMs over the entire BZ, an initial $O_{\text{init}}^{\mathbf{q}}$ and a final (target) $O_{\text{tgt}}^{\mathbf{q}}$. Here, ‘‘init’’ means the 1-RDM we used to start HF; ‘‘tgt’’ means the true final 1-RDM we obtained at zero temperature after self-consistent HF convergence. After flattening in Eqs. (A5) and (A7), they become:

$$X^{(\beta)} \equiv \begin{bmatrix} \mathbf{x}^{(\beta)}(\mathbf{k}_1)^\top \\ \vdots \\ \mathbf{x}^{(\beta)}(\mathbf{k}_{L^2})^\top \end{bmatrix} \in \mathbb{R}^{L^2 \times 2\xi^2}, \quad \beta \in \{\text{init}, \text{tgt}\}. \quad (\text{A9})$$

Define means and standard deviations over all \mathbf{k}_i and all N_{sample} training samples with $\beta \in \{\text{init}, \text{tgt}\}$, for each feature $f \in \{1, \dots, 2\xi^2\}$:

$$\mu_f^{(\beta)} \equiv \frac{1}{N_{\text{sample}}L^2} \sum_{\text{sample}} \sum_{i=1}^{L^2} X_{i,f}^{(\beta)}, \quad (\sigma_f^{(\beta)})^2 \equiv \frac{1}{N_{\text{sample}}L^2 - 1} \sum_{\text{sample}} \sum_{i=1}^{L^2} (X_{i,f}^{(\beta)} - \mu_f^{(\beta)})^2. \quad (\text{A10})$$

Note that for the translation-invariant case (Sec. C), we calculate the mean and standard deviation across all features (see Eq. (C23)). We then standardize $X_{\text{init}}, X_{\text{tgt}}$ (computing the z -score):

$$\tilde{X}_{i,f}^{(\text{init})} \equiv \frac{X_{i,f}^{(\text{init})} - \mu_f^{(\text{init})}}{\sigma_f^{(\text{init})}}, \quad \tilde{X}_{i,f}^{(\text{tgt})} \equiv \frac{X_{i,f}^{(\text{tgt})} - \mu_f^{(\text{tgt})}}{\sigma_f^{(\text{tgt})}}, \quad (\text{A11})$$

Equivalently, for each \mathbf{k}_i

$$\tilde{\mathbf{x}}^{(\beta)}(\mathbf{k}_i) \equiv (\tilde{X}_{i,1}^{(\beta)}, \dots, \tilde{X}_{i,2\xi^2}^{(\beta)})^\top \in \mathbb{R}^{2\xi^2}. \quad (\text{A12})$$

In what follows, the NN input is the standardized $\tilde{\mathbf{x}}^{(\text{init})}(\mathbf{k}_i)$; for brevity we write $\tilde{\mathbf{x}}_i \equiv \tilde{\mathbf{x}}^{(\text{init})}(\mathbf{k}_i)$ unless stated otherwise. Standardization ensures that both the input and output data in the training dataset have a mean of 0 and a standard deviation of 1, which improves numerical conditioning and speeds training [111, 112]. This combined set of transformations (flattening in Eq. (A5) and standardization in Eq. (A11)) is denoted in the preprocessing part of Fig. 2. Note that since these transformations are invertible, we can easily reverse the process to recover the predicted final 1-RDMs from the NN outputs. The matrices $\tilde{X}^{(\text{init})}$ and $\tilde{X}^{(\text{tgt})}$, containing exactly the information from $O_{\text{init}}^{\mathbf{q}}$ and $O_{\text{tgt}}^{\mathbf{q}}$, are thus the data we use to train the NN. During the training process, the self-attention NN parameters are optimized so that, starting from $O_{\text{init}}^{\mathbf{q}}$ defined on all L^2 momenta, it produces $O_{\text{out}}^{\mathbf{q}}$ whose values at each \mathbf{k}_i closely matches the $O_{\text{tgt}}^{\mathbf{q}}$. After the training, we would expect the NN to be able to make accurate predictions for $O_{\text{tgt}}^{\mathbf{q}}$ not only for the training system size but also for larger L .

c. Overall Structure of Attention Layers

With each local $O^{\mathbf{q}}(\mathbf{k}_i)$ now flattened and standardized (Eq. (A5)-Eq. (A7)) into token features $\tilde{\mathbf{x}}_i$, we now describe the overall structure of how our model processes them through stacked attention layers to produce the predicted final 1-RDM, as shown in Fig. 2(b).

Input layer. As shown in Eqs. (A5) and (A7), at each momentum \mathbf{k}_i we have a normalized real feature vector $\tilde{\mathbf{x}}_i \in \mathbb{R}^{2\xi^2}$ (flattened entries of the 1-RDM at some \mathbf{k}_i). We first map it to a vector of dimension D (where D is the “model width”):

$$\mathbf{h}_i^{(0)} = W_{\text{in}} \tilde{\mathbf{x}}_i + \mathbf{b}_{\text{in}} \in \mathbb{R}^D, \quad (\text{A13})$$

where $W_{\text{in}}, \mathbf{b}_{\text{in}}$ are learnable parameters. Stacking all $\mathbf{h}_i^{(0)}$ gives us a matrix $H^{(0)}$,

$$H^{(0)} = \begin{bmatrix} (\mathbf{h}_1^{(0)})^\top \\ \vdots \\ (\mathbf{h}_{L^2}^{(0)})^\top \end{bmatrix} \in \mathbb{R}^{L^2 \times D}. \quad (\text{A14})$$

Attention layers. We then apply N attention layers (Fig. 2(a)) to $H^{(0)}$ in sequence in order to produce $H^{(N)} \in \mathbb{R}^{L^2 \times D}$, where the i -th row is $h_i^{(N)} \in \mathbb{R}^D$. In general, we denote the matrix $H^{(\ell-1)} \in \mathbb{R}^{L^2 \times D}$ as the input to the ℓ^{th} layer of our model, $\ell \in \{1, \dots, N\}$. The structure of one attention layer consists of three components: (a) one attention block discussed in Sec. A1d, (b) Dropout and LayerNorm discussed in Sec. A1e and (c) one FFN, also discussed in Sec. A1e. As we will see in Sec. A1e, the first FFN layer (see construction in Sec. A1e) maps $\mathbb{R}^D \rightarrow \mathbb{R}^{D_{\text{ff}}}$ and the second maps back $\mathbb{R}^{D_{\text{ff}}} \rightarrow \mathbb{R}^D$.

Output head. Finally, we define a linear head with which learnable parameters $W_{\text{out}} \in \mathbb{R}^{2\xi^2 \times D}$, $\mathbf{b}_{\text{out}} \in \mathbb{R}^{2\xi^2}$ that maps each \mathbf{h}_i back to a vector $\hat{\mathbf{x}}_i$:

$$\hat{\mathbf{x}}_i = W_{\text{out}} \mathbf{h}_i^{(N)} + \mathbf{b}_{\text{out}}. \quad (\text{A15})$$

Stacking all $\hat{\mathbf{x}}_i$ gives

$$\tilde{X}_{\text{out}} = \begin{bmatrix} \hat{\mathbf{x}}_1^\top \\ \vdots \\ \hat{\mathbf{x}}_{L^2}^\top \end{bmatrix} \in \mathbb{R}^{L^2 \times 2\xi^2}. \quad (\text{A16})$$

To recover the physics of 1-RDM, we de-standardize elementwise (reverse of Eq. (A11)):

$$(X_{\text{out}})_{i,f} \equiv (\tilde{X}_{\text{out}})_{i,f} \sigma_f^{\text{tgt}} + \mu_f^{\text{tgt}}. \quad (\text{A17})$$

Note that when testing the trained NN for larger L , we use the same μ_f^{tgt} and σ_f^{tgt} computed from the smaller system size, since the assumption is that they possess similar distributions. We then reshape X_{out} to $L \times L \times \xi \times \xi$ and recombine the real/imag halves to invert the flattening in Eq. (A5) - Eq. (A7), yielding the final predicted 1-RDM:

$$\mathbf{x}_{\text{out}}(\mathbf{k}_i) \equiv (\tilde{\mathbf{x}}_{\text{out}}(\mathbf{k}_i))_f \sigma_f^{\text{tgt}} + \mu_f^{\text{tgt}}, \quad f = 1, \dots, 2\xi^2. \quad (\text{A18})$$

$$\text{Re } O_{\text{out}}^q(\mathbf{k}_i) \equiv \text{vec}^{-1} \left((\mathbf{x}_{\text{out}}(\mathbf{k}_i))_{1:\xi^2} \right), \quad \text{Im } O_{\text{out}}^q(\mathbf{k}_i) \equiv \text{vec}^{-1} \left((\mathbf{x}_{\text{out}}(\mathbf{k}_i))_{\xi^2+1:2\xi^2} \right), \quad (\text{A19})$$

$$O_{\text{out}}^q(\mathbf{k}_i) = \text{Re } O_{\text{out}}^q(\mathbf{k}_i) + i \text{Im } O_{\text{out}}^q(\mathbf{k}_i), \quad (\text{A20})$$

where μ_f, σ_f are defined in Eq. (A10). And vec^{-1} is the inverse of the vec in Eq. (A5), which takes a length- ξ^2 vector and reshapes it back into a $\xi \times \xi$ matrix using the same stacking convention from vec (see Eq. (A5)). The process from Eq. (A17) to Eq. (A20) are shown as the decoding step in Fig. 2.

Training. For computational efficiency, we divide the training dataset into several “minibatches” (according to standard practice), where each minibatch consists of N_b $(\tilde{X}_{\text{init}}, \tilde{X}_{\text{tgt}})$ pairs. For our loss function, we use the MSE between \tilde{X}_{out} and \tilde{X}_{tgt} (both of which have a total of L^2 elements):

$$\mathcal{L} = \frac{1}{N_b L^2 (2\xi^2)} \sum_{b=1}^{N_b} \sum_{i=1}^{L^2} \sum_{f=1}^{2\xi^2} (\tilde{X}_{\text{out},i,f}^{(b)} - \tilde{X}_{\text{tgt},i,f}^{(b)})^2. \quad (\text{A21})$$

as indicated in Fig. 2, then take the gradient of the loss \mathcal{L} with respect to the trainable parameters (defined in Sec. A1e) and update the values of parameters using the AdamW optimizer [127].

d. *Attention Block (multiple attention heads)*

Here we describe the detailed structure of the attention block we first mentioned in Sec. A 1 c as part of each attention layer. Each attention block includes N_{head} attention heads (Fig. 2(c)). The structure of one attention head is shown in Fig. 2(d). We first introduce the *Bias* block in Fig. 2(d). The bias block is constructed based on the geometry-aware relative positional bias that will be used in attention heads. Intuitively speaking, attention [55] decides “which \mathbf{k}_j should influence \mathbf{k}_i .” We want this decision to respect BZ geometry and periodicity. Precisely, for each ordered pair of momenta $(\mathbf{k}_i, \mathbf{k}_j)$ with $\mathbf{k}_i = \frac{l_{i,1}}{L}\mathbf{b}_1 + \frac{l_{i,2}}{L}\mathbf{b}_2$ and $\mathbf{k}_j = \frac{l_{j,1}}{L}\mathbf{b}_1 + \frac{l_{j,2}}{L}\mathbf{b}_2$ defined in Eq. (A2), we stack them to form the vector

$$\left(\frac{l_{i,1}}{L}, \frac{l_{i,2}}{L}, \frac{l_{j,1}}{L}, \frac{l_{j,2}}{L}\right) \in [0, 1)^4. \quad (\text{A22})$$

In each attention head, we then define a learnable continuous function $f_\theta : \mathbb{R}^4 \rightarrow \mathbb{R}$ that maps each such pair of momenta to a scalar bias that represents how closely correlated they are. In general, this f_θ can be parameterized as a standard NN, as in Sec. C. However, we can also explicitly incorporate our physical assumptions by using a carefully-chosen ansatz with a periodic basis, as is used in Sec. D and described below. Let $W_r \in \mathbb{R}^{m \times 2}$ be a learnable matrix, where m is a hyperparameter that determines the number of frequencies. Project each $\mathbf{k}_i, \mathbf{k}_j$, separately:

$$\mathbf{u}_i = W_r \begin{bmatrix} \frac{l_{i,1}}{L} \\ \frac{l_{i,2}}{L} \end{bmatrix} \in \mathbb{R}^m, \quad \mathbf{u}_j = W_r \begin{bmatrix} \frac{l_{j,1}}{L} \\ \frac{l_{j,2}}{L} \end{bmatrix} \in \mathbb{R}^m. \quad (\text{A23})$$

We build periodic features

$$\phi(\mathbf{k}) \equiv \cos \mathbf{u} + \sin \mathbf{u} \in \mathbb{R}^m \quad (\text{applied elementwise}), \quad (\text{A24})$$

and take the difference

$$\Delta_{ij} = \phi(\mathbf{k}_i) - \phi(\mathbf{k}_j) \in \mathbb{R}^m. \quad (\text{A25})$$

With a learnable vector of coefficients $\mathbf{C} \in \mathbb{R}^m$ (which is initially set to all 1’s before being optimized during training), we define a scalar, nonnegative “periodic distance” σ_{ij} ,

$$\sigma_{ij} \equiv |\langle \Delta_{ij}, \mathbf{C} \rangle| \geq 0, \quad (\text{A26})$$

(here \langle, \rangle means standard dot-product) and convert it to a decaying bias [125] f_θ :

$$f_\theta(\mathbf{k}_i, \mathbf{k}_j) \equiv \exp [-(\sigma_{ij} + \varepsilon)^p], \quad \varepsilon = 10^{-6}, \quad (\text{A27})$$

where $p \in [0.5, 3]$ is an exponent that serves as a practical stability constraint [128–130]. Repeating this process for each pair of momenta, we obtain a matrix $B \in \mathbb{R}^{L^2 \times L^2}$, where we define

$$B_{ij} \equiv f_\theta(\mathbf{k}_i, \mathbf{k}_j), \quad i, j \in \{1, \dots, L^2\}. \quad (\text{A28})$$

Thus B_{ij} acts as a smooth, periodic bias on the 1BZ [131, 132], which is shown as the *Bias* block in Fig. 2(d).

Besides the bias block, the attention head also involves the query Q matrix, key K matrix, value V matrix, and Scalable Softmax. For each attention head $h \in \{1, \dots, N_{\text{head}}\}$ with N_{head} the number of heads, we make matrices $Q^{(h)}, K^{(h)}, V^{(h)} \in \mathbb{R}^{L^2 \times d_k}$ [55] by multiplying $H^{(\ell-1)}$ (the current layer’s input) with learnable matrices $W_Q^{(h)}, W_K^{(h)}, W_V^{(h)} \in \mathbb{R}^{D \times d_k}$, where $d_k \equiv D/N_{\text{head}}$ is the width of each head and D is the model width as defined in Sec. A 1 c. Then we have:

$$Q^{(h)} = H^{(\ell-1)}W_Q^{(h)}, \quad K^{(h)} = H^{(\ell-1)}W_K^{(h)}, \quad V^{(h)} = H^{(\ell-1)}W_V^{(h)}. \quad (\text{A29})$$

With B_{ij} from Eq. (A28), define the pre-softmax logits [55, 133] as:

$$\Lambda_{ij}^{(h)} = \tau \left(\frac{\langle Q_i^{(h)}, K_j^{(h)} \rangle + B_{ij}}{\sqrt{d_k}} \right), \quad \text{where } \tau \equiv s \log(L^2), \quad (\text{A30})$$

and s is a learnable parameter. (We use the notation of Q_i, K_i , and V_i for the i^{th} row of Q, K , and V , respectively, with $i \in \{1, \dots, L^2\}$). Notice that $B_{ij} \in (0, 1]$ is large when \mathbf{k}_i and \mathbf{k}_j are close on 1BZ, so it adds extra preference to

mix nearby momenta. Meanwhile, the multiplication by $s \log(L^2)$ implements Scalable Softmax [115] to avoid the phenomenon of ‘‘attention fading’’; that is, it ensures that for a large number of \mathbf{k} points [133], the maximum value of the attention weights does not drop to 0, which could otherwise hinder the NN’s capacity for length generalization. The attention weights and head outputs are

$$A_{ij}^{(h)} = \frac{e^{\tau \Lambda_{ij}^{(h)}}}{\sum_{m=1}^{L^2} e^{\tau \Lambda_{im}^{(h)}}}, \quad \sum_j A_{ij}^{(h)} = 1, \quad A_{ij}^{(h)} > 0. \quad (\text{A31})$$

i.e., Softmax [134] is applied here (row-wise normalization that turns attention scores into positive weights summing to 1). Then,

$$\mathbf{z}_i^{(h)} = \sum_{j=1}^{L^2} A_{ij}^{(h)} V_j^{(h)} \in \mathbb{R}^{d_k}. \quad (\text{A32})$$

We can stack all the $\mathbf{z}_i^{(h)}$ s constructed in this way to form a matrix:

$$Z^{(h)} = \begin{bmatrix} \mathbf{z}_1^{(h)} \\ \vdots \\ \mathbf{z}_{L^2}^{(h)} \end{bmatrix} \in \mathbb{R}^{L^2 \times d_k}. \quad (\text{A33})$$

Therefore, a summary of the attention head we just discussed in Eq. (A29)-Eq. (A31) is the following (see the red box in Fig. 2):

$$\text{AttentionHead}^{(h)}(H^{(\ell-1)}) := Z^{(h)} \quad \text{with} \quad \begin{cases} Q^{(h)} = H^{(\ell-1)} W_Q^{(h)}, & K^{(h)} = H^{(\ell-1)} W_K^{(h)}, & V^{(h)} = H^{(\ell-1)} W_V^{(h)}, \\ \Lambda_{ij}^{(h)} = \tau \left(\frac{\langle Q_i^{(h)}, K_j^{(h)} \rangle + B_{ij}}{\sqrt{d_k}} \right), & \text{where } \tau \equiv s \log(L^2), \\ A_{ij}^{(h)} = \frac{e^{\tau \Lambda_{ij}^{(h)}}}{\sum_{m=1}^{L^2} e^{\tau \Lambda_{im}^{(h)}}}, & \sum_j A_{ij}^{(h)} = 1, \quad A_{ij}^{(h)} > 0, \\ Z^{(h)} = A^{(h)} V^{(h)}. \end{cases} \quad (\text{A34})$$

Finally, the $N_{\text{head}} \geq 1$ attention heads form an attention block. Parameters are not shared between different attention heads (even if they are in the same attention block), (*i.e.*, each individual attention head has its own set of learnable parameters which are optimized independently from the others). For all $i \in \{1, \dots, L^2\}$, we concatenate (*i.e.* ‘‘stack’’) the output vectors $\mathbf{z}_i^{(h)} \in \mathbb{R}^{d_k}$ from each attention head into a single vector of size $N_{\text{head}} d_k = D$:

$$\text{Concat}(Z^{(1)}, \dots, Z^{(N_{\text{head}})}) = [Z^{(1)} \quad Z^{(2)} \quad \dots \quad Z^{(N_{\text{head}})}] \in \mathbb{R}^{L^2 \times D}. \quad (\text{A35})$$

and then apply an output linear map with learnable parameters $W_O \in \mathbb{R}^{D \times D}$, $\mathbf{b}_O \in \mathbb{R}^D$:

$$Z = \text{Concat}(Z^{(1)}, \dots, Z^{(N_{\text{head}})}) W_O + \mathbf{1} \mathbf{b}_O^\top, \quad (\text{A36})$$

and here $\mathbf{1}$ is a length- L^2 column of ones. This mixes information across heads and returns to the model width D .

e. Dropout, Layer Normalization, and FFN

We now discuss the dropout, layer normalization, and FFN in each each attention layer (we first introduced them in Sec. A1c) as shown in Fig. 2(b).

Applying Dropout to a vector or matrix means that we randomly set each element of the vector or matrix to zero with a probability p or keep it with a probability of $1 - p$ [113]. We apply dropout to the attention output Z (Eq. (A37)), add the result to the layer input $H^{(\ell-1)}$ (Eq. (A38)), and then apply LayerNorm per \mathbf{k}_i :

$$\hat{Z} = \text{Dropout}(Z), \quad \text{where } \text{Dropout}(Z)_{ij} = \frac{m_{ij} Z_{ij}}{1 - p}, \quad m_{ij} \sim \text{Bernoulli}(1 - p), \quad (\text{A37})$$

$$U_i = \text{LayerNorm}(H_i^{(\ell-1)} + \hat{Z}_i), \quad U \in \mathbb{R}^{L^2 \times D}. \quad (\text{A38})$$

Here LayerNorm is applied independently to each $\mathbf{U}_i \in \mathbb{R}^D$, and is defined as follows: define the mean and variance over $d = 1, \dots, D$:

$$\mu_i \equiv \frac{1}{D} \sum_{d=1}^D U_{i,d}, \quad \sigma_i^2 \equiv \frac{1}{D} \sum_{d=1}^D (U_{i,d} - \mu_i)^2, \quad (\text{A39})$$

then, with learnable parameters $\boldsymbol{\gamma}, \boldsymbol{\beta} \in \mathbb{R}^D$ and a small $\epsilon > 0$, we set

$$\text{LayerNorm}(\mathbf{U}_i) \equiv \boldsymbol{\gamma} \odot \frac{\mathbf{U}_i - \mu_i \mathbf{1}}{\sqrt{\sigma_i^2 + \epsilon}} + \boldsymbol{\beta} \in \mathbb{R}^D, \quad (\text{A40})$$

where \odot is the element-wise product. Namely,

$$[\text{LayerNorm}(U_i)]_d = \gamma_d \frac{U_{i,d} - \mu_i}{\sqrt{\sigma_i^2 + \epsilon}} + \beta_d, \quad d = 1, \dots, D. \quad (\text{A41})$$

For every \mathbf{k}_i , take its current vector $\mathbf{U}_i \in \mathbb{R}^D$ and apply a learned linear map which increases the dimension to a larger width D_{ff} , to get $\mathbf{F}_i = W_1 \mathbf{U}_i + \mathbf{b}_1$ with $W_1 \in \mathbb{R}^{D \times D_{\text{ff}}}$ and $\mathbf{b}_1 \in \mathbb{R}^{D_{\text{ff}}}$:

$$\mathbf{F} = U W_1 + \mathbf{1} \mathbf{b}_1^\top \in \mathbb{R}^{L^2 \times D_{\text{ff}}}. \quad (\text{A42})$$

Apply the GELU (“Gaussian Error Linear Unit” [135]) element-wise to F , which smoothly gates each component of F : small negative values are damped, large positive values pass through almost linearly. It is written using the error function erf, then mapped back from the hidden width to the model width:

$$\widehat{U} = W_2 \text{GELU}(F) + \mathbf{1} \mathbf{b}_2^\top \in \mathbb{R}^{L^2 \times D} \quad \text{where} \quad \text{GELU}(F) \equiv \frac{F}{2} \left(\mathbf{1} + \text{erf} \left(\frac{F}{\sqrt{2}} \right) \right), \quad (\text{A43})$$

with $W_2 \in \mathbb{R}^{D_{\text{ff}} \times D}$, $\mathbf{b}_2 \in \mathbb{R}^D$, and $\mathbf{1} \in \mathbb{R}^{L^2}$ (column of ones). Then,

$$H^{(\ell)} = \text{LayerNorm} \left(\mathbf{U} + \text{Dropout}(\widehat{U}) \right). \quad (\text{A44})$$

Eq. (A43) is labeled as FFN in Fig. 2.

2. SIREN with Custom Loss Function

Alternatively, rather than learning a map from a random initial n-RDM to a final n-RDM, we may treat the task purely as interpolation: we learn a continuous function Φ (the interpolant) represented by a NN that takes momentum–space coordinates \mathbf{k} (or normalized coordinates $\mathbf{v} \in [-1, 1]^2$, see Eq. (A46)) as input, and outputs a matrix $O^q(\mathbf{k}_i)$ representing the n-RDM, e.g. $\Phi(\mathbf{k}) \approx O_{\alpha\alpha'}^q(\mathbf{k})$ (or $\text{Re}/\text{Im } O_{\alpha\alpha'}^q(\mathbf{k})$ when training the real/imaginary parts separately). The explicit structure is in Sec. A 2 c. One way to achieve this interpolation is the SIREN architecture. In the following, we will discuss it using the example of fixed- q 1-RDM that only depends on one \mathbf{k} . Nevertheless, the discussion holds for a matrix that depends on more than one Bloch momenta, as shown in Sec. B.

a. physical set-up

We keep the BZ discretization of Eq. (A2). All n -RDM are defined as in Sec. A 1 a. As discussed in Sec. A 1 a, we focus on considering the fixed- q 1-RDMs ($O_{\mathbf{k},\alpha\alpha'}^q$) over BZ with a shape of $L \times L \times \xi \times \xi$. The overall goal of the SIREN [97] approach is to train one continuous function $\Phi(k_x, k_y)$ that predicts each 1-RDM block over the BZ. In particular, we train a function $\Phi(k_x, k_y)$ per (α, α') and per real/imaginary part of $O_{\mathbf{k},\alpha\alpha'}^q$, if needed, such that

$$\Phi(\mathbf{k}) \approx \text{Re} \left[O_{\mathbf{k},\alpha\alpha'}^q \right] \quad \text{or} \quad \text{Im} \left[O_{\mathbf{k},\alpha\alpha'}^q \right]. \quad (\text{A45})$$

(In practice, both the Hubbard (Sec. D) and the Richardson (Sec. B) model exhibit a vanishing imaginary part, so we only consider the real part for training in those cases.) Stacking all different Φ for all different values of (α, α') reconstructs $O^q(\mathbf{k})$. We will train on smaller BZ grids, and then evaluate Φ on denser BZ grids.

b. NN input

For an $L \times L$ BZ with \mathbf{k}_i from Eq. (A2), we define the normalized coordinate

$$\mathbf{v}(\mathbf{k}) \equiv \left(2 \frac{\ell_1}{L} - 1, 2 \frac{\ell_2}{L} - 1 \right) \in [-1, 1]^2, \quad \text{for } \mathbf{k} = \frac{\ell_1}{L} \mathbf{b}_1 + \frac{\ell_2}{L} \mathbf{b}_2. \quad (\text{A46})$$

For each fixed (α, α') , evaluate $\text{Re}[O^q(\mathbf{k})]$ and $\text{Im}[O^q(\mathbf{k})]$ for all \mathbf{k} . To enforce periodicity at the boundaries, extend each to a wrapped array

$$\text{Re}[\tilde{O}^q], \text{Im}[\tilde{O}^q] \in \mathbb{R}^{(L+1) \times (L+1)} \quad (\text{A47})$$

by repeating the first row and column:

$$\tilde{O}_{m,n}^q \equiv O_{m \bmod L, n \bmod L}^q, \quad m, n \in \{0, 1, \dots, L\} \quad (\text{A48})$$

So \tilde{O}^q is just O^q with its first row/column copied to the end—this “closes” the matrix at finite L .

c. SIREN architecture

Given input to our NN in the form of Eq. (A46), we build one SIREN [97] (depicted in Fig. 3) to predict each block of the 1-RDM respectively (e.g., $\text{Re}[O(\mathbf{k})]$ or $\text{Im}[O(\mathbf{k})]$). Each SIREN has 4 hidden sine layers: $\mathbf{h}_1, \mathbf{h}_2, \mathbf{h}_3, \mathbf{h}_4$, followed by a final linear layer. Explicitly,

$$\begin{aligned} \mathbf{h}_1(\mathbf{v}) &= \sin(6(W_1 \mathbf{v} + \mathbf{b}_1)) \in \mathbb{R}^{d_H}, \\ \mathbf{h}_2(\mathbf{v}) &= \sin(30(W_2 \mathbf{h}_1(\mathbf{v}) + \mathbf{b}_2)) \in \mathbb{R}^{d_H}, \\ \mathbf{h}_3(\mathbf{v}) &= \sin(30(W_3 \mathbf{h}_2(\mathbf{v}) + \mathbf{b}_3)) \in \mathbb{R}^{d_H}, \\ \mathbf{h}_4(\mathbf{v}) &= \sin(30(W_4 \mathbf{h}_3(\mathbf{v}) + \mathbf{b}_4)) \in \mathbb{R}^{d_H}, \\ \Phi_\theta(\mathbf{v}) &= \mathbf{w}^\top \mathbf{h}_4(\mathbf{v}) + b_{\text{out}} \in \mathbb{R}. \end{aligned} \quad (\text{A49})$$

where

$$\mathbf{v} \in \mathbb{R}^2, \quad W_1 \in \mathbb{R}^{d_H \times 2}, W_2, W_3, W_4 \in \mathbb{R}^{d_H \times d_H}, \mathbf{b}_1, \mathbf{b}_2, \mathbf{b}_3, \mathbf{b}_4 \in \mathbb{R}^{d_H}, \mathbf{w} \in \mathbb{R}^{d_H}, b_{\text{out}} \in \mathbb{R}. \quad (\text{A50})$$

Eq. (A49) maps a BZ coordinate from Eq. (A46), $\mathbf{v} = (v_x, v_y) \in [-1, 1]^2$, to a scalar $\Phi_\theta(\mathbf{v}) \in \mathbb{R}$ that predicts the corresponding element of either $\text{Re}[O^q(\mathbf{k}_i)]$ or $\text{Im}[O^q(\mathbf{k}_i)]$. The layer widths are: $d_0 = 2$ for the input vector \mathbf{v} (from Eq. (A46)), and $d_1 = d_2 = d_3 = d_4 = d_H$ for the hidden layers ($h_{1,2,3,4}$ in Eq. (A49)) for which we usually select $d_H \in [256, 800]$. We choose sines because they naturally model smooth, periodic patterns across the BZ. Additionally, to keep gradients healthy, we incorporate a special weight initialization scheme [97]: define $W \sim \mathcal{U}(a, b)$ to mean “sample uniformly at random between a and b .” Here $W \sim \mathcal{U}$ denotes element-wise initialization: each entry W_{ij} is drawn independently from $\mathcal{U}(a, b)$. Then we initialize the weights in Eq. (A49) with:

$$W_1 \sim \mathcal{U}\left(-\frac{1}{d_0}, \frac{1}{d_0}\right), \quad \text{and } w^\top, W_\ell \sim \mathcal{U}\left(-\frac{\sqrt{6/d_H}}{30}, \frac{\sqrt{6/d_H}}{30}\right) \text{ elementwise, } \quad 2 \leq \ell \leq 4. \quad (\text{A51})$$

The full model can then be written as Φ_θ , where θ represents all the tunable parameters mentioned above.

d. Datasets, standardization, and evaluation grids

For $\text{Re}[\tilde{O}^q] \in \mathbb{R}^{(L+1) \times (L+1)}$ defined in Eq. (A47), we compute the mean and standard deviation over all entries:

$$\mu = \text{mean}(\text{Re}[\tilde{O}^q]), \quad \sigma = \text{std}(\text{Re}[\tilde{O}^q]), \quad (\text{A52})$$

and form the standardized version of \tilde{O}^q :

$$Z_L \equiv \frac{\text{Re}[\tilde{O}^q] - \mu}{\sigma} \in \mathbb{R}^{(L+1) \times (L+1)}. \quad (\text{A53})$$

A similar standardization procedure applies for $\text{Im}[\tilde{O}^q]$. For evaluation on larger L , we use the same μ and σ (computed from the O^q used for training) to normalize the data. Also notice that the unstandardized SIREN predictions for the target channel can be recovered after training by reversing Eq. (A53). Each input point is a normalized BZ coordinate $\nu \in [-1, 1]^2$ (see Eq. (A46)). Define the coordinate grid $X_L \equiv \{\mathbf{v}(\mathbf{k}_{ij}) : i, j = 0, \dots, L\} \subset [-1, 1]^{(L+1) \times (L+1) \times 2}$, $\mathbf{k}_{ij} \equiv \frac{i}{L}\mathbf{b}_1 + \frac{j}{L}\mathbf{b}_2$. Our training data thus consists of the set of input coordinates $X_L \in [-1, 1]^{(L+1) \times (L+1) \times 2}$ and the normalized values Z_L .

When calculating the loss, we also evaluate SIREN on a $L' \times L'$ mesh with $L' > L$ and output $Z_{L'} \in [-1, 1]^{(L'+1) \times (L'+1) \times 2}$, as seen in Sec. A2e. However, we will eventually downsample the $Z_{L'}$ back to $L \times L$ mesh to compare to the training data. In this process, we do *not* use any true final RDMs on the $L' \times L'$ mesh as training data, since doing so would defeat our entire purpose of generalizing to larger system sizes.

e. Loss function

Define $\Phi_\theta : [-1, 1]^2 \rightarrow \mathbb{R}$ to be the SIREN we constructed in Sec. A2c with tunable parameters denoted as θ , which takes a normalized BZ coordinate $\mathbf{v}(\mathbf{k}) \in [-1, 1]^2$ as input and outputs a scalar prediction for the corresponding element of the chosen 1-RDM block:

$$\hat{Z}(\mathbf{k}) \equiv \Phi_\theta(\mathbf{v}(\mathbf{k})), \quad (\text{A54})$$

For small-mesh MSE,

$$\mathcal{L}_{\text{small}}(\theta) = \frac{1}{(L+1)^2} \sum_{\mathbf{v} \in X_L} \left(\hat{Z}(X_L)[\mathbf{v}] - Z_L[\mathbf{v}] \right)^2. \quad (\text{A55})$$

Let G be any finite symmetry subgroup of the symmetry group of the system acting on normalized BZ coordinates $\mathbf{v} \in [-1, 1]^2$ (e.g., rotations/reflections of the square). Define the symmetrization operator S_G by averaging over the group action. For example, for a square lattice we take $G = D_4$ (order 8, consisting of four rotations $0^\circ, 90^\circ, 180^\circ, 270^\circ$ and four reflections across the two axes and two diagonals). Let ζ be a fixed downsampler (e.g. bilinear or bicubic interpolation [136, 137]), which is effectively a classical algorithm used to interpolate the SIREN predictions on the denser coordinate mesh $X_{L'}$ back to the training system size. This allows us to control behavior at finer scales, without the need for additional training data (e.g. $Z_{L'}$) from the larger system. As such, we evaluate the SIREN on the dense grid $X_{L'}$, symmetrize, and then downsample back down to X_L :

$$\hat{Z}^\downarrow(X_L) \equiv \zeta(S_G[\hat{Z}(X_{L'})] \rightarrow X_L), \quad (\text{A56})$$

$$\mathcal{L}_{\text{cons}}(\theta) = \frac{1}{(L+1)^2} \sum_{\mathbf{v} \in X_L} \left(\hat{Z}^\downarrow(X_L)[\mathbf{v}] - Z_L[\mathbf{v}] \right)^2. \quad (\text{A57})$$

(Note that for the Richardson model in Sec. B2, we employ a slightly different technique to learn the symmetry group during training; see Eq. (B134) for details.) Randomly sample N points $U = \{u_i\}_{i=1}^N \subset [-1, 1]^2$. With ∇_u the gradient and Hess_u the Hessian w.r.t. u , and with $\|\cdot\|_1$ the ℓ^1 norm and $\|\cdot\|_F$ the Frobenius norm:

$$\mathcal{P}_{\text{TV}}(\theta) \equiv \frac{1}{N} \sum_{i=1}^N \|\nabla_u \Phi_\theta(u_i)\|_1, \quad \mathcal{P}_{\text{FH}}(\theta) \equiv \frac{1}{N} \sum_{i=1}^N \|\text{Hess}_u \Phi_\theta(u_i)\|_F. \quad (\text{A58})$$

The total loss is:

$$\mathcal{L}(\theta) = \mathcal{L}_{\text{small}}(\theta) + \mathcal{L}_{\text{cons}}(\theta) + \lambda \mathcal{P}(\theta), \quad \mathcal{P} \in \{\mathcal{P}_{\text{TV}}, \mathcal{P}_{\text{FH}}, 0\}, \quad (\text{A59})$$

with $\lambda \in [10^{-7}, 10^{-5}]$ in practice. We then take the gradient of \mathcal{L} w.r.t. θ and train the SIREN using the Adam optimizer [138]. For all trainings using a SIREN-based NN in this paper, we set the constant learning rate for the optimizer equal to 1×10^{-4} .

Appendix B: Richardson Model

1. Model Formulation

We start by reviewing the Richardson model for superconductivity [104–106].

a. Analytic Solution via the Richardson Equations

We begin with deriving the Richardson model for spinful fermions on a Bravais lattice with one atom per unit cell. We label the hopping by $t_{\mathbf{r}\mathbf{r}'}$ and introduce an attraction $V(\mathbf{r} - \mathbf{r}') \leq 0$ that depends only on separation $\mathbf{r} - \mathbf{r}'$ [139]:

$$H = \sum_{\mathbf{r}, \mathbf{r}', s} t_{\mathbf{r}\mathbf{r}'} c_{\mathbf{r}s}^\dagger c_{\mathbf{r}'s} + \frac{1}{2} \sum_{\mathbf{r}, \mathbf{r}'} V(\mathbf{r} - \mathbf{r}') c_{\mathbf{r}\uparrow}^\dagger c_{\mathbf{r}'\downarrow}^\dagger c_{\mathbf{r}'\downarrow} c_{\mathbf{r}\uparrow}, \quad (\text{B1})$$

Introduce lattice Fourier modes

$$c_{\mathbf{r},s} = \frac{1}{L} \sum_{\mathbf{k} \in \text{BZ}} e^{i\mathbf{k} \cdot \mathbf{r}} c_{\mathbf{k},s}, \quad c_{\mathbf{k},s} = \frac{1}{L} \sum_{\mathbf{r}} e^{-i\mathbf{k} \cdot \mathbf{r}} c_{\mathbf{r},s}, \quad \sum_{\mathbf{r}} e^{i(\mathbf{k} - \mathbf{k}') \cdot \mathbf{r}} = L^2 \delta_{\mathbf{k}, \mathbf{k}'}. \quad (\text{B2})$$

so that the kinetic term diagonalizes as

$$H_0 = \sum_{\mathbf{r}, \mathbf{r}', s} t_{\mathbf{r}-\mathbf{r}'} c_{\mathbf{r}s}^\dagger c_{\mathbf{r}'s} \quad (\text{B3})$$

$$= \sum_{\mathbf{r}, \mathbf{r}', s} t_{\mathbf{r}-\mathbf{r}'} \left[\frac{1}{L} \sum_{\mathbf{k}} e^{-i\mathbf{k} \cdot \mathbf{r}} c_{\mathbf{k}s}^\dagger \right] \left[\frac{1}{L} \sum_{\mathbf{k}'} e^{i\mathbf{k}' \cdot \mathbf{r}'} c_{\mathbf{k}'s} \right] \quad (\text{B4})$$

$$= \frac{1}{L^2} \sum_{\mathbf{k}, \mathbf{k}', s} \left[\sum_{\mathbf{r}, \mathbf{r}'} t_{\mathbf{r}-\mathbf{r}'} e^{-i\mathbf{k} \cdot \mathbf{r}} e^{i\mathbf{k}' \cdot \mathbf{r}'} \right] c_{\mathbf{k}s}^\dagger c_{\mathbf{k}'s} \quad (\text{B5})$$

$$= \frac{1}{L^2} \sum_{\mathbf{k}, \mathbf{k}', s} \left[\sum_{\mathbf{r}-\mathbf{r}'} t_{\mathbf{r}-\mathbf{r}'} \sum_{\mathbf{r}'} e^{-i\mathbf{k} \cdot (\mathbf{r}' + (\mathbf{r} - \mathbf{r}'))} e^{i\mathbf{k}' \cdot \mathbf{r}'} \right] c_{\mathbf{k}s}^\dagger c_{\mathbf{k}'s} \quad (\text{B6})$$

$$= \frac{1}{L^2} \sum_{\mathbf{k}, \mathbf{k}', s} \left[\sum_{\mathbf{r}-\mathbf{r}'} t_{\mathbf{r}-\mathbf{r}'} e^{-i\mathbf{k} \cdot (\mathbf{r} - \mathbf{r}')} \right] \left[\sum_{\mathbf{r}'} e^{i(\mathbf{k}' - \mathbf{k}) \cdot \mathbf{r}'} \right] c_{\mathbf{k}s}^\dagger c_{\mathbf{k}'s} \quad (\text{B7})$$

$$= \sum_{\mathbf{k}, s} \underbrace{\left[\sum_{\mathbf{r}-\mathbf{r}'} t_{\mathbf{r}-\mathbf{r}'} e^{i\mathbf{k} \cdot (\mathbf{r} - \mathbf{r}')} \right]}_{\varepsilon_{\mathbf{k}}} c_{\mathbf{k}s}^\dagger c_{\mathbf{k}s} \quad \left(\sum_{\mathbf{r}'} e^{i(\mathbf{k}' - \mathbf{k}) \cdot \mathbf{r}'} = L^2 \delta_{\mathbf{k}, \mathbf{k}'} \right) \quad (\text{B8})$$

$$= \sum_{\mathbf{k}, s} \varepsilon_{\mathbf{k}} c_{\mathbf{k}s}^\dagger c_{\mathbf{k}s}, \quad (\text{B9})$$

The interaction becomes a pair-pair scattering in momentum space,

$$H_{\text{int}} = \frac{1}{2} \sum_{\mathbf{r}, \mathbf{r}'} V(\mathbf{r} - \mathbf{r}') c_{\mathbf{r}\uparrow}^\dagger c_{\mathbf{r}'\downarrow}^\dagger c_{\mathbf{r}'\downarrow} c_{\mathbf{r}\uparrow} \quad (\text{B10})$$

$$= \frac{1}{2} \sum_{\mathbf{r}, \mathbf{r}'} V(\mathbf{r} - \mathbf{r}') \left[\frac{1}{L} \sum_{\mathbf{k}} e^{-i\mathbf{k} \cdot \mathbf{r}} c_{\mathbf{k}\uparrow}^\dagger \right] \left[\frac{1}{L} \sum_{\mathbf{p}} e^{-i\mathbf{p} \cdot \mathbf{r}'} c_{\mathbf{p}\downarrow}^\dagger \right] \left[\frac{1}{L} \sum_{\mathbf{p}'} e^{i\mathbf{p}' \cdot \mathbf{r}'} c_{\mathbf{p}'\downarrow} \right] \left[\frac{1}{L} \sum_{\mathbf{k}'} e^{i\mathbf{k}' \cdot \mathbf{r}} c_{\mathbf{k}'\uparrow} \right] \quad (\text{B11})$$

$$= \frac{1}{2L^4} \sum_{\mathbf{k}, \mathbf{k}', \mathbf{p}, \mathbf{p}'} \left[\sum_{\mathbf{r}, \mathbf{r}'} V(\mathbf{r} - \mathbf{r}') e^{-i\mathbf{k} \cdot \mathbf{r}} e^{-i\mathbf{p} \cdot \mathbf{r}'} e^{i\mathbf{p}' \cdot \mathbf{r}'} e^{i\mathbf{k}' \cdot \mathbf{r}} \right] c_{\mathbf{k}\uparrow}^\dagger c_{\mathbf{p}\downarrow}^\dagger c_{\mathbf{p}'\downarrow} c_{\mathbf{k}'\uparrow} \quad (\text{B12})$$

$$= \frac{1}{2L^4} \sum_{\mathbf{k}, \mathbf{k}', \mathbf{p}, \mathbf{p}'} \left[\sum_{\mathbf{r}-\mathbf{r}'} V(\mathbf{r} - \mathbf{r}') \sum_{\mathbf{r}'} e^{-i\mathbf{k} \cdot (\mathbf{r}' + (\mathbf{r} - \mathbf{r}'))} e^{-i\mathbf{p} \cdot \mathbf{r}'} e^{i\mathbf{p}' \cdot \mathbf{r}'} e^{i\mathbf{k}' \cdot (\mathbf{r}' + (\mathbf{r} - \mathbf{r}'))} \right] c_{\mathbf{k}\uparrow}^\dagger c_{\mathbf{p}\downarrow}^\dagger c_{\mathbf{p}'\downarrow} c_{\mathbf{k}'\uparrow} \quad (\text{B13})$$

$$= \frac{1}{2L^4} \sum_{\mathbf{k}, \mathbf{k}', \mathbf{p}, \mathbf{p}'} \left[\sum_{\mathbf{r}-\mathbf{r}'} V(\mathbf{r} - \mathbf{r}') \sum_{\mathbf{r}'} e^{i(\mathbf{k}' - \mathbf{k}) \cdot (\mathbf{r} - \mathbf{r}')} e^{-i\mathbf{k} \cdot \mathbf{r}'} e^{i\mathbf{k}' \cdot \mathbf{r}'} e^{-i\mathbf{p} \cdot \mathbf{r}'} e^{i\mathbf{p}' \cdot \mathbf{r}'} \right] c_{\mathbf{k}\uparrow}^\dagger c_{\mathbf{p}\downarrow}^\dagger c_{\mathbf{p}'\downarrow} c_{\mathbf{k}'\uparrow} \quad (\text{B14})$$

$$= \frac{1}{2L^2} \sum_{\mathbf{k}, \mathbf{k}', \mathbf{p}, \mathbf{p}'} \left[\sum_{\mathbf{r}-\mathbf{r}'} V(\mathbf{r} - \mathbf{r}') e^{i(\mathbf{k}' - \mathbf{k}) \cdot (\mathbf{r} - \mathbf{r}')} \right] \delta_{\mathbf{k} + \mathbf{p}, \mathbf{k}' + \mathbf{p}'} c_{\mathbf{k}\uparrow}^\dagger c_{\mathbf{p}\downarrow}^\dagger c_{\mathbf{p}'\downarrow} c_{\mathbf{k}'\uparrow} \quad (\text{B15})$$

Define

$$V(\mathbf{q}) \equiv \sum_{\mathbf{r}-\mathbf{r}'} V(\mathbf{r} - \mathbf{r}') e^{i\mathbf{q} \cdot (\mathbf{r} - \mathbf{r}')}, \quad \mathbf{q} \equiv \mathbf{k}' - \mathbf{k} \quad (\text{B16})$$

and use $\mathbf{p}' = \mathbf{k} + \mathbf{p} - \mathbf{k}'$ from the Kronecker delta to obtain,

$$H_{\text{int}} = \frac{1}{2L^2} \sum_{\mathbf{k}, \mathbf{p}, \mathbf{q}} V(\mathbf{q}) c_{\mathbf{k}\uparrow}^\dagger c_{\mathbf{p}\downarrow}^\dagger c_{\mathbf{p}-\mathbf{q},\downarrow} c_{\mathbf{k}+\mathbf{q},\uparrow}. \quad (\text{B17})$$

To obtain the Richardson model from Eq. (B1), we select the subspace of time-reversed pairs with the following constraints:

$$\mathbf{k} + \mathbf{p} = \mathbf{0}, \quad \mathbf{k}' + \mathbf{p}' = \mathbf{0} \iff \mathbf{p} = -\mathbf{k}, \quad \mathbf{p}' = -\mathbf{k}'. \quad (\text{B18})$$

where \mathbf{k} and \mathbf{p} are the crystal momenta of the two electrons that form a pair, we set their total momentum to be zero:

$$H_{\text{int}}^{\text{red}} = \frac{1}{2L^2} \sum_{\mathbf{k}, \mathbf{k}'} V(\mathbf{k}' - \mathbf{k}) c_{\mathbf{k}\uparrow}^\dagger c_{-\mathbf{k}\downarrow}^\dagger c_{-\mathbf{k}'\downarrow} c_{\mathbf{k}'\uparrow} = \frac{1}{2L^2} \sum_{\mathbf{k}, \mathbf{k}'} V(\mathbf{k}' - \mathbf{k}) A_{\mathbf{k}}^\dagger A_{\mathbf{k}'}, \quad (\text{B19})$$

with

$$A_{\mathbf{k}}^\dagger \equiv c_{\mathbf{k}\uparrow}^\dagger c_{-\mathbf{k}\downarrow}^\dagger, \quad \text{and} \quad A_{\mathbf{k}} \equiv c_{-\mathbf{k}\downarrow} c_{\mathbf{k}\uparrow}. \quad (\text{B20})$$

Therefore, the Richardson model is

$$H = \sum_{\mathbf{k}, s} \varepsilon_{\mathbf{k}} c_{\mathbf{k}s}^\dagger c_{\mathbf{k}s} + g \left(\sum_{\mathbf{k}} A_{\mathbf{k}}^\dagger \right) \left(\sum_{\mathbf{k}'} A_{\mathbf{k}'} \right), \quad (\text{B21})$$

where $u = \frac{1}{2}V(\mathbf{k}' - \mathbf{k})$ and $g = u/L^2$ with $g < 0$ denoting attractive pairing, and we choose $\varepsilon_{-\mathbf{k}} = \varepsilon_{\mathbf{k}}$. Define $N_{\mathbf{k}} \equiv n_{\mathbf{k}\uparrow} + n_{-\mathbf{k}\downarrow} = c_{\mathbf{k}\uparrow}^\dagger c_{\mathbf{k}\uparrow} + c_{-\mathbf{k}\downarrow}^\dagger c_{-\mathbf{k}\downarrow}$. The quasi-spin algebra reads

$$[A_{\mathbf{k}}, A_{\mathbf{p}}^\dagger] = \delta_{\mathbf{k}\mathbf{p}} (1 - N_{\mathbf{k}}), \quad [N_{\mathbf{k}}, A_{\mathbf{p}}^\dagger] = 2\delta_{\mathbf{k}\mathbf{p}} A_{\mathbf{k}}^\dagger, \quad [A_{\mathbf{k}}^\dagger, A_{\mathbf{p}}^\dagger] = 0. \quad (\text{B22})$$

In the seniority-zero (all particles paired) sector with M pairs, eigenstates take the factorized form [106],

$$|\Psi_{2M}\rangle = \prod_{\alpha=1}^M B_{\alpha}^\dagger |0\rangle, \quad B_{\alpha}^\dagger = \sum_{\mathbf{k}} \frac{A_{\mathbf{k}}^\dagger}{2\varepsilon_{\mathbf{k}} - E_{\alpha}}, \quad (\text{B23})$$

where the unknown ‘‘rapidities’’ $\{E_{\alpha}\}_{\alpha=1}^M$ are determined by the eigenequation. Demanding $H|\Psi_{2M}\rangle = E|\Psi_{2M}\rangle$ and using Eq. (B22) yields the set of coupled equations

$$\frac{1}{g} + \sum_{\mathbf{k}} \frac{1}{2\varepsilon_{\mathbf{k}} - E_{\alpha}} - 2 \sum_{\beta(\neq\alpha)} \frac{1}{E_{\beta} - E_{\alpha}} = 0, \quad \alpha = 1, \dots, M \quad (\text{B24})$$

and the total many-body energy

$$E = \sum_{\alpha=1}^M E_{\alpha}. \quad (\text{B25})$$

Here, we will derive Eq. (B24) explicitly. Use $\{c_i, c_j^\dagger\} = \delta_{ij}$ and $\{c_i, c_j\} = \{c_i^\dagger, c_j^\dagger\} = 0$, we can show Eq. (B22):

$$\begin{aligned} [A_{\mathbf{k}}, A_{\mathbf{k}}^\dagger] &= A_{\mathbf{k}} A_{\mathbf{k}}^\dagger - A_{\mathbf{k}}^\dagger A_{\mathbf{k}} = c_{-\mathbf{k}\downarrow} c_{\mathbf{k}\uparrow} c_{\mathbf{k}\uparrow}^\dagger c_{-\mathbf{k}\downarrow}^\dagger - c_{\mathbf{k}\uparrow}^\dagger c_{-\mathbf{k}\downarrow}^\dagger c_{-\mathbf{k}\downarrow} c_{\mathbf{k}\uparrow} = c_{-\mathbf{k}\downarrow} (1 - c_{\mathbf{k}\uparrow}^\dagger c_{\mathbf{k}\uparrow}) c_{-\mathbf{k}\downarrow}^\dagger - c_{\mathbf{k}\uparrow}^\dagger (c_{-\mathbf{k}\downarrow}^\dagger c_{-\mathbf{k}\downarrow}) c_{\mathbf{k}\uparrow} \\ &= c_{-\mathbf{k}\downarrow} c_{-\mathbf{k}\downarrow}^\dagger - c_{-\mathbf{k}\downarrow} c_{\mathbf{k}\uparrow}^\dagger c_{\mathbf{k}\uparrow} c_{-\mathbf{k}\downarrow}^\dagger - c_{\mathbf{k}\uparrow}^\dagger c_{-\mathbf{k}\downarrow}^\dagger c_{-\mathbf{k}\downarrow} c_{\mathbf{k}\uparrow} = (1 - c_{-\mathbf{k}\downarrow}^\dagger c_{-\mathbf{k}\downarrow}) - c_{\mathbf{k}\uparrow}^\dagger c_{\mathbf{k}\uparrow} (1 - c_{-\mathbf{k}\downarrow}^\dagger c_{-\mathbf{k}\downarrow}) - c_{\mathbf{k}\uparrow}^\dagger c_{-\mathbf{k}\downarrow}^\dagger c_{-\mathbf{k}\downarrow} c_{\mathbf{k}\uparrow} \\ &= 1 - n_{-\mathbf{k}\downarrow} - n_{\mathbf{k}\uparrow} + n_{\mathbf{k}\uparrow} n_{-\mathbf{k}\downarrow} - n_{\mathbf{k}\uparrow} n_{-\mathbf{k}\downarrow} = 1 - n_{\mathbf{k}\uparrow} - n_{-\mathbf{k}\downarrow} = 1 - N_{\mathbf{k}}; \end{aligned} \quad (\text{B26})$$

$$[A_{\mathbf{k}}, A_{\mathbf{q}}^\dagger] = c_{-\mathbf{k}\downarrow} c_{\mathbf{k}\uparrow} c_{\mathbf{q}\uparrow}^\dagger c_{-\mathbf{q}\downarrow}^\dagger - c_{\mathbf{q}\uparrow}^\dagger c_{-\mathbf{q}\downarrow}^\dagger c_{-\mathbf{k}\downarrow} c_{\mathbf{k}\uparrow} = c_{-\mathbf{k}\downarrow} c_{\mathbf{k}\uparrow} c_{\mathbf{q}\uparrow}^\dagger c_{-\mathbf{q}\downarrow}^\dagger - c_{-\mathbf{k}\downarrow} c_{\mathbf{k}\uparrow} c_{\mathbf{q}\uparrow}^\dagger c_{-\mathbf{q}\downarrow}^\dagger = 0 \quad (\mathbf{k} \neq \mathbf{q}); \quad (\text{B27})$$

$$[N_{\mathbf{k}}, A_{\mathbf{p}}^\dagger] = [n_{\mathbf{k}\uparrow} + n_{-\mathbf{k}\downarrow}, c_{\mathbf{p}\uparrow}^\dagger c_{-\mathbf{p}\downarrow}^\dagger] = [n_{\mathbf{k}\uparrow}, c_{\mathbf{p}\uparrow}^\dagger c_{-\mathbf{p}\downarrow}^\dagger] + [n_{-\mathbf{k}\downarrow}, c_{\mathbf{p}\uparrow}^\dagger c_{-\mathbf{p}\downarrow}^\dagger]$$

$$\begin{aligned}
&= [n_{\mathbf{k}\uparrow}, c_{\mathbf{p}\uparrow}^\dagger] c_{-\mathbf{p}\downarrow}^\dagger + c_{\mathbf{p}\uparrow}^\dagger [n_{\mathbf{k}\uparrow}, c_{-\mathbf{p}\downarrow}^\dagger] + [n_{-\mathbf{k}\downarrow}, c_{\mathbf{p}\uparrow}^\dagger] c_{-\mathbf{p}\downarrow}^\dagger + c_{\mathbf{p}\uparrow}^\dagger [n_{-\mathbf{k}\downarrow}, c_{-\mathbf{p}\downarrow}^\dagger] \\
&= [n_{\mathbf{k}\uparrow}, c_{\mathbf{p}\uparrow}^\dagger] c_{-\mathbf{p}\downarrow}^\dagger + c_{\mathbf{p}\uparrow}^\dagger [n_{-\mathbf{k}\downarrow}, c_{-\mathbf{p}\downarrow}^\dagger] \quad (\text{two terms vanish}) \\
&= \delta_{\mathbf{k}\mathbf{p}} c_{\mathbf{p}\uparrow}^\dagger c_{-\mathbf{p}\downarrow}^\dagger + \delta_{-\mathbf{k}, -\mathbf{p}} c_{\mathbf{p}\uparrow}^\dagger c_{-\mathbf{p}\downarrow}^\dagger \quad (\text{since } [n_i, c_j^\dagger] = \delta_{ij} c_j^\dagger) \\
&= (\delta_{\mathbf{k}\mathbf{p}} + \delta_{\mathbf{k}\mathbf{p}}) c_{\mathbf{p}\uparrow}^\dagger c_{-\mathbf{p}\downarrow}^\dagger = 2\delta_{\mathbf{k}\mathbf{p}} A_{\mathbf{p}}^\dagger = 2\delta_{\mathbf{k}\mathbf{p}} A_{\mathbf{k}}^\dagger;
\end{aligned} \tag{B28}$$

$$[A_{\mathbf{k}}^\dagger, A_{\mathbf{p}}^\dagger] = c_{\mathbf{k}\uparrow}^\dagger c_{-\mathbf{k}\downarrow}^\dagger c_{\mathbf{p}\uparrow}^\dagger c_{-\mathbf{p}\downarrow}^\dagger - c_{\mathbf{p}\uparrow}^\dagger c_{-\mathbf{p}\downarrow}^\dagger c_{\mathbf{k}\uparrow}^\dagger c_{-\mathbf{k}\downarrow}^\dagger = 0. \tag{B29}$$

We introduce the shorthand for Eq. (B23)

$$\phi_\alpha(\mathbf{k}) \equiv \frac{1}{2\varepsilon_{\mathbf{k}} - E_\alpha}. \tag{B30}$$

Thus $B_\alpha^\dagger = \sum_{\mathbf{k}} \phi_\alpha(\mathbf{k}) A_{\mathbf{k}}^\dagger$. For later convenience define the collective pair operators

$$A^\dagger \equiv \sum_{\mathbf{k}} A_{\mathbf{k}}^\dagger, \quad K_\alpha \equiv \sum_{\mathbf{k}} \phi_\alpha(\mathbf{k}) (1 - N_{\mathbf{k}}), \tag{B31}$$

i.e. K_α is obtained from B_α^\dagger expression by replacing $A_{\mathbf{k}}^\dagger$ with $(1 - N_{\mathbf{k}})$. We split the Hamiltonian as

$$H = H_0 + V, \quad H_0 = \sum_{\mathbf{k}, s} \varepsilon_{\mathbf{k}} c_{\mathbf{k}s}^\dagger c_{\mathbf{k}s}, \quad V = g \sum_{\mathbf{k}, \mathbf{k}'} A_{\mathbf{k}}^\dagger A_{\mathbf{k}'} = g A^\dagger A. \tag{B32}$$

Evaluate the following commutators using Eq. (B22):

$$[H_0, A_{\mathbf{p}}^\dagger] = \left[\sum_{\mathbf{k}} \varepsilon_{\mathbf{k}} N_{\mathbf{k}}, A_{\mathbf{p}}^\dagger \right] = \sum_{\mathbf{k}} \varepsilon_{\mathbf{k}} [N_{\mathbf{k}}, A_{\mathbf{p}}^\dagger] = \sum_{\mathbf{k}} \varepsilon_{\mathbf{k}} 2\delta_{\mathbf{k}\mathbf{p}} A_{\mathbf{k}}^\dagger = 2\varepsilon_{\mathbf{p}} A_{\mathbf{p}}^\dagger. \tag{B33}$$

$$[V, A_{\mathbf{p}}^\dagger] = g \sum_{\mathbf{k}, \mathbf{k}'} A_{\mathbf{k}}^\dagger [A_{\mathbf{k}'}, A_{\mathbf{p}}^\dagger] = g \sum_{\mathbf{k}} A_{\mathbf{k}}^\dagger (1 - N_{\mathbf{p}}) = g A^\dagger (1 - N_{\mathbf{p}}) \tag{B34}$$

Combine them:

$$[H, A_{\mathbf{p}}^\dagger] = 2\varepsilon_{\mathbf{p}} A_{\mathbf{p}}^\dagger + g A^\dagger (1 - N_{\mathbf{p}}). \tag{B35}$$

Using Eq. (B23),

$$[H, B_\alpha^\dagger] = \sum_{\mathbf{p}} \phi_\alpha(\mathbf{p}) [H, A_{\mathbf{p}}^\dagger] = \sum_{\mathbf{p}} \phi_\alpha(\mathbf{p}) 2\varepsilon_{\mathbf{p}} A_{\mathbf{p}}^\dagger + g A^\dagger \sum_{\mathbf{p}} \phi_\alpha(\mathbf{p}) (1 - N_{\mathbf{p}}) \tag{B36}$$

We have the identity

$$\frac{2\varepsilon_{\mathbf{p}}}{2\varepsilon_{\mathbf{p}} - E_\alpha} = \frac{(2\varepsilon_{\mathbf{p}} - E_\alpha) + E_\alpha}{2\varepsilon_{\mathbf{p}} - E_\alpha} = 1 + \frac{E_\alpha}{2\varepsilon_{\mathbf{p}} - E_\alpha} \tag{B37}$$

Hence the first sum becomes

$$\sum_{\mathbf{p}} \phi_\alpha(\mathbf{p}) 2\varepsilon_{\mathbf{p}} A_{\mathbf{p}}^\dagger = \sum_{\mathbf{p}} \left[1 + \frac{E_\alpha}{2\varepsilon_{\mathbf{p}} - E_\alpha} \right] A_{\mathbf{p}}^\dagger = A^\dagger + E_\alpha \sum_{\mathbf{p}} \frac{A_{\mathbf{p}}^\dagger}{2\varepsilon_{\mathbf{p}} - E_\alpha} = A^\dagger + E_\alpha B_\alpha^\dagger. \tag{B38}$$

Therefore,

$$[H, B_\alpha^\dagger] = E_\alpha B_\alpha^\dagger + A^\dagger + g A^\dagger K_\alpha, \quad K_\alpha \equiv \sum_{\mathbf{p}} \phi_\alpha(\mathbf{p}) (1 - N_{\mathbf{p}}). \tag{B39}$$

We will need how K_α commutes with B_β^\dagger . Using Eq. (B31) with Eq. (B30),

$$[K_\alpha, B_\beta^\dagger] = \left[\sum_{\mathbf{k}} \phi_\alpha(\mathbf{k}) (1 - N_{\mathbf{k}}), \sum_{\mathbf{p}} \phi_\beta(\mathbf{p}) A_{\mathbf{p}}^\dagger \right] = \sum_{\mathbf{k}, \mathbf{p}} \phi_\alpha(\mathbf{k}) \phi_\beta(\mathbf{p}) [1 - N_{\mathbf{k}}, A_{\mathbf{p}}^\dagger] = \sum_{\mathbf{k}, \mathbf{p}} \phi_\alpha(\mathbf{k}) \phi_\beta(\mathbf{p}) (-2\delta_{\mathbf{k}\mathbf{p}} A_{\mathbf{k}}^\dagger) \tag{B40}$$

$$= -2 \sum_{\mathbf{k}} \phi_{\alpha}(\mathbf{k}) \phi_{\beta}(\mathbf{k}) A_{\mathbf{k}}^{\dagger} = -2 \sum_{\mathbf{k}} \frac{1}{(2\varepsilon_{\mathbf{k}} - E_{\alpha})(2\varepsilon_{\mathbf{k}} - E_{\beta})} A_{\mathbf{k}}^{\dagger}. \quad (\text{B41})$$

Using the identity $\frac{1}{x-a} - \frac{1}{x-b} = \frac{a-b}{(x-a)(x-b)}$ with $x \equiv 2\varepsilon_{\mathbf{k}}$, $a \equiv E_{\alpha}$, $b \equiv E_{\beta}$, we obtain

$$\frac{1}{(2\varepsilon_{\mathbf{k}} - E_{\alpha})(2\varepsilon_{\mathbf{k}} - E_{\beta})} = \frac{1}{E_{\alpha} - E_{\beta}} \left[\frac{1}{2\varepsilon_{\mathbf{k}} - E_{\alpha}} - \frac{1}{2\varepsilon_{\mathbf{k}} - E_{\beta}} \right]. \quad (\text{B42})$$

Multiplying by $A_{\mathbf{k}}^{\dagger}$ and summing over k gives

$$\sum_{\mathbf{k}} \frac{A_{\mathbf{k}}^{\dagger}}{(2\varepsilon_{\mathbf{k}} - E_{\alpha})(2\varepsilon_{\mathbf{k}} - E_{\beta})} = \frac{1}{E_{\alpha} - E_{\beta}} \sum_{\mathbf{k}} \left[\frac{A_{\mathbf{k}}^{\dagger}}{2\varepsilon_{\mathbf{k}} - E_{\alpha}} - \frac{A_{\mathbf{k}}^{\dagger}}{2\varepsilon_{\mathbf{k}} - E_{\beta}} \right] = \frac{1}{E_{\alpha} - E_{\beta}} (B_{\alpha}^{\dagger} - B_{\beta}^{\dagger}) = \frac{B_{\alpha}^{\dagger} - B_{\beta}^{\dagger}}{E_{\alpha} - E_{\beta}}. \quad (\text{B43})$$

Insert it into Eq. (B41):

$$[K_{\alpha}, B_{\beta}^{\dagger}] = -2 \frac{B_{\alpha}^{\dagger} - B_{\beta}^{\dagger}}{E_{\alpha} - E_{\beta}}. \quad (\text{B44})$$

Equivalently, $K_{\alpha} B_{\beta}^{\dagger} = B_{\beta}^{\dagger} K_{\alpha} - 2 \frac{B_{\alpha}^{\dagger} - B_{\beta}^{\dagger}}{E_{\alpha} - E_{\beta}}$. Now act with H on the ansatz state $|\Psi_{2M}\rangle = \prod_{\lambda=1}^M B_{\lambda}^{\dagger} |0\rangle$. Since $H|0\rangle = 0$, the commutator trick gives

$$\begin{aligned} H|\Psi_{2M}\rangle &= H \left(\prod_{\alpha=1}^M B_{\alpha}^{\dagger} \right) |0\rangle = \left([H, \prod_{\alpha=1}^M B_{\alpha}^{\dagger}] + \prod_{\alpha=1}^M B_{\alpha}^{\dagger} H \right) |0\rangle \\ &= [H, \prod_{\alpha=1}^M B_{\alpha}^{\dagger}] |0\rangle \quad (\text{because } H|0\rangle = 0) \\ &= \left(\sum_{\alpha=1}^M \left(\prod_{\gamma < \alpha} B_{\gamma}^{\dagger} \right) [H, B_{\alpha}^{\dagger}] \left(\prod_{\gamma > \alpha} B_{\gamma}^{\dagger} \right) \right) |0\rangle \quad (\text{using } [H, XY] = [H, X]Y + X[H, Y]). \end{aligned} \quad (\text{B45})$$

Insert Eq. (B39),

$$\begin{aligned} H|\Psi_{2M}\rangle &= \sum_{\alpha} \left(\prod_{\gamma < \alpha} B_{\gamma}^{\dagger} \right) (E_{\alpha} B_{\alpha}^{\dagger} + A^{\dagger} + g A^{\dagger} K_{\alpha}) \left(\prod_{\gamma > \alpha} B_{\gamma}^{\dagger} \right) |0\rangle \\ &= \sum_{\alpha} E_{\alpha} \left(\prod_{\gamma} B_{\gamma}^{\dagger} \right) |0\rangle + A^{\dagger} \sum_{\alpha} \left(\prod_{\gamma \neq \alpha} B_{\gamma}^{\dagger} \right) |0\rangle + g A^{\dagger} \sum_{\alpha} \left(\prod_{\gamma < \alpha} B_{\gamma}^{\dagger} \right) K_{\alpha} \left(\prod_{\gamma > \alpha} B_{\gamma}^{\dagger} \right) |0\rangle \\ &= \sum_{\alpha} E_{\alpha} |\Psi_{2M}\rangle + A^{\dagger} \sum_{\alpha} \left(\prod_{\gamma \neq \alpha} B_{\gamma}^{\dagger} \right) |0\rangle \\ &\quad + g A^{\dagger} \sum_{\alpha} \left(\prod_{\gamma < \alpha} B_{\gamma}^{\dagger} \right) \left[\left(\prod_{\gamma > \alpha} B_{\gamma}^{\dagger} \right) K_{\alpha} + \sum_{\beta > \alpha} \left(\prod_{\alpha < \gamma < \beta} B_{\gamma}^{\dagger} \right) [K_{\alpha}, B_{\beta}^{\dagger}] \left(\prod_{\gamma > \beta} B_{\gamma}^{\dagger} \right) \right] |0\rangle \\ &= \sum_{\alpha} E_{\alpha} |\Psi_{2M}\rangle + A^{\dagger} \sum_{\alpha} \left(\prod_{\gamma \neq \alpha} B_{\gamma}^{\dagger} \right) |0\rangle + g A^{\dagger} \sum_{\alpha} \left(\prod_{\gamma \neq \alpha} B_{\gamma}^{\dagger} \right) K_{\alpha} |0\rangle + g A^{\dagger} \sum_{\alpha} \sum_{\beta > \alpha} \left(\prod_{\gamma \neq \alpha, \beta} B_{\gamma}^{\dagger} \right) [K_{\alpha}, B_{\beta}^{\dagger}] |0\rangle \end{aligned} \quad (\text{B46})$$

$$H|\Psi_{2M}\rangle = \left(\sum_{\alpha} E_{\alpha} \right) |\Psi_{2M}\rangle + A^{\dagger} \sum_{\alpha} \left[1 + g \sum_{\mathbf{k}} \phi_{\alpha}(\mathbf{k}) \right] \prod_{\gamma \neq \alpha} B_{\gamma}^{\dagger} |0\rangle - g A^{\dagger} \sum_{\alpha} \sum_{\beta (\neq \alpha)} \frac{B_{\alpha}^{\dagger} - B_{\beta}^{\dagger}}{E_{\alpha} - E_{\beta}} \prod_{\gamma \neq \alpha, \beta} B_{\gamma}^{\dagger} |0\rangle. \quad (\text{B47})$$

Then,

$$\begin{aligned}
& \sum_{\alpha} \sum_{\beta(\neq\alpha)} \frac{B_{\alpha}^{\dagger} - B_{\beta}^{\dagger}}{E_{\alpha} - E_{\beta}} \prod_{\substack{\gamma \neq \alpha \\ \gamma \neq \beta}} B_{\gamma}^{\dagger} = \sum_{\alpha} \sum_{\beta(\neq\alpha)} \frac{1}{E_{\alpha} - E_{\beta}} \prod_{\gamma \neq \beta} B_{\gamma}^{\dagger} - \sum_{\alpha} \sum_{\beta(\neq\alpha)} \frac{1}{E_{\alpha} - E_{\beta}} \prod_{\gamma \neq \alpha} B_{\gamma}^{\dagger} \\
& = \sum_{\alpha} \sum_{\beta(\neq\alpha)} \frac{1}{E_{\beta} - E_{\alpha}} \prod_{\gamma \neq \alpha} B_{\gamma}^{\dagger} - \sum_{\alpha} \sum_{\beta(\neq\alpha)} \frac{1}{E_{\alpha} - E_{\beta}} \prod_{\gamma \neq \alpha} B_{\gamma}^{\dagger} \quad (\text{swapped dummy indices in the first term}) \\
& = 2 \sum_{\alpha} \sum_{\beta(\neq\alpha)} \frac{1}{E_{\beta} - E_{\alpha}} \prod_{\gamma \neq \alpha} B_{\gamma}^{\dagger},
\end{aligned} \tag{B48}$$

which leads to

$$\begin{aligned}
H|\Psi_{2M}\rangle & = \left(\sum_{\alpha} E_{\alpha} \right) |\Psi_{2M}\rangle + A^{\dagger} \sum_{\alpha} \left[1 + g \sum_{\mathbf{k}} \phi_{\alpha}(\mathbf{k}) \right] \prod_{\gamma \neq \alpha} B_{\gamma}^{\dagger} |0\rangle - 2g A^{\dagger} \sum_{\alpha} \sum_{\beta(\neq\alpha)} \frac{1}{E_{\beta} - E_{\alpha}} \prod_{\gamma \neq \alpha} B_{\gamma}^{\dagger} |0\rangle \\
& = \left(\sum_{\alpha} E_{\alpha} \right) |\Psi_{2M}\rangle + A^{\dagger} \sum_{\alpha} \left[1 + g \sum_{\mathbf{k}} \phi_{\alpha}(\mathbf{k}) - 2g \sum_{\beta(\neq\alpha)} \frac{1}{E_{\beta} - E_{\alpha}} \right] \prod_{\gamma \neq \alpha} B_{\gamma}^{\dagger} |0\rangle,
\end{aligned} \tag{B49}$$

which gives the following equation:

$$\frac{1}{g} + \sum_{\mathbf{k}} \frac{1}{2\varepsilon_{\mathbf{k}} - E_{\mu}} - \sum_{\nu \neq \mu} \frac{2}{E_{\nu} - E_{\mu}} = 0, \quad \mu = 1, \dots, M. \tag{B50}$$

as claimed [106].

After obtaining the Richardson equations, it is convenient to introduce the Jacobian matrix with respect to the rapidities:

$$G_{\mu\nu} = \frac{\partial R_{\mu}}{\partial E_{\nu}}, \tag{B51}$$

where $R_{\mu}(\{E\}) \equiv \frac{1}{g} + \sum_{\mathbf{k}} \frac{1}{2\varepsilon_{\mathbf{k}} - E_{\mu}} - \sum_{\nu \neq \mu}^M \frac{2}{E_{\nu} - E_{\mu}} = 0$. For off-diagonal elements ($\nu \neq \mu$), only the third term depends on E_{ν} , and only through the ν th term:

$$G_{\mu\nu} = \frac{\partial}{\partial E_{\nu}} \left(-\frac{2}{E_{\nu} - E_{\mu}} \right) = \frac{2}{(E_{\nu} - E_{\mu})^2}, \quad \nu \neq \mu. \tag{B52}$$

For diagonal elements ($\nu = \mu$), differentiating with respect to E_{μ} yields

$$G_{\mu\mu} = \frac{\partial R_{\mu}}{\partial E_{\mu}} = \sum_{\mathbf{k}} \frac{\partial}{\partial E_{\mu}} (2\varepsilon_{\mathbf{k}} - E_{\mu})^{-1} - \sum_{\nu \neq \mu} 2 \frac{\partial}{\partial E_{\mu}} (E_{\nu} - E_{\mu})^{-1} \tag{B53}$$

$$= \sum_{\mathbf{k}} [-(2\varepsilon_{\mathbf{k}} - E_{\mu})^{-2} \cdot (-1)] - 2 \sum_{\nu \neq \mu}^M [-(E_{\nu} - E_{\mu})^{-2} \cdot (-1)] = \sum_{\mathbf{k}} \frac{1}{(2\varepsilon_{\mathbf{k}} - E_{\mu})^2} - 2 \sum_{\nu \neq \mu}^M \frac{1}{(E_{\nu} - E_{\mu})^2}. \tag{B54}$$

Together,

$$G_{\mu\nu} = \begin{cases} \sum_{\mathbf{k}} \frac{1}{(2\varepsilon_{\mathbf{k}} - E_{\mu})^2} - 2 \sum_{\lambda \neq \mu} \frac{1}{(E_{\lambda} - E_{\mu})^2}, & \nu = \mu, \\ \frac{2}{(E_{\nu} - E_{\mu})^2}, & \nu \neq \mu. \end{cases} \tag{B55}$$

This is called Gaudin matrix [106], which will be useful later in Sec. B 1 b when expressing correlation functions.

b. *Pair–Pair Correlators: Exact Formula*

With the Cooper-pair operator $A_{\mathbf{k}}^\dagger$ and $A_{\mathbf{k}}$ defined in Eq. (B20), for a general many-body state, the pair–pair correlator is

$$\tilde{C}_{\mathbf{k}\mathbf{k}'} \equiv \langle A_{\mathbf{k}}^\dagger A_{\mathbf{k}'} \rangle - \langle A_{\mathbf{k}}^\dagger \rangle \langle A_{\mathbf{k}'} \rangle, \quad (\text{B56})$$

where $\langle \dots \rangle$ is the average with respect to the state of interest. In the Richardson model we work with number-conserving eigenstates $|\Psi_{2M}\rangle$ (fixed particle number $2M$). Since $A_{\mathbf{k}}$ lowers particle number by two, $A_{\mathbf{k}}|\Psi_{2M}\rangle$ lies in the $2M - 2$ sector and is orthogonal to $|\Psi_{2M}\rangle$, hence

$$\langle A_{\mathbf{k}} \rangle = \langle \Psi_{2M} | A_{\mathbf{k}} | \Psi_{2M} \rangle = 0. \quad (\text{B57})$$

Therefore the connected and full correlators coincide,

$$\tilde{C}_{\mathbf{k}\mathbf{k}'} = \langle A_{\mathbf{k}}^\dagger A_{\mathbf{k}'} \rangle. \quad (\text{B58})$$

Writing out $A_{\mathbf{k}}^\dagger$ and $A_{\mathbf{k}'}$,

$$\langle A_{\mathbf{k}}^\dagger A_{\mathbf{k}'} \rangle = \langle c_{\mathbf{k}\uparrow}^\dagger c_{-\mathbf{k}\downarrow}^\dagger c_{-\mathbf{k}'\downarrow} c_{\mathbf{k}'\uparrow} \rangle, \quad (\text{B59})$$

which is exactly the Cooper-channel combination of the 2-RDM defined in Eq. (1), i.e.

$$C_{\mathbf{k}\mathbf{k}'} \equiv \tilde{C}_{\mathbf{k}\mathbf{k}'} = O_{\mathbf{k}\uparrow, -\mathbf{k}\downarrow, \mathbf{k}'\uparrow, -\mathbf{k}'\downarrow}. \quad (\text{B60})$$

(For U(1)–breaking mean-field states we may have $\langle A_{\mathbf{k}} \rangle \neq 0$, in which case the connected correlator (B56) differs from the full 2-RDM matrix element by $\langle A_{\mathbf{k}}^\dagger \rangle \langle A_{\mathbf{k}'} \rangle$; in our number-conserving case, (B57) ensures they are identical.)

Now we derive a general expression of $\langle \Psi_{2M} | A_{\mathbf{k}}^\dagger A_{\mathbf{k}'} | \Psi_{2M} \rangle$. Let's start from

$$A_{\mathbf{k}'} | \Psi_{2M} \rangle = A_{\mathbf{k}'} \left(\prod_{\epsilon=1}^M B_\epsilon^\dagger \right) | 0 \rangle. \quad (\text{B61})$$

Because $A_{\mathbf{k}'} | 0 \rangle = 0$, we can commute $A_{\mathbf{k}'}$ through the product and keep only commutators:

$$A_{\mathbf{k}'} \left(\prod_{\epsilon=1}^M B_\epsilon^\dagger \right) | 0 \rangle = \prod_{\epsilon=1}^M B_\epsilon^\dagger A_{\mathbf{k}'} | 0 \rangle + \sum_{\mu=1}^M \left(\prod_{\epsilon < \mu} B_\epsilon^\dagger \right) [A_{\mathbf{k}'}, B_\mu^\dagger] \left(\prod_{\epsilon > \mu} B_\epsilon^\dagger \right) | 0 \rangle \quad (\text{B62})$$

$$= \sum_{\mu=1}^M \left(\prod_{\epsilon < \mu} B_\epsilon^\dagger \right) [A_{\mathbf{k}'}, B_\mu^\dagger] \left(\prod_{\epsilon > \mu} B_\epsilon^\dagger \right) | 0 \rangle. \quad (\text{B63})$$

We can compute the commutator using $B_\mu^\dagger = \sum_{\mathbf{p}} \phi_\mu(\mathbf{p}) A_{\mathbf{p}}^\dagger$ and $[A_{\mathbf{k}'}, A_{\mathbf{p}}^\dagger] = \delta_{\mathbf{k}'\mathbf{p}}(1 - N_{\mathbf{k}'})$:

$$[A_{\mathbf{k}'}, B_\mu^\dagger] = \sum_{\mathbf{p}} \phi_\mu(\mathbf{p}) [A_{\mathbf{k}'}, A_{\mathbf{p}}^\dagger] = \sum_{\mathbf{p}} \phi_\mu(\mathbf{p}) \delta_{\mathbf{k}'\mathbf{p}}(1 - N_{\mathbf{k}'}) = \phi_\mu(\mathbf{k}')(1 - N_{\mathbf{k}'}). \quad (\text{B64})$$

Therefore,

$$A_{\mathbf{k}'} | \Psi_{2M} \rangle = \sum_{\mu=1}^M \phi_\mu(\mathbf{k}') \left(\prod_{\epsilon < \mu} B_\epsilon^\dagger \right) (1 - N_{\mathbf{k}'}) \left(\prod_{\epsilon > \mu} B_\epsilon^\dagger \right) | 0 \rangle \quad (\text{B65})$$

$$= \sum_{\mu=1}^M \phi_\mu(\mathbf{k}') \left(\prod_{\epsilon < \mu} B_\epsilon^\dagger \right) \left[\left(\prod_{\epsilon > \mu} B_\epsilon^\dagger \right) (1 - N_{\mathbf{k}'}) | 0 \rangle + \sum_{\nu > \mu} \left(\prod_{\mu < \epsilon < \nu} B_\epsilon^\dagger \right) [1 - N_{\mathbf{k}'}, B_\nu^\dagger] \left(\prod_{\epsilon > \nu} B_\epsilon^\dagger \right) | 0 \rangle \right], \quad (\text{B66})$$

where $[N_{\mathbf{k}'}, B_\nu^\dagger] = \sum_{\mathbf{p}} \phi_\nu(\mathbf{p}) [N_{\mathbf{k}'}, A_{\mathbf{p}}^\dagger] = 2\phi_\nu(\mathbf{k}') A_{\mathbf{k}'}^\dagger$, using Eq. (B22), so $[1 - N_{\mathbf{k}'}, B_\nu^\dagger] = -2\phi_\nu(\mathbf{k}') A_{\mathbf{k}'}^\dagger$. Thus,

$$A_{\mathbf{k}'} | \Psi_{2M} \rangle = \sum_{\mu=1}^M \phi_\mu(\mathbf{k}') \left(\prod_{\epsilon < \mu} B_\epsilon^\dagger \right) \left[\left(\prod_{\epsilon > \mu} B_\epsilon^\dagger \right) | 0 \rangle - \sum_{\nu > \mu} \left(\prod_{\mu < \epsilon < \nu} B_\epsilon^\dagger \right) 2\phi_\nu(\mathbf{k}') A_{\mathbf{k}'}^\dagger \left(\prod_{\epsilon > \nu} B_\epsilon^\dagger \right) | 0 \rangle \right] \quad (\text{B67})$$

$$= \sum_{\mu=1}^M \phi_{\mu}(\mathbf{k}') \left(\prod_{\epsilon \neq \mu} B_{\epsilon}^{\dagger} \right) |0\rangle - \sum_{\mu=1}^M \phi_{\mu}(\mathbf{k}') \left(\prod_{\epsilon < \mu} B_{\epsilon}^{\dagger} \right) \sum_{\nu > \mu} \left(\prod_{\mu < \epsilon < \nu} B_{\epsilon}^{\dagger} \right) 2\phi_{\nu}(\mathbf{k}') A_{\mathbf{k}'}^{\dagger} \left(\prod_{\epsilon > \nu} B_{\epsilon}^{\dagger} \right) |0\rangle \quad (\text{B68})$$

$$= \sum_{\mu=1}^M \phi_{\mu}(\mathbf{k}') \left(\prod_{\epsilon \neq \mu} B_{\epsilon}^{\dagger} \right) |0\rangle - 2A_{\mathbf{k}'}^{\dagger} \sum_{\mu=1}^M \sum_{\nu > \mu} \phi_{\mu}(\mathbf{k}') \phi_{\nu}(\mathbf{k}') \left(\prod_{\epsilon < \mu} B_{\epsilon}^{\dagger} \right) \left(\prod_{\mu < \epsilon < \nu} B_{\epsilon}^{\dagger} \right) \left(\prod_{\epsilon > \nu} B_{\epsilon}^{\dagger} \right) |0\rangle \quad (\text{B69})$$

$$= \sum_{\mu=1}^M \phi_{\mu}(\mathbf{k}') \left(\prod_{\epsilon \neq \mu} B_{\epsilon}^{\dagger} \right) |0\rangle - 2A_{\mathbf{k}'}^{\dagger} \sum_{1 \leq \mu < \nu \leq M} \phi_{\mu}(\mathbf{k}') \phi_{\nu}(\mathbf{k}') \left(\prod_{\epsilon \neq \mu, \nu} B_{\epsilon}^{\dagger} \right) |0\rangle. \quad (\text{B70})$$

Define the shorthand:

$$|\Psi^{(\mu)}\rangle \equiv \left(\prod_{\epsilon \neq \mu} B_{\epsilon}^{\dagger} \right) |0\rangle, \quad |\Psi^{(\mu\nu)}\rangle \equiv \left(\prod_{\epsilon \neq \mu, \nu} B_{\epsilon}^{\dagger} \right) |0\rangle, \quad \langle \Psi^{(\rho)} | \equiv \langle 0 | \left(\prod_{\omega \neq \rho} B_{\omega} \right), \quad \langle \Psi^{(\rho\sigma)} | \equiv \langle 0 | \left(\prod_{\omega \neq \rho, \sigma} B_{\omega} \right). \quad (\text{B71})$$

Therefore,

$$\langle \Psi_{2M} | A_{\mathbf{k}}^{\dagger} A_{\mathbf{k}'} | \Psi_{2M} \rangle = \langle \Psi_{2M} | A_{\mathbf{k}}^{\dagger} \left[\sum_{\mu} \phi_{\mu}(\mathbf{k}') |\Psi^{(\mu)}\rangle - 2A_{\mathbf{k}'}^{\dagger} \sum_{\mu < \nu} \phi_{\mu}(\mathbf{k}') \phi_{\nu}(\mathbf{k}') |\Psi^{(\mu\nu)}\rangle \right] \quad (\text{B72})$$

$$= \sum_{\mu} \phi_{\mu}(\mathbf{k}') \langle \Psi_{2M} | A_{\mathbf{k}}^{\dagger} |\Psi^{(\mu)}\rangle - 2 \sum_{\mu < \nu} \phi_{\mu}(\mathbf{k}') \phi_{\nu}(\mathbf{k}') \langle \Psi_{2M} | A_{\mathbf{k}}^{\dagger} A_{\mathbf{k}'}^{\dagger} |\Psi^{(\mu\nu)}\rangle \quad (\text{B73})$$

$$= \sum_{\mu} \phi_{\mu}(\mathbf{k}') F_{\mathbf{k}}^{(\mu)} - 2 \sum_{\mu < \nu} \phi_{\mu}(\mathbf{k}') \phi_{\nu}(\mathbf{k}') F_{\mathbf{k}\mathbf{k}'}^{(\mu\nu)}. \quad (\text{B74})$$

where we define the form factors

$$F_{\mathbf{k}}^{(\mu)} \equiv \langle \Psi_{2M} | A_{\mathbf{k}}^{\dagger} |\Psi^{(\mu)}\rangle, \quad F_{\mathbf{k}\mathbf{k}'}^{(\mu\nu)} \equiv \langle \Psi_{2M} | A_{\mathbf{k}}^{\dagger} A_{\mathbf{k}'}^{\dagger} |\Psi^{(\mu\nu)}\rangle. \quad (\text{B75})$$

Define the general pair-creation operators

$$B^{\dagger}(u) \equiv \sum_{\mathbf{p}} \frac{A_{\mathbf{p}}^{\dagger}}{d_{\mathbf{p}} - u}, \quad u \in \mathbb{C}. \quad (\text{B76})$$

where $d_{\mathbf{p}} = 2\varepsilon_{\mathbf{p}}$. For any choice of parameters $\{u_{\mu}\}_{\mu=1}^M$, this generates the general M -pair state

$$|\{u\}\rangle \equiv \prod_{\mu=1}^M B^{\dagger}(u_{\mu}) |0\rangle. \quad (\text{B77})$$

In particular, taking $u_{\mu} = E_{\mu}$ equal to the Richardson rapidities, we recover the Richardson state $|\Psi_{2M}\rangle = \prod_{\mu=1}^M B^{\dagger}(E_{\mu}) |0\rangle$, $B^{\dagger}(E_{\mu}) = \sum_{\mathbf{p}=1} \frac{A_{\mathbf{p}}^{\dagger}}{d_{\mathbf{p}} - E_{\mu}}$, which matches the amplitudes $\phi_{\mu}(\mathbf{p}) = 1/(d_{\mathbf{p}} - E_{\mu})$ we discussed. Now we can show the residue identity for $A_{\mathbf{k}}^{\dagger}$. From Eq. (B76),

$$(d_{\mathbf{k}} - u) B^{\dagger}(u) = (d_{\mathbf{k}} - u) \sum_{\mathbf{p}} \frac{A_{\mathbf{p}}^{\dagger}}{d_{\mathbf{p}} - u} = \sum_{\mathbf{p}} (d_{\mathbf{k}} - u) \frac{A_{\mathbf{p}}^{\dagger}}{d_{\mathbf{p}} - u} \quad (\text{B78})$$

$$= (d_{\mathbf{k}} - u) \frac{A_{\mathbf{k}}^{\dagger}}{d_{\mathbf{k}} - u} + \sum_{\mathbf{p} \neq \mathbf{k}} (d_{\mathbf{k}} - u) \frac{A_{\mathbf{p}}^{\dagger}}{d_{\mathbf{p}} - u} = A_{\mathbf{k}}^{\dagger} + \sum_{\mathbf{p} \neq \mathbf{k}} \frac{d_{\mathbf{k}} - u}{d_{\mathbf{p}} - u} A_{\mathbf{p}}^{\dagger} \quad (\text{B79})$$

$$\lim_{u \rightarrow d_{\mathbf{k}}} (d_{\mathbf{k}} - u) B^{\dagger}(u) = \lim_{u \rightarrow d_{\mathbf{k}}} \left[A_{\mathbf{k}}^{\dagger} + \sum_{\mathbf{p} \neq \mathbf{k}} \frac{d_{\mathbf{k}} - u}{d_{\mathbf{p}} - u} A_{\mathbf{p}}^{\dagger} \right] = A_{\mathbf{k}}^{\dagger} + \sum_{\mathbf{p} \neq \mathbf{k}} \left(\lim_{u \rightarrow d_{\mathbf{k}}} \frac{d_{\mathbf{k}} - u}{d_{\mathbf{p}} - u} \right) A_{\mathbf{p}}^{\dagger} = A_{\mathbf{k}}^{\dagger} + \sum_{\mathbf{p} \neq \mathbf{k}} 0 \cdot A_{\mathbf{p}}^{\dagger} = A_{\mathbf{k}}^{\dagger}. \quad (\text{B80})$$

Therefore,

$$A_{\mathbf{k}}^{\dagger} = \lim_{u \rightarrow d_{\mathbf{k}}} (d_{\mathbf{k}} - u) B^{\dagger}(u). \quad (\text{B81})$$

We can re-write the form factors in Eq. (B75):

$$F_{\mathbf{k}}^{(\mu)} = \langle \Psi | A_{\mathbf{k}}^\dagger | \Psi^{(\mu)} \rangle = \langle \{E\} | A_{\mathbf{k}}^\dagger \prod_{\nu \neq \mu} B^\dagger(E_\nu) | 0 \rangle = \langle \{E\} | \lim_{u \rightarrow d_{\mathbf{k}}} (d_{\mathbf{k}} - u) B^\dagger(u) \prod_{\nu \neq \mu} B^\dagger(E_\nu) | 0 \rangle \quad (\text{B82})$$

$$= \lim_{u \rightarrow d_{\mathbf{k}}} (d_{\mathbf{k}} - u) S \left(\{E\}, \{F^{(\mu)}(u)\} \right), \quad (\text{B83})$$

where we defined $S(\{E\}, \{F^{(\mu)}(u)\}) \equiv \langle \{E\} | \{F^{(\mu)}(u)\} \rangle$, and $|\{F^{(\mu)}(u)\}\rangle \equiv B^\dagger(u) \prod_{\nu \neq \mu} B^\dagger(E_\nu) | 0 \rangle$. Notice that, here we denote $\{F^{(\mu)}(u)\} = \{E_1, \dots, E_{\mu-1}, u, E_{\mu+1}, \dots, E_M\}$, the set obtained from $\{E\}$ by replacing only the μ -th element with u . Similarly,

$$F_{\mathbf{k}\mathbf{k}'}^{(\mu\nu)} = \lim_{u \rightarrow d_{\mathbf{k}}} \lim_{v \rightarrow d_{\mathbf{k}'}} (d_{\mathbf{k}} - u)(d_{\mathbf{k}'} - v) S \left(\{E\}, \{F^{(\mu\nu)}(u, v)\} \right), \quad (\text{B84})$$

where we defined $|\{F^{(\mu\nu)}(u, v)\}\rangle \equiv B^\dagger(u) B^\dagger(v) \prod_{\lambda \neq \mu, \nu} B^\dagger(E_\lambda) | 0 \rangle$.

Now all we need is to evaluate the form factors from Eq. (B83) and Eq. (B84), so that we can plug into the correlator expression in Eq. (B74). To do so, we use the standard Slavnov's formula [140–143] that gives an exact determinant expression for $S(\{E\}, \{F\})$ when $\{E\}$ are the solution from Richardson equations (which we will show explicitly in Sec. B1c); we can derive:

$$F_{\mathbf{k}}^{(\mu)} = (d_{\mathbf{k}} - E_\mu) \det(G(\mu \rightarrow C^{(\mathbf{k})})), \quad (\text{B85})$$

$$F_{\mathbf{k}\mathbf{k}'}^{(\mu\nu)} = \frac{(d_{\mathbf{k}} - E_\mu)(d_{\mathbf{k}} - E_\nu)(d_{\mathbf{k}'} - E_\mu)(d_{\mathbf{k}'} - E_\nu)}{(d_{\mathbf{k}} - d_{\mathbf{k}'})(E_\nu - E_\mu)} \det(G(\mu, \nu \rightarrow C^{(\mathbf{k})}, C^{(\mathbf{k}')})), \quad (\mathbf{k} \neq \mathbf{k}') \quad (\text{B86})$$

where G is the Gaudin matrix derived in Eq. (B55), and $G(\mu \rightarrow C^{(\mathbf{k})})$ here denotes the matrix obtained from G by replacing its μ -th column with the vector $C^{(\mathbf{k})}$ whose elements are $C_\alpha^{(\mathbf{k})} = \frac{1}{(d_{\mathbf{k}} - E_\alpha)^2}$, while $G(\mu, \nu \rightarrow C^{(\mathbf{k})}, C^{(\mathbf{k}')})$ denotes the matrix obtained by replacing the μ -th and ν -th columns of G with $C^{(\mathbf{k})}$ and $C^{(\mathbf{k}'})$, respectively. Now plug Eq. (B85) and Eq. (B86) into Eq. (B74),

$$\langle \Psi_{2M} | A_{\mathbf{k}}^\dagger A_{\mathbf{k}'} | \Psi_{2M} \rangle = \sum_{\mu} \phi_{\mu}(\mathbf{k}') F_{\mathbf{k}}^{(\mu)} - 2 \sum_{\mu < \nu} \phi_{\mu}(\mathbf{k}') \phi_{\nu}(\mathbf{k}') F_{\mathbf{k}\mathbf{k}'}^{(\mu\nu)} \quad (\text{B87})$$

$$= \sum_{\mu} \phi_{\mu}(\mathbf{k}') (d_{\mathbf{k}} - E_\mu) \det(G(\mu \rightarrow C^{(\mathbf{k})})) \quad (\text{B88})$$

$$- 2 \sum_{\mu < \nu} \phi_{\mu}(\mathbf{k}') \phi_{\nu}(\mathbf{k}') \frac{(d_{\mathbf{k}} - E_\mu)(d_{\mathbf{k}} - E_\nu)(d_{\mathbf{k}'} - E_\mu)(d_{\mathbf{k}'} - E_\nu)}{(d_{\mathbf{k}} - d_{\mathbf{k}'})(E_\nu - E_\mu)} \det(G(\mu, \nu \rightarrow C^{(\mathbf{k})}, C^{(\mathbf{k}')})) \quad (\text{B89})$$

$$= \sum_{\mu} \frac{d_{\mathbf{k}} - E_\mu}{d_{\mathbf{k}'} - E_\mu} \det(G(\mu \rightarrow C^{(\mathbf{k})})) - 2 \sum_{\mu < \nu} \frac{(d_{\mathbf{k}} - E_\mu)(d_{\mathbf{k}} - E_\nu)}{(d_{\mathbf{k}} - d_{\mathbf{k}'})(E_\nu - E_\mu)} \det(G(\mu, \nu \rightarrow C^{(\mathbf{k})}, C^{(\mathbf{k}')})). \quad (\text{B90})$$

We normalize it by $\langle \Psi_{2M} | \Psi_{2M} \rangle = \det G$:

$$\frac{\langle \Psi_{2M} | A_{\mathbf{k}}^\dagger A_{\mathbf{k}'} | \Psi_{2M} \rangle}{\langle \Psi_{2M} | \Psi_{2M} \rangle} = \sum_{\mu} \frac{d_{\mathbf{k}} - E_\mu}{d_{\mathbf{k}'} - E_\mu} \frac{\det(G(\mu \rightarrow C^{(\mathbf{k})}))}{\det G} - 2 \sum_{\mu < \nu} \frac{(d_{\mathbf{k}} - E_\mu)(d_{\mathbf{k}} - E_\nu)}{(d_{\mathbf{k}} - d_{\mathbf{k}'})(E_\nu - E_\mu)} \frac{\det(G(\mu, \nu \rightarrow C^{(\mathbf{k})}, C^{(\mathbf{k}')}))}{\det G} \quad (\text{B91})$$

Now all we need is to simplify the terms $\frac{\det(G(\mu \rightarrow C^{(\mathbf{k})}))}{\det G}$ and $\frac{\det(G(\mu, \nu \rightarrow C^{(\mathbf{k})}, C^{(\mathbf{k}')}))}{\det G}$, here is how we derive an expression for them:

We differentiate Richardson equations:

$$0 = \frac{\partial R_\alpha}{\partial d_{\mathbf{k}}} = \frac{\partial}{\partial d_{\mathbf{k}}} \left[\frac{1}{g} + \sum_i \frac{1}{d_i - E_\alpha} - 2 \sum_{\beta \neq \alpha} \frac{1}{E_\beta - E_\alpha} \right] \quad (\text{B92})$$

$$= \frac{\partial}{\partial d_{\mathbf{k}}} \left(\frac{1}{d_{\mathbf{k}} - E_{\alpha}} \right) + \sum_{i \neq \mathbf{k}} \frac{\partial}{\partial d_{\mathbf{k}}} \left(\frac{1}{d_i - E_{\alpha}} \right) - 2 \sum_{\beta \neq \alpha} \frac{\partial}{\partial d_{\mathbf{k}}} \left(\frac{1}{E_{\beta} - E_{\alpha}} \right) \quad (\text{B93})$$

$$= \frac{-1}{(d_{\mathbf{k}} - E_{\alpha})^2} \frac{\partial}{\partial d_{\mathbf{k}}} (d_{\mathbf{k}} - E_{\alpha}) + \sum_{i \neq \mathbf{k}} \left[\frac{-1}{(d_i - E_{\alpha})^2} \frac{\partial}{\partial d_{\mathbf{k}}} (d_i - E_{\alpha}) \right] - 2 \sum_{\beta \neq \alpha} \left[\frac{\partial}{\partial E_{\beta}} \left(\frac{1}{E_{\beta} - E_{\alpha}} \right) \frac{\partial E_{\beta}}{\partial d_{\mathbf{k}}} + \frac{\partial}{\partial E_{\alpha}} \left(\frac{1}{E_{\beta} - E_{\alpha}} \right) \frac{\partial E_{\alpha}}{\partial d_{\mathbf{k}}} \right] \quad (\text{B94})$$

$$= \frac{-1}{(d_{\mathbf{k}} - E_{\alpha})^2} \left(1 - \frac{\partial E_{\alpha}}{\partial d_{\mathbf{k}}} \right) + \sum_{i \neq \mathbf{k}} \left[-\frac{1}{(d_i - E_{\alpha})^2} \left(0 - \frac{\partial E_{\alpha}}{\partial d_{\mathbf{k}}} \right) \right] - 2 \sum_{\beta \neq \alpha} \left[\left(-\frac{1}{(E_{\beta} - E_{\alpha})^2} \right) \frac{\partial E_{\beta}}{\partial d_{\mathbf{k}}} + \left(\frac{1}{(E_{\beta} - E_{\alpha})^2} \right) \frac{\partial E_{\alpha}}{\partial d_{\mathbf{k}}} \right] \quad (\text{B95})$$

$$= \frac{-1}{(d_{\mathbf{k}} - E_{\alpha})^2} + \frac{1}{(d_{\mathbf{k}} - E_{\alpha})^2} \frac{\partial E_{\alpha}}{\partial d_{\mathbf{k}}} + \sum_{i \neq \mathbf{k}} \frac{1}{(d_i - E_{\alpha})^2} \frac{\partial E_{\alpha}}{\partial d_{\mathbf{k}}} + 2 \sum_{\beta \neq \alpha} \frac{1}{(E_{\beta} - E_{\alpha})^2} \frac{\partial E_{\beta}}{\partial d_{\mathbf{k}}} - 2 \sum_{\beta \neq \alpha} \frac{1}{(E_{\beta} - E_{\alpha})^2} \frac{\partial E_{\alpha}}{\partial d_{\mathbf{k}}} \quad (\text{B96})$$

$$= -\frac{1}{(d_{\mathbf{k}} - E_{\alpha})^2} + \left[\sum_i \frac{1}{(d_i - E_{\alpha})^2} - 2 \sum_{\beta \neq \alpha} \frac{1}{(E_{\beta} - E_{\alpha})^2} \right] \frac{\partial E_{\alpha}}{\partial d_{\mathbf{k}}} + \sum_{\beta \neq \alpha} \frac{2}{(E_{\beta} - E_{\alpha})^2} \frac{\partial E_{\beta}}{\partial d_{\mathbf{k}}} \quad (\text{B97})$$

We can identify the Gaudin matrix from Eq. (B55), then

$$0 = -\frac{1}{(d_{\mathbf{k}} - E_{\alpha})^2} + G_{\alpha\alpha} x_{\alpha}^{(\mathbf{k})} + \sum_{\beta \neq \alpha} G_{\alpha\beta} x_{\beta}^{(\mathbf{k})}, \quad x_{\beta}^{(\mathbf{k})} \equiv \frac{\partial E_{\beta}}{\partial d_{\mathbf{k}}}, \quad (\text{B98})$$

$$G_{\alpha\alpha} x_{\alpha}^{(\mathbf{k})} + \sum_{\beta \neq \alpha} G_{\alpha\beta} x_{\beta}^{(\mathbf{k})} = \frac{1}{(d_{\mathbf{k}} - E_{\alpha})^2}, \quad (\text{B99})$$

$$\sum_{\beta=1}^M G_{\alpha\beta} x_{\beta}^{(\mathbf{k})} = \frac{1}{(d_{\mathbf{k}} - E_{\alpha})^2}. \quad (\text{B100})$$

Namely, $G\hat{x} = C^{(\mathbf{k})}$, where $C^{(\mathbf{k})} \equiv \frac{1}{(d_{\mathbf{k}} - E_{\alpha})^2}$.

According to Cramer's rule, if a matrix $A \in \mathbb{C}^{n \times n}$ is invertible and $Ax = b$, then for each i ,

$$x_i = \frac{\det A^{(i)}}{\det A} \quad (i = 1, \dots, n). \quad (\text{B101})$$

where $A^{(i)}$ is obtained from A by replacing its i -th column with b . Applying Eq. (B101) with $A = G$ and $b = C^{(\mathbf{k})}$ gives

$$x_{\mu}^{(\mathbf{k})} = \frac{\det (G(\mu \rightarrow C^{(\mathbf{k})}))}{\det G}, \quad (\text{B102})$$

where $G(\mu \rightarrow C^{(\mathbf{k})})$ denotes the matrix obtained by replacing the μ th column of G by the vector $C^{(\mathbf{k})}$. Since $x_{\mu}^{(\mathbf{k})} = \partial E_{\mu} / \partial d_{\mathbf{k}}$, we conclude

$$\frac{\det (G(\mu \rightarrow C^{(\mathbf{k})}))}{\det G} = \frac{\partial E_{\mu}}{\partial d_{\mathbf{k}}}. \quad (\text{B103})$$

Similarly, consider the matrix $G(\mu, \nu \rightarrow C^{(\mathbf{k})}, C^{(\mathbf{k}')})$ obtained from G by replacing the μ th column by $C^{(\mathbf{k})}$ and the ν th column by $C^{(\mathbf{k}')}$. We can also get the standard identity

$$\frac{\det (G(\mu, \nu \rightarrow C^{(\mathbf{k})}, C^{(\mathbf{k}')}))}{\det G} = x_{\mu}^{(\mathbf{k})} x_{\nu}^{(\mathbf{k}')} - x_{\nu}^{(\mathbf{k})} x_{\mu}^{(\mathbf{k}')}. \quad (\text{B104})$$

Substituting $x_{\mu}^{(\mathbf{k})} = \partial E_{\mu} / \partial d_{\mathbf{k}}$ and $x_{\mu}^{(\mathbf{k}')} = \partial E_{\mu} / \partial d_{\mathbf{k}'}$ leads to

$$\frac{\det (G(\mu, \nu \rightarrow C^{(\mathbf{k})}, C^{(\mathbf{k}')}))}{\det G} = \frac{\partial E_{\mu}}{\partial d_{\mathbf{k}}} \frac{\partial E_{\nu}}{\partial d_{\mathbf{k}'}} - \frac{\partial E_{\nu}}{\partial d_{\mathbf{k}}} \frac{\partial E_{\mu}}{\partial d_{\mathbf{k}'}}. \quad (\text{B105})$$

We plug Eq. (B103) and Eq. (B105) into Eq. (B91):

$$\frac{\langle \Psi_{2M} | A_{\mathbf{k}}^\dagger A_{\mathbf{k}'} | \Psi_{2M} \rangle}{\langle \Psi_{2M} | \Psi_{2M} \rangle} = \sum_{\mu} \frac{d_{\mathbf{k}} - E_{\mu}}{d_{\mathbf{k}'} - E_{\mu}} \frac{\partial E_{\mu}}{\partial d_{\mathbf{k}}} - 2 \sum_{\mu < \nu} \frac{(d_{\mathbf{k}} - E_{\mu})(d_{\mathbf{k}} - E_{\nu})}{(d_{\mathbf{k}} - d_{\mathbf{k}'})(E_{\nu} - E_{\mu})} \left(\frac{\partial E_{\mu}}{\partial d_{\mathbf{k}}} \frac{\partial E_{\nu}}{\partial d_{\mathbf{k}'}} - \frac{\partial E_{\nu}}{\partial d_{\mathbf{k}}} \frac{\partial E_{\mu}}{\partial d_{\mathbf{k}'}} \right), \quad (\mathbf{k} \neq \mathbf{k}'). \quad (\text{B106})$$

We derived the correlator formula for $\mathbf{k} \neq \mathbf{k}'$ case, now for $\mathbf{k} = \mathbf{k}'$ we have:

$$H = \sum_{\mathbf{k}, s} \varepsilon_{\mathbf{k}} c_{\mathbf{k}s}^\dagger c_{\mathbf{k}s} + g \sum_{\mathbf{k}} A_{\mathbf{k}}^\dagger \sum_{\mathbf{k}'} A_{\mathbf{k}'} = \sum_{\mathbf{k}} \varepsilon_{\mathbf{k}} (n_{\mathbf{k}\uparrow} + n_{-\mathbf{k}\downarrow}) + g \sum_{\mathbf{k}, \mathbf{k}'} A_{\mathbf{k}}^\dagger A_{\mathbf{k}'} \quad (\text{B107})$$

$$= \frac{1}{2} \sum_{\mathbf{k}} d_{\mathbf{k}} N_{\mathbf{k}} + g \sum_{\mathbf{k}, \mathbf{k}'} A_{\mathbf{k}}^\dagger A_{\mathbf{k}'}, \quad (N_{\mathbf{k}} \equiv n_{\mathbf{k}\uparrow} + n_{-\mathbf{k}\downarrow}). \quad (\text{B108})$$

Take derivative:

$$\frac{\partial H}{\partial d_{\mathbf{k}}} = \frac{1}{2} N_{\mathbf{k}} = n_{\mathbf{k}\uparrow} n_{-\mathbf{k}\downarrow} = c_{\mathbf{k}\uparrow}^\dagger c_{-\mathbf{k}\downarrow}^\dagger c_{-\mathbf{k}\downarrow} c_{\mathbf{k}\uparrow} = A_{\mathbf{k}}^\dagger A_{\mathbf{k}}. \quad (\text{B109})$$

where we focus on the seniority-zero (fully paired) subspace. We apply the Hellmann–Feynman theorem [144] to the exact eigenstate $|\Psi_{2M}\rangle$:

$$\frac{\partial E}{\partial d_{\mathbf{k}}} = \frac{\langle \Psi_{2M} | \frac{\partial H}{\partial d_{\mathbf{k}}} | \Psi_{2M} \rangle}{\langle \Psi_{2M} | \Psi_{2M} \rangle} = \frac{\langle \Psi_{2M} | A_{\mathbf{k}}^\dagger A_{\mathbf{k}} | \Psi_{2M} \rangle}{\langle \Psi_{2M} | \Psi_{2M} \rangle}. \quad (\text{B110})$$

Therefore,

$$\frac{\langle \Psi_{2M} | A_{\mathbf{k}}^\dagger A_{\mathbf{k}} | \Psi_{2M} \rangle}{\langle \Psi_{2M} | \Psi_{2M} \rangle} = \frac{\partial E}{\partial d_{\mathbf{k}}} = \sum_{\mu=1}^M \frac{\partial E_{\mu}}{\partial d_{\mathbf{k}}}, \quad (\mathbf{k} = \mathbf{k}') \quad (\text{B111})$$

Eq. (B106) and Eq. (B111) are the final expressions of the pair-pair correlator, where $d_{\mathbf{k}} = 2\varepsilon_{\mathbf{k}}$, matching the result from [143].

c. Slavnov's Formula and Application

In this section, we will derive Eq. (B85) and Eq. (B86) used in Pair–Pair Correlators section (Sec. B1b). Recall the M -pair states

$$|\{u\}\rangle \equiv \prod_{\alpha=1}^M B^\dagger(u_\alpha) |0\rangle, \quad B^\dagger(u) = \sum_{\mathbf{p}} \frac{A_{\mathbf{p}}^\dagger}{d_{\mathbf{p}} - u}, \quad (\text{B112})$$

and we defined the overlap

$$S(\{E\}, \{F\}) \equiv \langle \{E\} | \{F\} \rangle. \quad (\text{B113})$$

In this subsection, we assume $\{E\}$ is on-shell (namely, $\{E\}$ solves the Richardson equations), while $\{F\}$ is arbitrary and it does not need to solve the Richardson equations (we call it off-shell).

According to Slavnov's formula and its application in Richardson model [140–143], for on-shell $\{E\} = \{E_1, \dots, E_M\}$ and arbitrary $\{F\} = \{F_1, \dots, F_M\}$,

$$S(\{E\}, \{F\}) = \frac{\prod_{b=1}^M \prod_{\substack{a=1 \\ a \neq b}}^M (E_a - F_b)}{\prod_{1 \leq a < b \leq M} (E_b - E_a) \prod_{1 \leq b < a \leq M} (F_b - F_a)} \det \mathcal{S}(\{E\}, \{F\}). \quad (\text{B114})$$

and the $M \times M$ matrix \mathcal{S} has entries (with $a, b = 1, \dots, M$)

$$\mathcal{S}_{ab}(\{E\}, \{F\}) = \frac{E_b - F_b}{E_a - F_b} \left[\sum_i \frac{1}{(E_a - d_i)(F_b - d_i)} - 2 \sum_{\substack{c=1 \\ c \neq a}}^M \frac{1}{(E_a - E_c)(F_b - E_c)} \right]. \quad (\text{B115})$$

We now apply (B114)–(B115) to the specific sets in our case

$$\{F^{(\mu)}(u)\} = \{E_1, \dots, E_{\mu-1}, u, E_{\mu+1}, \dots, E_M\}, \quad \{F^{(\mu\nu)}(u, v)\} = \{E_1, \dots, u, \dots, v, \dots, E_M\}, \quad (\text{B116})$$

because they are exactly the sets in our form factors (the factors to compute correlators) in Eq. (B83) and Eq. (B84):

$$F_{\mathbf{k}}^{(\mu)} = \lim_{u \rightarrow d_{\mathbf{k}}} (d_{\mathbf{k}} - u) S(\{E\}, \{F^{(\mu)}(u)\}), \quad F_{\mathbf{k}\mathbf{k}'}^{(\mu\nu)} = \lim_{u \rightarrow d_{\mathbf{k}}} \lim_{v \rightarrow d_{\mathbf{k}'}} (d_{\mathbf{k}} - u)(d_{\mathbf{k}'} - v) S(\{E\}, \{F^{(\mu\nu)}(u, v)\}). \quad (\text{B117})$$

For $\{F\} = \{F^{(\mu)}(u)\}$ we have $F_b = E_b$ for $b \neq \mu$ and $F_\mu = u$, so the prefactor in Eq. (B114) can be reduced to 1:

$$\frac{\prod_b \prod_{a \neq b} (E_a - F_b)}{\prod_{a < b} (E_b - E_a) \prod_{b < a} (F_b - F_a)} = \frac{\prod_{b \neq \mu, a \neq b} (E_a - E_b) \prod_{a < b = \mu} (E_a - u) \prod_{a > b = \mu} (E_a - u)}{\prod_{a < b} (E_b - E_a) \prod_{\substack{b < a \\ b, a \neq \mu}} (E_b - E_a) \prod_{b < a = \mu} (E_b - u) \prod_{a > b = \mu} (u - E_a)} \quad (\text{B118})$$

$$= \left(\frac{\prod_{b \neq \mu, a \neq b} (E_a - E_b)}{\prod_{a < b} (E_b - E_a) \prod_{\substack{b < a \\ b, a \neq \mu}} (E_b - E_a)} \right) \left(\frac{\prod_{a < b = \mu} (E_a - u)}{\prod_{b < a = \mu} (E_b - u)} \right) \left(\frac{\prod_{a > b = \mu} (E_a - u)}{\prod_{a > b = \mu} (u - E_a)} \right) \quad (\text{B119})$$

$$= (-1)^{M-\mu} (1) (-1)^{M-\mu} = (-1)^{2(M-\mu)} = 1. \quad (\text{B120})$$

Hence Eq. (B114) becomes

$$S(\{E\}, \{F^{(\mu)}(u)\}) = \det \mathcal{S}(\{E\}, \{F^{(\mu)}(u)\}). \quad (\text{B121})$$

We now evaluate the limit $F_b \rightarrow E_b$ in (B115). First, for the columns $b \neq \mu$, according to Eq. (B116), we have $F_b = E_b$, then

Off-diagonal ($a \neq b$):

$$\lim_{F_b \rightarrow E_b} \mathcal{S}_{ab} = \lim_{F_b \rightarrow E_b} \frac{E_b - F_b}{E_a - F_b} \cdot \frac{-2}{(E_a - E_b)(F_b - E_b)} = \frac{-2}{(E_a - E_b)} \lim_{F_b \rightarrow E_b} \frac{E_b - F_b}{(E_a - F_b)(F_b - E_b)} \quad (\text{B122})$$

$$= \frac{-2}{(E_a - E_b)} \lim_{F_b \rightarrow E_b} \frac{-(F_b - E_b)}{(E_a - F_b)(F_b - E_b)} = \frac{2}{(E_a - E_b)} \lim_{F_b \rightarrow E_b} \frac{1}{E_a - F_b} = \frac{2}{(E_a - E_b)^2}. \quad (\text{B123})$$

Diagonal ($a = b$):

$$\lim_{F_b \rightarrow E_b} \mathcal{S}_{bb} = \lim_{F_b \rightarrow E_b} \frac{E_b - F_b}{E_b - F_b} \left[\sum_i \frac{1}{(E_b - d_i)(F_b - d_i)} - 2 \sum_{c \neq b} \frac{1}{(E_b - E_c)(F_b - E_c)} \right] = \sum_i \frac{1}{(E_b - d_i)^2} - 2 \sum_{c \neq b} \frac{1}{(E_b - E_c)^2}. \quad (\text{B124})$$

Comparing (B123)–(B124) with the Gaudin matrix G in Eq. (B55), we conclude: for every $b \neq \mu$, the b -th column of $\mathcal{S}(\{E\}, \{F^{(\mu)}(u)\})$ matches exactly the b -th column of G in the limit $F_b \rightarrow E_b$. Hence, inside the determinant (B121), all columns except the μ -th become Gaudin columns.

Second, for the special column $b = \mu$, we have $F_\mu = u$. Multiply (B115) by $(d_{\mathbf{k}} - u)$ and take $u \rightarrow d_{\mathbf{k}}$. Only the $i = \mathbf{k}$ term in the first sum is singular, therefore,

$$\lim_{u \rightarrow d_{\mathbf{k}}} (d_{\mathbf{k}} - u) \mathcal{S}_{a\mu} = \lim_{u \rightarrow d_{\mathbf{k}}} (d_{\mathbf{k}} - u) \frac{E_\mu - u}{E_a - u} \frac{1}{(E_a - d_{\mathbf{k}})(u - d_{\mathbf{k}})} = \frac{E_\mu - d_{\mathbf{k}}}{E_a - d_{\mathbf{k}}} \frac{-1}{E_a - d_{\mathbf{k}}} = \frac{d_{\mathbf{k}} - E_\mu}{(d_{\mathbf{k}} - E_a)^2}. \quad (\text{B125})$$

Define the vector $C_a^{(\mathbf{k})} \equiv \frac{1}{(d_{\mathbf{k}} - E_a)^2}$, with $a = 1, \dots, M$, then

$$\lim_{u \rightarrow d_{\mathbf{k}}} (d_{\mathbf{k}} - u) \mathcal{S}_{a\mu} = (d_{\mathbf{k}} - E_\mu) C_a^{(\mathbf{k})}. \quad (\text{B126})$$

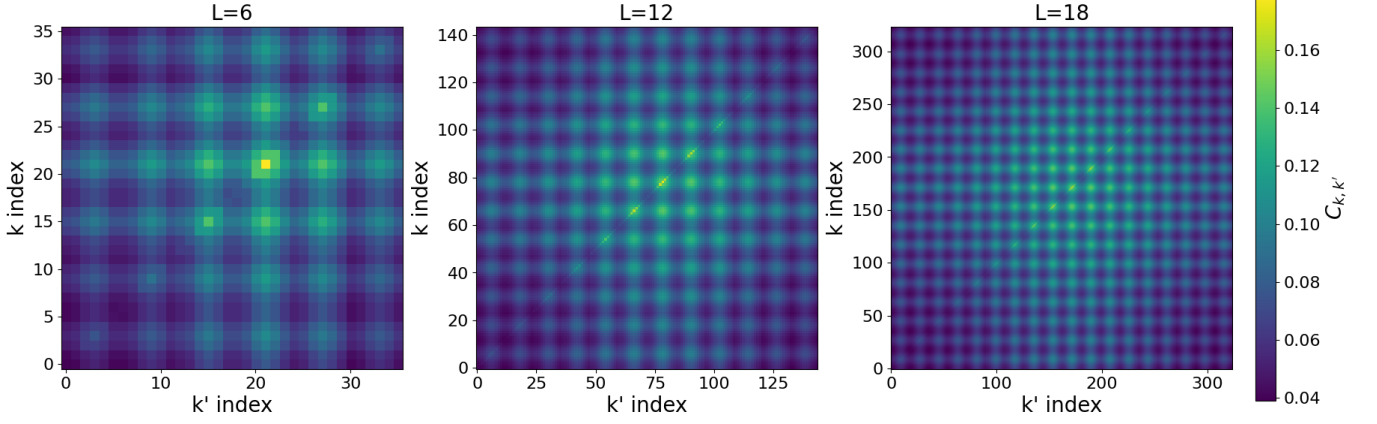


FIG. 8. **Exact pair-pair correlators from the 2-dimensional Richardson model across mesh sizes.** Heat maps of the ground-state $C_{\mathbf{k},\mathbf{k}'}$ on the BZ for $L = 6, 12, 18$, computed from the exact solutions of Richardson equations.

Namely, as a column vector statement:

$$\lim_{u \rightarrow d_{\mathbf{k}}} (d_{\mathbf{k}} - u) \mathcal{S}_{\mu}(u) = (d_{\mathbf{k}} - E_{\mu}) C^{(\mathbf{k})}, \quad (\text{B127})$$

where $C^{(\mathbf{k})}$ is the column vector with components $C_a^{(\mathbf{k})}$.

Multiply Eq. (B121) by $(d_{\mathbf{k}} - u)$ and take the limit:

$$\lim_{u \rightarrow d_{\mathbf{k}}} (d_{\mathbf{k}} - u) \mathcal{S}(\{E\}, \{F^{(\mu)}(u)\}) = \lim_{u \rightarrow d_{\mathbf{k}}} (d_{\mathbf{k}} - u) \det(\mathcal{S}(\{E\}, \{F^{(\mu)}(u)\})). \quad (\text{B128})$$

Since only the μ -th column of $\mathcal{S}(\{E\}, \{F^{(\mu)}(u)\})$ contains a pole as we take the limit (having finite limit), multiplying its determinant by $(d_{\mathbf{k}} - u)$ and taking $u \rightarrow d_{\mathbf{k}}$ is equivalent to replacing the μ -th column by $(d_{\mathbf{k}} - E_{\mu}) C^{(\mathbf{k})}$ (see Eq. (B127)), while all other columns become Gaudin matrix's columns (see (B123)–(B124)). Thus,

$$\lim_{u \rightarrow d_{\mathbf{k}}} (d_{\mathbf{k}} - u) \mathcal{S}(\{E\}, \{F^{(\mu)}(u)\}) = (d_{\mathbf{k}} - E_{\mu}) \det G(\mu \rightarrow C^{(\mathbf{k})}), \quad (\text{B129})$$

where $G(\mu \rightarrow C^{(\mathbf{k})})$ denotes the matrix obtained from G by replacing its μ -th column with $C^{(\mathbf{k})}$. Using Eq. (B83) gives precisely Eq. (B85) that we used in the previous subsection:

$$F_{\mathbf{k}}^{(\mu)} = (d_{\mathbf{k}} - E_{\mu}) \det(G(\mu \rightarrow C^{(\mathbf{k})})), \quad (\text{B130})$$

Similarly, we can also show that

$$F_{\mathbf{k}\mathbf{k}'}^{(\mu\nu)} = \frac{(d_{\mathbf{k}} - E_{\mu})(d_{\mathbf{k}} - E_{\nu})(d_{\mathbf{k}'} - E_{\mu})(d_{\mathbf{k}'} - E_{\nu})}{(d_{\mathbf{k}} - d_{\mathbf{k}'})(E_{\nu} - E_{\mu})} \det(G(\mu, \nu \rightarrow C^{(\mathbf{k})}, C^{(\mathbf{k}')}), \quad (\mathbf{k} \neq \mathbf{k}') \quad (\text{B131})$$

as claimed in Eq. (B86), where $G(\mu, \nu \rightarrow C^{(\mathbf{k})}, C^{(\mathbf{k}')})$ denotes the matrix obtained from G by replacing the μ -th and ν -th columns by $C^{(\mathbf{k})}$ and $C^{(\mathbf{k}'})$, respectively.

d. Numerical Exact Pair-Pair Correlator Data

We solve the Richardson equations Eq. (B50) on 2-dimensional Richardson models [104–106] on $L = 6, 12, 18$ respectively, with fixed electron filling $2M/L^2 = 1/6$. On each $L \times L$ BZ mesh we sample

$$\mathbf{k} = (k_x, k_y), \quad k_x = \frac{2\pi}{L} n_x, \quad k_y = \frac{2\pi}{L} n_y, \quad n_x, n_y \in \{0, 1, \dots, L-1\}, \quad (\text{B132})$$

with single-particle energy

$$\varepsilon_{\mathbf{k}} = t(\cos k_x + \cos k_y). \quad (\text{B133})$$

We choose hopping $t = 0.1$ in this work. For each of the meshes, we calculate the numerical pair-pair correlator data using Eq. (B106) and Eq. (B111).

L	electron number	g	u	$\sqrt{\sum_{\mu=1}^M R_{\mu} ^2}$.
2	2	-0.250000	-1	2.22×10^{-16}
4	4	-0.062500	-1	0.0
6	6	-0.027778	-1	2.52×10^{-12}
12	24	-0.006944	-1	1.80×10^{-10}
18	54	-0.003086	-1	1.18×10^{-12}

TABLE I. **Verification metrics across mesh sizes.** For each L , we report the electron number, coupling $g \equiv u/L^2$ and Richardson-equation residual 2-norm $\sqrt{\sum_{\mu=1}^M |R_{\mu}|^2}$ where $R_{\mu} \equiv \frac{1}{g} + \sum_{\mathbf{k}} \frac{1}{2\varepsilon_{\mathbf{k}} - E_{\mu}} - \sum_{\nu \neq \mu} \frac{2}{E_{\nu} - E_{\mu}}$. Here, $L = 2$ and $L = 4$ are used to benchmark against Exact-Diagonalization (ED) calculation, $L = 6$ provides training data for our SIREN, and $L = 12, 18$ are reserved for SIREN benchmarking; for $L = 6, 12, 18$ we fix the electron filling to $1/6$.

e. Exact-Diagonalization (ED) Validation

We validate our numerical Richardson-equation solver by benchmarking against ED calculation on small system sizes in the fully-paired sector. For each $L \times L$ momentum grid and coupling $g = u/L^2$ with $u = -1$, we solve the Richardson equations for the rapidities $\{E_{\mu}\}_{\mu=1}^M$ and compute the many-body energy $E_{\text{numerical}} = \sum_{\mu=1}^M E_{\mu}$. For the cases $L = 2, N_e = 2$ and $L = 4, N_e = 4$, our $E_{\text{numerical}}$ matches the ED ground-state energy exactly (with differences at most $\sim 10^{-16}$), and the $\frac{1}{g} + \sum_{\mathbf{k}} \frac{1}{2\varepsilon_{\mathbf{k}} - E_{\mu}} - \sum_{\nu \neq \mu} \frac{2}{E_{\nu} - E_{\mu}}$ are negligible ($\sim 10^{-16}$ and $\sim 10^{-14}$ respectively), confirming that our solver converges to the exact solution.

We also further validate our pair-pair correlator evaluation by benchmarking against ED. Using the same momentum grid, electron filling, u , and g , we compute the correlator matrix in two independent ways: (i) from the Richardson rapidities $\{E_{\mu}\}$ via the closed-form expressions, Eq. (B106) and Eq. (B111), and (ii) directly from the ED ground-state wavefunction in the M -pair Hilbert space. For the small-size test cases (e.g., $L = 2, N_e = 2$ and $L = 4, N_e = 4$), the resulting $C_{\mathbf{k}\mathbf{k}'}$ agree exactly, confirming the correctness of our numerical correlator solver.

2. ML Results

We wish to train a NN on the pair-pair correlation function (a special 2-RDM) $C \in \mathbb{R}^{L^2 \times L^2}$, which is a symmetric positive semi-definite real matrix with L^4 elements in total. Since the self-attention mechanism has quadratic time and space complexity, the memory requirements are proportional to L^8 , which can be extremely difficult for large L . Therefore, we chose to focus exclusively on the SIREN architecture for this model.

Numerically, the eigenvalue spectrum of C is dominated by a single eigenvalue, with the remaining eigenvalues suppressed by several orders of magnitude. Consequently, the matrix has an effective rank close to 1. As such, we can diagonalize C for each value of L and choose $\mathbf{A} \in \mathbb{R}^{L^2 \times 1}$ to be a normalized (i.e., $\|\mathbf{A}\|_2 = 1$) eigenvector corresponding to the largest eigenvalue. Since the trace of the correlator is equal to $\frac{L^2}{12}$ (electron pair number), C can then be approximately reconstructed as $C \approx \frac{L^2}{12} \mathbf{A} \mathbf{A}^T$.

Note that we can reshape \mathbf{A} into a matrix of shape $L \times L$, which matches the matrix dimensions in the 1-RDM case. Thus, we train a SIREN to output the elements of \mathbf{A} given 2D normalized coordinates, as described in Sec. A 2. For inference, we enforce full D_4 symmetry by averaging the SIREN predictions for large L with all of their rotations and reflections (i.e. the entire group of symmetries of the square). However, during training, we instead allow the SIREN to learn the symmetry by adding another term to the loss function in Eq. (A59):

$$\mathcal{L}_{\text{symmetry}} = \lambda_{\text{symmetry}} \left(\frac{1}{|S|} \right) \sum_{g \in S} \text{MSE} \left(\tilde{\mathbf{A}}, g(\tilde{\mathbf{A}}) \right), \quad (\text{B134})$$

where $\tilde{\mathbf{A}} \in \mathbb{R}^{(L+1) \times (L+1)}$ is the ‘‘wrapped around’’ version of the reshaped \mathbf{A} matrix for large L (see Sec. A 2 b for details), S is a generating subset of D_4 (i.e., $D_4 = \langle S \rangle$), which we choose to be $S = \{R_{90}, D\}$ (R_{90} denotes rotation by 90° and D denotes a reflection across the main diagonal), $|S|$ is the cardinality of S ($|S| = 2$ in our case), and the $\lambda_{\text{symmetry}}$ coefficient (a hyperparameter) controls the contribution to the total loss function. This symmetry loss is added after a small number of warmup steps (50 steps in our case) to prevent gradients from misleading the training by chasing a moving target. For training on the Richardson model, we omit the optional statistical prior (TV/FH) described in the general SIREN architecture (see Sec. A 2 e for details), so we choose $\mathcal{P} = 0$ in Eq. (A59). Finally,

L	$\sqrt{\text{MSE}}$	r_n
12	0.0074	94.56%
18	0.0077	94.29%

TABLE II. **Pair-Pair Correlation function of Richardson model interpolation with SIREN.** Metrics at evaluation mesh size $L \times L$ for a SIREN trained on 6×6 . Columns report root-mean-square error ($\sqrt{\text{MSE}}$) and relative accuracy (r_n) between SIREN predictions and true final 2-RDM on the evaluation mesh.

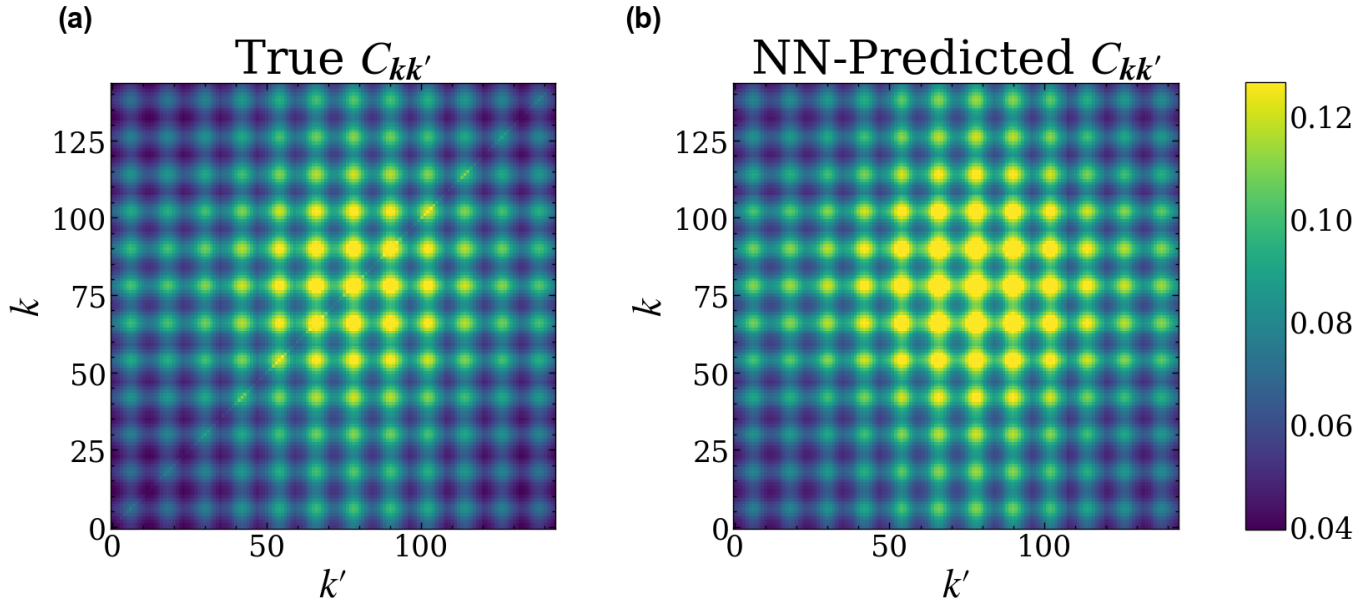


FIG. 9. Comparison between (a) the true final $C_{\mathbf{k}\mathbf{k}'}$ for $L = 12$ and (b) the predicted final $C_{\mathbf{k}\mathbf{k}'}$ for $L = 12$ given by a SIREN trained on $L = 6$. Indices $k, k' \in \{0, \dots, L^2 - 1\}$ enumerate the $L \times L$ \mathbf{k} points by flattening (ℓ_1, ℓ_2) with $\ell_{1,2} \in \{0, \dots, L - 1\}$ via $k = \ell_1 + L \ell_2$ with its momentum vector in Eq. (A2), and similarly for k' .

we use the Tree-Structured Parzen Estimation (TPE) [120] algorithm to search for the optimal hyperparameter configuration that can enable the SIREN to generalize effectively to larger L , as intended. For each trial, the SIREN is allowed to be trained for a total of 500 epochs, although we also save intermediate checkpoints in order to find the optimal parameter values.

Using the above method, we trained a SIREN on \mathbf{A} for $L = 6$, and then used it to predict \mathbf{A} for $L = 12$ and $L = 18$. For each test size, \mathbf{A} is first normalized such that $\|\mathbf{A}\|_2 = 1$ (where $\|\cdot\|_2$ denotes the ℓ^2 norm) before reconstructing the predicted final 2-RDM via:

$$C^{\text{SIREN}} = \frac{L^2}{12} \mathbf{A} \mathbf{A}^T. \quad (\text{B135})$$

For the Richardson model, the MSE is defined as:

$$\text{MSE}(C, C^{\text{SIREN}}) = \frac{1}{L^4} \sum_{i=1}^{L^2} \sum_{j=1}^{L^2} (C_{ij}^{\text{SIREN}} - C_{ij})^2, \quad (\text{B136})$$

where C^{SIREN} and C are the SIREN-predicted final values and the true final values for the 2-RDM of pair-pair correlators, respectively. In order to evaluate the trained SIREN's performance, we take the square root of Eq. (B136), *i.e.* $\sqrt{\text{MSE}}$, in order to ensure that the power on the unit of the error is the same as that for C and C^{SIREN} . To measure the relative accuracy r_n , we normalize the $\sqrt{\text{MSE}}$ by the total range of values of the original C , and subtract this fraction from unity. Results are shown in Tab. II. We can also compare the predicted final 2-RDM from the SIREN to the true final 2-RDM (*i.e.* the actual values of C) visually, as shown in Fig. 9 for a test size of $L = 12$. (See Fig. 4 in the maintext for a comparison on $L = 18$.)

Next, we train an additional SIREN on 4 $L_1 \times L_2$ tilted meshes with different side lengths $L_1, L_2 \in \mathbb{Z}_{>0}$. Define $\mathbf{b}_1 = (2\pi, 0)$ and $\mathbf{b}_2 = (0, 2\pi)$ to be the primitive reciprocal lattice vectors. For each tilted mesh, we construct the

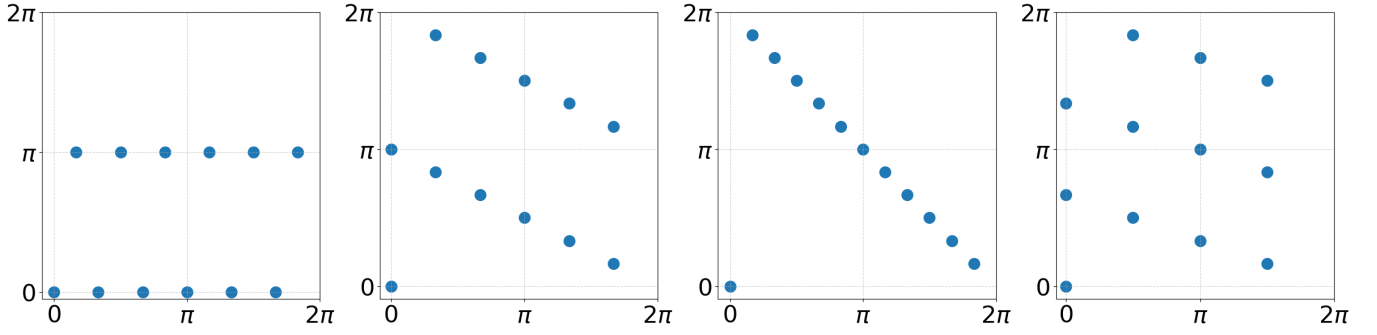


FIG. 10. The \mathbf{k} points chosen for the tilted meshes the SIREN is trained on for the Richardson model. The coordinates are wrapped around modulo 2π in each direction.

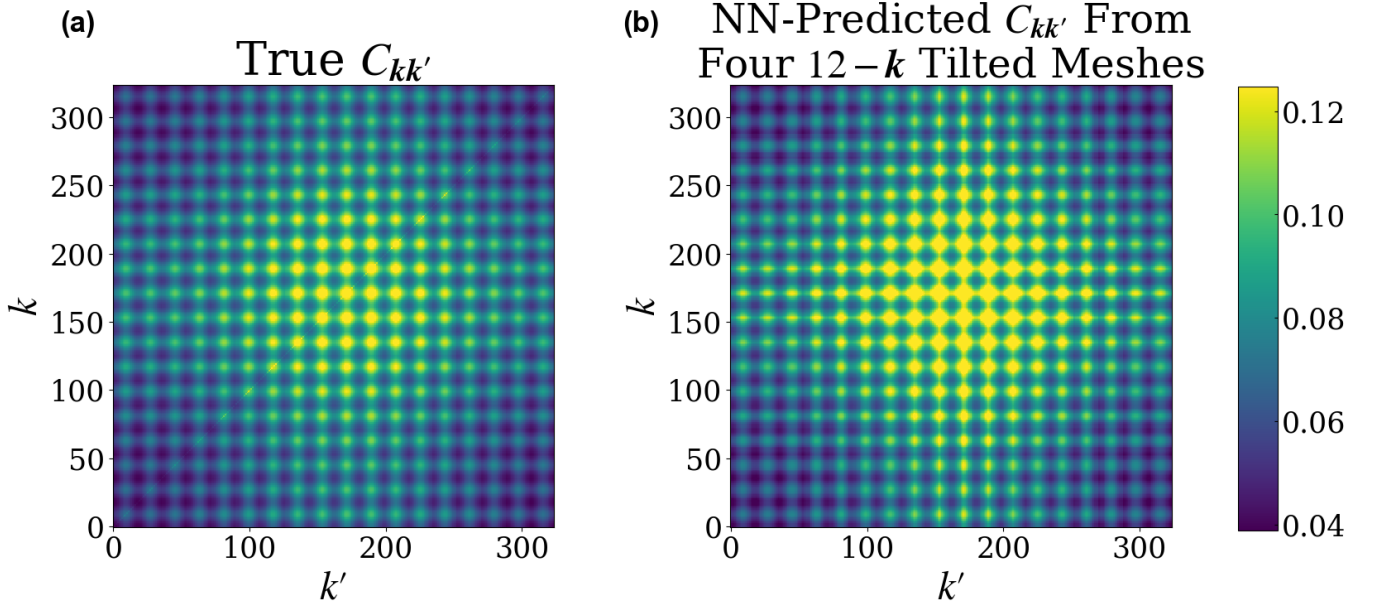


FIG. 11. Comparison between (a) the true final $C_{\mathbf{k}\mathbf{k}'}$ for $L = 18$ and (b) the predicted final $C_{\mathbf{k}\mathbf{k}'}$ for $L = 18$ given by a SIREN trained on four tilted meshes with 12 \mathbf{k} points each. Indices $k, k' \in \{0, \dots, L^2 - 1\}$ enumerate the $L \times L$ \mathbf{k} points by flattening (ℓ_1, ℓ_2) with $\ell_{1,2} \in \{0, \dots, L - 1\}$ via $k = \ell_1 + L\ell_2$ with its momentum vector in Eq. (A2), and similarly for k' .

transformed reciprocal lattice vectors \mathbf{f}_1 and \mathbf{f}_2 as a linear combination of \mathbf{b}_1 and \mathbf{b}_2 , *i.e.* $(\mathbf{f}_1, \mathbf{f}_2)^T = M(\mathbf{b}_1, \mathbf{b}_2)^T$, where $M \in \mathbb{Z}^{2 \times 2}$ is different for each tilted mesh. The side lengths and transformed reciprocal lattice vectors are chosen so that each tilted mesh has $L_1 L_2 = 12$ \mathbf{k} points, and so that the overlap between different meshes (*i.e.*, the number of \mathbf{k} points in common) is minimized as shown in Fig. 10. We diagonalize $C_{\mathbf{k}\mathbf{k}'}$ for each tilted mesh, and choose the normalized eigenvector $\mathbf{A} \in \mathbb{R}^{L_1 L_2}$ corresponding to the highest eigenvalue, which can be viewed as a function of $L_1 L_2$ \mathbf{k} points. By combining the eigenvectors for all four of the tilted meshes, we obtain the training dataset for the SIREN after normalizing the \mathbf{k} points to lie in $[-1, 1]^2$ and enforcing periodic boundary conditions for each reshaped eigenvector (see Sec. A2b). We train for a total of 1000 epochs, and apply the D_4 symmetry loss according to Eq. (B134) after the first 20 epochs. Note that we do not use TPE [120] to optimize hyperparameters, as was done when training on $L = 6$. After training, the resulting SIREN is then used to predict a new eigenvector, which we divide by its ℓ^2 norm to produce $\mathbf{A} \in \mathbb{R}^{18^2}$ for $L = 18$, where $\|\mathbf{A}\| = 1$. The corresponding $C_{\mathbf{k}\mathbf{k}'}$ is again reconstructed via Eq. (B135), after which we compute the accuracy with respect to the true final $C_{\mathbf{k}\mathbf{k}'}$ using Eq. (B136). The result yields a relative accuracy of $r_n = 93.77\%$. A comparison between C^{SIREN} and the true $C_{\mathbf{k}\mathbf{k}'}$ for this case can be seen in Fig. 11.

Appendix C: Translation-invariant 1-RDM in a four-band model

1. Model Set-Up

We work on an $L \times L$ Bravais lattice with a four-component orbital (or layer/sublattice) spinor $\psi_{\mathbf{r}} = (\psi_{\mathbf{r},1}, \dots, \psi_{\mathbf{r},4})^\top$ at site $\mathbf{r} \in \mathbb{Z}^2$. The real-space single-particle Hamiltonian contains on-site and short-range hoppings written with 4×4 matrices $h(\boldsymbol{\delta})$ that connect \mathbf{r} to $\mathbf{r} + \boldsymbol{\delta}$:

$$H_0 = \sum_{\mathbf{r}} \psi_{\mathbf{r}}^\dagger h(\mathbf{0}) \psi_{\mathbf{r}} + \sum_{\mathbf{r}} \sum_{\boldsymbol{\delta} \neq \mathbf{0}} \left(\psi_{\mathbf{r}+\boldsymbol{\delta}}^\dagger h(\boldsymbol{\delta}) \psi_{\mathbf{r}} + \text{h.c.} \right). \quad (\text{C1})$$

We choose the five gamma matrices as

$$\Gamma_1 = \sigma_x \otimes \sigma_x, \quad \Gamma_2 = \sigma_x \otimes \sigma_y, \quad \Gamma_3 = \sigma_x \otimes \sigma_z, \quad \Gamma_4 = \sigma_y \otimes \mathbb{I}, \quad \Gamma_5 = \sigma_z \otimes \mathbb{I}, \quad (\text{C2})$$

where σ_x, σ_y and σ_z are Pauli matrices. The hoppings have the following form:

$$\begin{aligned} \text{on-site:} & \quad h(\mathbf{0}) = \Gamma_5, \\ \text{NN (odd, along } x, y): & \quad h(+\hat{x}) = \frac{1}{2i}\Gamma_1, \quad h(-\hat{x}) = -\frac{1}{2i}\Gamma_1, \quad h(+\hat{y}) = \frac{1}{2i}\Gamma_2, \quad h(-\hat{y}) = -\frac{1}{2i}\Gamma_2, \\ \text{NNN(odd, along } x, y): & \quad h(+2\hat{x}) = \frac{1}{2i}\Gamma_3, \quad h(-2\hat{x}) = -\frac{1}{2i}\Gamma_3, \quad h(+2\hat{y}) = \frac{1}{2i}\Gamma_4, \quad h(-2\hat{y}) = -\frac{1}{2i}\Gamma_4, \\ \text{NN (even, in the } \Gamma_5 \text{ channel):} & \quad h(\pm\hat{x}) = \frac{1}{2}\Gamma_5, \quad h(\pm\hat{y}) = \frac{1}{2}\Gamma_5. \end{aligned} \quad (\text{C3})$$

Here ‘‘NN’’ denotes nearest-neighbor displacements $\boldsymbol{\delta}$ with $|\boldsymbol{\delta}| = 1$ ($\pm\hat{x}, \pm\hat{y}$); ‘‘NNN’’ denotes next-nearest neighbors along the axes $|\boldsymbol{\delta}| = 2$ ($\pm 2\hat{x}, \pm 2\hat{y}$). Unlisted $h(\boldsymbol{\delta})$ are zero. With the lattice Fourier transform

$$\psi_{\mathbf{r}} = \frac{1}{\sqrt{L^2}} \sum_{\mathbf{k}} e^{i\mathbf{k}\cdot\mathbf{r}} \psi_{\mathbf{k}}, \quad \mathbf{k} = (k_x, k_y) \in [0, 2\pi)^2, \quad (\text{C4})$$

Eq. (C1) becomes

$$\begin{aligned} H_0 &= \sum_{\mathbf{r}} \psi_{\mathbf{r}}^\dagger h(\mathbf{0}) \psi_{\mathbf{r}} + \sum_{\mathbf{r}} \sum_{\boldsymbol{\delta} \neq \mathbf{0}} \left(\psi_{\mathbf{r}+\boldsymbol{\delta}}^\dagger h(\boldsymbol{\delta}) \psi_{\mathbf{r}} + \text{h.c.} \right) \\ &= \frac{1}{L^2} \sum_{\mathbf{r}} \sum_{\mathbf{k}, \mathbf{k}'} e^{-i\mathbf{k}'\cdot\mathbf{r}} \psi_{\mathbf{k}'}^\dagger h(\mathbf{0}) e^{i\mathbf{k}\cdot\mathbf{r}} \psi_{\mathbf{k}} + \frac{1}{L^2} \sum_{\mathbf{r}} \sum_{\boldsymbol{\delta} \neq \mathbf{0}} \sum_{\mathbf{k}, \mathbf{k}'} e^{-i\mathbf{k}'\cdot(\mathbf{r}+\boldsymbol{\delta})} \psi_{\mathbf{k}'}^\dagger h(\boldsymbol{\delta}) e^{i\mathbf{k}\cdot\mathbf{r}} \psi_{\mathbf{k}} + \text{h.c.} \\ &= \sum_{\mathbf{k}, \mathbf{k}'} \psi_{\mathbf{k}'}^\dagger h(\mathbf{0}) \psi_{\mathbf{k}} \frac{1}{L^2} \sum_{\mathbf{r}} e^{i(\mathbf{k}-\mathbf{k}')\cdot\mathbf{r}} + \sum_{\boldsymbol{\delta} \neq \mathbf{0}} \sum_{\mathbf{k}, \mathbf{k}'} \psi_{\mathbf{k}'}^\dagger h(\boldsymbol{\delta}) \psi_{\mathbf{k}} \frac{1}{L^2} \sum_{\mathbf{r}} e^{i(\mathbf{k}-\mathbf{k}')\cdot\mathbf{r}} e^{-i\mathbf{k}'\cdot\boldsymbol{\delta}} + \text{h.c.} \\ &= \sum_{\mathbf{k}} \psi_{\mathbf{k}}^\dagger h(\mathbf{0}) \psi_{\mathbf{k}} + \sum_{\boldsymbol{\delta} \neq \mathbf{0}} \sum_{\mathbf{k}} \psi_{\mathbf{k}}^\dagger \left(e^{i\mathbf{k}\cdot\boldsymbol{\delta}} h(\boldsymbol{\delta}) \right) \psi_{\mathbf{k}} + \text{h.c.} \quad \left(\frac{1}{L^2} \sum_{\mathbf{r}} e^{i(\mathbf{k}-\mathbf{k}')\cdot\mathbf{r}} = \delta_{\mathbf{k}, \mathbf{k}'} \right) \\ &= \sum_{\mathbf{k}} \psi_{\mathbf{k}}^\dagger \left[h(\mathbf{0}) + \sum_{\boldsymbol{\delta} \neq \mathbf{0}} \left(e^{i\mathbf{k}\cdot\boldsymbol{\delta}} h(\boldsymbol{\delta}) + e^{-i\mathbf{k}\cdot\boldsymbol{\delta}} h^\dagger(\boldsymbol{\delta}) \right) \right] \psi_{\mathbf{k}} \\ &\equiv \sum_{\mathbf{k}} \psi_{\mathbf{k}}^\dagger H_0(\mathbf{k}) \psi_{\mathbf{k}}, \quad H_0(\mathbf{k}) = h(\mathbf{0}) + \sum_{\boldsymbol{\delta} \neq \mathbf{0}} \left(e^{i\mathbf{k}\cdot\boldsymbol{\delta}} h(\boldsymbol{\delta}) + e^{-i\mathbf{k}\cdot\boldsymbol{\delta}} h^\dagger(\boldsymbol{\delta}) \right) = \sum_{a=1}^5 d_a(\mathbf{k}) \Gamma_a, \end{aligned} \quad (\text{C5})$$

and the form factors are

$$d_1 = \sin k_x, \quad d_2 = \sin k_y, \quad d_3 = \sin(2k_x), \quad d_4 = \sin(2k_y), \quad d_5 = 1 + \cos k_x + \cos k_y. \quad (\text{C6})$$

The odd/even harmonics follow from $e^{\pm i\mathbf{k}\cdot\boldsymbol{\delta}} = (\cos \mathbf{k}\cdot\boldsymbol{\delta}) \pm i(\sin \mathbf{k}\cdot\boldsymbol{\delta})$: antisymmetric pairs $h(+\boldsymbol{\delta}) = -h(-\boldsymbol{\delta})$ generate sin, while symmetric pairs $h(+\boldsymbol{\delta}) = h(-\boldsymbol{\delta})$ generate cos. By the Clifford algebra of the Γ_a , the spectrum is doubly degenerate with

$$E_{\pm}(\mathbf{k}) = \pm \|d(\mathbf{k})\| = \pm \sqrt{\sum_{a=1}^5 d_a(\mathbf{k})^2}. \quad (\text{C7})$$

At filling $f = 1$ we occupy the lower band. We diagnose its topology via the Wilson loop $W_x(k_y)$ of the occupied projector $P(\mathbf{k})$ in Eq. (C13), yielding the \mathbb{Z}_2 index $\nu_{\mathbb{Z}_2} = 1$. This certifies that our training/benchmark data come from a \mathbb{Z}_2 non-trivial phase. For the interaction in second quantization and its lattice Fourier transform Eq. (B2),

$$\begin{aligned}
H_{\text{int}} &= \frac{1}{2} \sum_{\mathbf{r}} \sum_{\mathbf{R}} V(\mathbf{R}) n_{\mathbf{r}} n_{\mathbf{r}+\mathbf{R}} \\
&= \frac{1}{2} \sum_{\mathbf{r}, \mathbf{R}} V(\mathbf{R}) \left(\frac{1}{\sqrt{N}} \sum_{\mathbf{k}} e^{i\mathbf{k}\cdot\mathbf{r}} \psi_{\mathbf{k}}^\dagger \right) \left(\frac{1}{\sqrt{N}} \sum_{\mathbf{k}'} e^{-i\mathbf{k}'\cdot\mathbf{r}} \psi_{\mathbf{k}'} \right) \left(\frac{1}{\sqrt{N}} \sum_{\mathbf{p}} e^{i\mathbf{p}\cdot(\mathbf{r}+\mathbf{R})} \psi_{\mathbf{p}}^\dagger \right) \left(\frac{1}{\sqrt{N}} \sum_{\mathbf{p}'} e^{-i\mathbf{p}'\cdot(\mathbf{r}+\mathbf{R})} \psi_{\mathbf{p}'} \right) \\
&= \frac{1}{2N^2} \sum_{\mathbf{R}} V(\mathbf{R}) \sum_{\mathbf{k}, \mathbf{k}', \mathbf{p}, \mathbf{p}'} \left(\sum_{\mathbf{r}} e^{i(\mathbf{k}-\mathbf{k}'+\mathbf{p}-\mathbf{p}')\cdot\mathbf{r}} \right) e^{i(\mathbf{p}-\mathbf{p}')\cdot\mathbf{R}} \psi_{\mathbf{k}}^\dagger \psi_{\mathbf{k}'} \psi_{\mathbf{p}}^\dagger \psi_{\mathbf{p}'} \\
&= \frac{1}{2N} \sum_{\mathbf{R}} V(\mathbf{R}) \sum_{\mathbf{k}, \mathbf{k}', \mathbf{q}} e^{-i\mathbf{q}\cdot\mathbf{R}} \psi_{\mathbf{k}+\mathbf{q}}^\dagger \psi_{\mathbf{k}} \psi_{\mathbf{k}'-\mathbf{q}}^\dagger \psi_{\mathbf{k}'} \quad (\mathbf{q} \equiv \mathbf{p}' - \mathbf{p}) \\
&= \frac{1}{2N} \sum_{\mathbf{q}} \underbrace{\left(\sum_{\mathbf{R}} V(\mathbf{R}) e^{-i\mathbf{q}\cdot\mathbf{R}} \right)}_{U(\mathbf{q})} \sum_{\mathbf{k}, \mathbf{k}'} \psi_{\mathbf{k}+\mathbf{q}}^\dagger \psi_{\mathbf{k}} \psi_{\mathbf{k}'-\mathbf{q}}^\dagger \psi_{\mathbf{k}'}. \tag{C8}
\end{aligned}$$

Thus the translation-invariant interaction enters through the lattice Fourier transform,

$$U(\mathbf{q}) = \sum_{\mathbf{R}} V(\mathbf{R}) e^{-i\mathbf{q}\cdot\mathbf{R}}. \tag{C9}$$

For our specific short-range choice

$$V(\mathbf{R}) = U_0 \left[\delta_{\mathbf{R}, \mathbf{0}} + \frac{1}{2} (\delta_{\mathbf{R}, \hat{x}} + \delta_{\mathbf{R}, -\hat{x}} + \delta_{\mathbf{R}, \hat{y}} + \delta_{\mathbf{R}, -\hat{y}}) \right] \tag{C10}$$

Therefore,

$$U(\mathbf{q}) = \sum_{\mathbf{R}} V(\mathbf{R}) e^{-i\mathbf{q}\cdot\mathbf{R}} = U_0 \left[1 + \frac{1}{2} (e^{-iq_x} + e^{+iq_x} + e^{-iq_y} + e^{+iq_y}) \right] = U_0 (1 + \cos q_x + \cos q_y). \tag{C11}$$

So the momentum-space interaction is

$$H_{\text{int}} = \frac{1}{2N} \sum_{\mathbf{q}} U_0 (1 + \cos q_x + \cos q_y) \sum_{\mathbf{k}, \mathbf{k}'} \psi_{\mathbf{k}+\mathbf{q}}^\dagger \psi_{\mathbf{k}} \psi_{\mathbf{k}'-\mathbf{q}}^\dagger \psi_{\mathbf{k}'}. \tag{C12}$$

The mean-field order parameter is the 1-RDM (projector onto occupied HF bands) at each momentum:

$$P(\mathbf{k}) = \sum_{n=1}^f |u_n(\mathbf{k})\rangle \langle u_n(\mathbf{k})|, \tag{C13}$$

where n is the band index, and $f \in \{1, 2, 3, 4\}$ is the filling (number of occupied bands per \mathbf{k}). We choose $f = 1$ for our ML training. The projector obeys

$$P^\dagger(\mathbf{k}) = P(\mathbf{k}), \quad P^2(\mathbf{k}) = P(\mathbf{k}), \quad \text{tr} P(\mathbf{k}) = f. \tag{C14}$$

Normal ordering the interaction with respect to $P(\mathbf{k})$ yields the self-consistent HF Hamiltonian

$$H_{\text{HF}}(\mathbf{k}) = H_0(\mathbf{k}) + \Sigma_H + \Sigma_F(\mathbf{k}; [P]), \tag{C15}$$

with a Hartree shift

$$\Sigma_H = U(0) \bar{n} \mathbb{I}_4, \quad \bar{n} \equiv \frac{1}{L^2} \sum_{\mathbf{k}} \text{tr} P(\mathbf{k}), \tag{C16}$$

and a Fock self-energy given by a BZ convolution

$$\Sigma_F(\mathbf{k}; [P]) = -\frac{1}{L^2} \sum_{\mathbf{q}} U(\mathbf{q}) P(\mathbf{k} + \mathbf{q}). \quad (\text{C17})$$

Because $\Sigma_H \propto \mathbb{I}_4$ and $\text{tr} P(\mathbf{k}) = f$ is fixed by the filling, the Hartree term produces a uniform band shift and does not affect the projector; symmetry breaking (if any) is controlled by Σ_F . We monitor the total energy density (per unit cell)

$$\mathcal{E}[P] = \frac{1}{2L^2} \sum_{\mathbf{k}} \text{tr} \left[(H_{\text{HF}}(\mathbf{k}) + H_0(\mathbf{k})) P(\mathbf{k}) \right], \quad (\text{C18})$$

where the factor 1/2 avoids double counting. The stopping criterion is $|\mathcal{E}_{n+1} - \mathcal{E}_n| < 10^{-6}$, supplemented by the mean-squared change of the projector between iterations. Arrays $H_0(\mathbf{k})$, $U(\mathbf{q})$, and $P(\mathbf{k})$ live on the BZ grid. Given $P^{(n)}$, we build $\Sigma_H[P^{(n)}]$ and $\Sigma_F[P^{(n)}]$, diagonalize $H_{\text{HF}}[P^{(n)}](\mathbf{k})$ at each \mathbf{k} , and update

$$P^{(n+1)}(\mathbf{k}) = \sum_{m=1}^f |u_m^{(n)}(\mathbf{k})\rangle \langle u_m^{(n)}(\mathbf{k})|, \quad (\text{C19})$$

selecting the f eigenvectors with the lowest eigenvalues (ordered by real part).

The four-band model supplies the final HF labels — $P(\mathbf{k})$ at filling $f = 1$ and band energies \mathcal{E} — from a translation-invariant HF calculation, by which we pretrain and validate our NN architectures. It provides a clean benchmark to quantify acceleration: we compare HF iteration counts when initialized with the NN-predicted final 1-RDM versus a random initial 1-RDM at a fixed tolerance.

2. ML Results

Translation-invariant systems are simpler because the one-body correlator is diagonal in momentum ($\mathbf{k} = \mathbf{k}'$), so inference reduces to a sequence of L^2 matrices. The lower dimensionality lets us use a conventional self-attention NN without neural representation (SIREN). We again work on the discrete BZ with \mathbf{k} in Eq. (A2). Index grid points by their integers (l_1, l_2) with $l_{1,2} \in \{0, \dots, L-1\}$, so that

$$\mathbf{k}(l_1, l_2) = \frac{l_1}{L} \mathbf{b}_1 + \frac{l_2}{L} \mathbf{b}_2.$$

To encode relative position with periodic boundary conditions, use the wrapped (minimum-image) index differences

$$\Delta l_1 = ((l_1 - l'_1 + \lfloor L/2 \rfloor) \bmod L) - \lfloor L/2 \rfloor, \quad \Delta l_2 = ((l_2 - l'_2 + \lfloor L/2 \rfloor) \bmod L) - \lfloor L/2 \rfloor, \quad (\text{C20})$$

so we can define the 2D coordinate

$$\mathbf{x}_{(l_1, l_2), (l'_1, l'_2)} = \left(\frac{\Delta l_1}{L}, \frac{\Delta l_2}{L} \right). \quad (\text{C21})$$

For brevity we denote $\mathbf{x}_{(l_1, l_2), (l'_1, l'_2)}$ as \mathbf{x}_{ij} .

For the four-band model we keep the architecture of Sec. A1 but, given the simplicity here, replace the custom Fourier-based bias by a small MLP, following the formulation of Ref. [131]. That is,

$$B_{ij} = f_\theta(\mathbf{k}_i, \mathbf{k}_j) = \text{GELU}(\mathbf{x}_{ij} W_1 + \mathbf{b}_1) W_2 + b_2. \quad (\text{C22})$$

where \mathbf{x}_{ij} represents the relative coordinate between two k -points in 2D momentum space and $W_1 \in \mathcal{M}_{2 \times d_{\text{MLP}}}(\mathbb{R})$, $\mathbf{b}_1 \in \mathbb{R}^{d_{\text{MLP}}}$, $W_2 \in \mathcal{M}_{d_{\text{MLP}} \times 1}(\mathbb{R})$, $b_2 \in \mathbb{R}$ are all filled with learnable parameters to be optimized during training, and d_{MLP} represents the size of the hidden layer in the MLP. Eq. (C22) replaces Eq. (A27) for the bias function in the four-band model. Thus, the output of f_θ is a scalar bias (that quantifies how closely related the corresponding \mathbf{k} points are), which is then added to the self-attention computation via Eq. (A30), thereby injecting relative positional information into the NN.

a. Hyperparameters

To train the self-attention NN, we used a constant learning rate of 3×10^{-4} . A full list of the hyperparameters used can be seen in Tab. III.

Hyperparameter	Value
Epochs	300
N	3
N_{head}	2
D	32
D_{ff}	256
d_{MLP}	32
p	0.0

TABLE III. List of hyperparameters for training a self-attention NN on the four-band model. “Epochs” is the number of training iterations. N is the number of attention layers in the NN and D is the dimensionality (*i.e.* the “model width”) as defined in Sec. A 1 c. N_{head} is the number of attention heads in a single attention block, as defined in Sec. A 1 d. D_{ff} is the size of the hidden layer in the FFN, as defined in Sec. A 1 e. p is the probability with which elements are set to 0 in the Dropout operation, according to Eq. (A37).

b. Standardization

For the translation-invariant case, given $O_{\mathbf{k},\alpha\alpha}^{q=0}$, we construct X_{init} and X_{tgt} as in Eq. (A11) and Eq. (A5). To standardize the data, we compute the mean and standard deviations across all features $f \in \{1, \dots, 2\xi^2\}$. That is, for all N_{sample} training samples with $\beta \in \{\text{init}, \text{tgt}\}$:

$$\mu_f^{(\beta)} \equiv \frac{1}{N_{\text{sample}} L^2 (2\xi^2)} \sum_{\text{sample}} \sum_{i=1}^{L^2} \sum_{f=1}^{2\xi^2} X_{i,f}^{(\beta)}, \quad \left(\sigma_f^{(\beta)}\right)^2 \equiv \frac{1}{N_{\text{sample}} L^2 (2\xi^2) - 1} \sum_{\text{sample}} \sum_{i=1}^{L^2} \sum_{f=1}^{2\xi^2} \left(X_{i,f}^{(\beta)} - \mu_f^{(\beta)}\right)^2. \quad (\text{C23})$$

Eq. (C23) replaces Eq. (A10) for computing $\mu_f^{(\beta)}$ and $\sigma_f^{(\beta)}$ in the four-band model. We then use these values to standardize X_{init} and X_{tgt} following Eq. (A11).

c. Weight Initialization

The initial values for all NN parameters were drawn from the default distributions in PyTorch’s initialization scheme. Specifically, we use Kaiming (He) [123] initialization for all weight matrices and bias vectors in the input and output layers (*i.e.* $W_{\text{in}}, b_{\text{in}}$ and $W_{\text{out}}, b_{\text{out}}$) as well as in the FFNs (see Eq. (A43)) and the MLPs for f_θ (from Eq. (C22)), and in the self-attention mechanism (*i.e.* $W_Q^{(h)}, W_K^{(h)}, W_V^{(h)}, W_O$). Unlike the general case in Eq. (A36), we do not use a learnable bias vector b_O when mixing information across attention heads. For the LayerNorm operation (see Eq. (A40)), the weights γ and the biases β are initialized to all 1’s and all 0’s, respectively. Finally, we choose the learnable scalar s in Eq. (A30) in each attention head to be initialized to 1. All learnable parameters are trained by backpropagation to minimize the loss.

d. Results

We train a self-attention model on 10,000 (input,label) 1-RDM pairs at $L = 6$ and $L = 8$, and evaluate on 1,000 held-out systems with $L \in \{10, 12, \dots, 50\}$. For each test instance we run two HF solvers with identical tolerance and settings: (i) initialized from a random 1-RDM, and (ii) initialized from the NN-predicted final 1-RDM. We report the percent reduction in iteration count. At $L = 50$ the mean reduction is 91.63%. Results for all L are in Fig. 12 and Tab. IV.

In order to test how well the NN generalizes to larger system sizes, we also computed the MSE loss between the predicted final 1-RDM from the NN and the true final 1-RDM for up to $L = 50$, where the MSE is defined as in Eq. (A21). The results can be seen in Fig. 13.

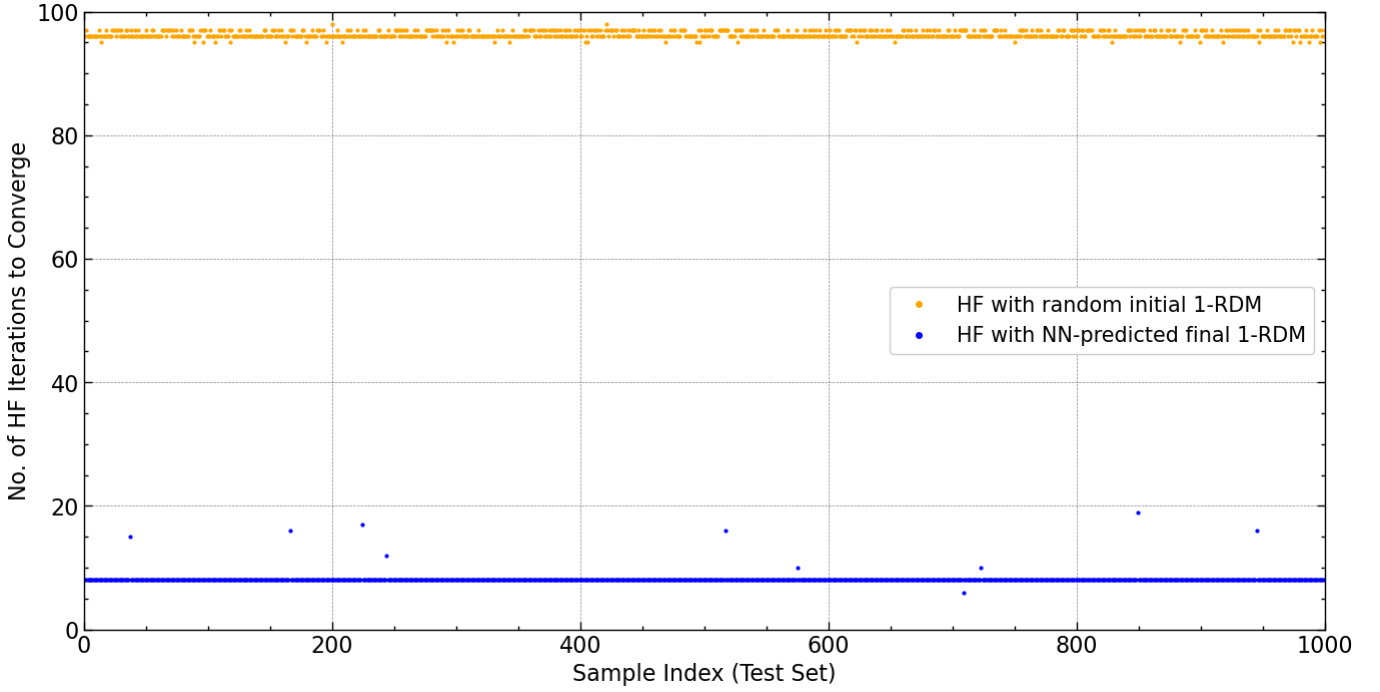


FIG. 12. HF iteration test on translationally-invariant four-band model (see Eqs. (C1) to (C19)) for $L = 50$ using a self-attention NN trained only on $L = 6$ and $L = 8$. The x-axis enumerates the 1000 test samples; the y-axis shows the number of HF iterations required to reach the convergence criterion when using the predicted final 1-RDM from the NN as the initial 1-RDM (blue) and when using a random initial 1-RDM (orange).

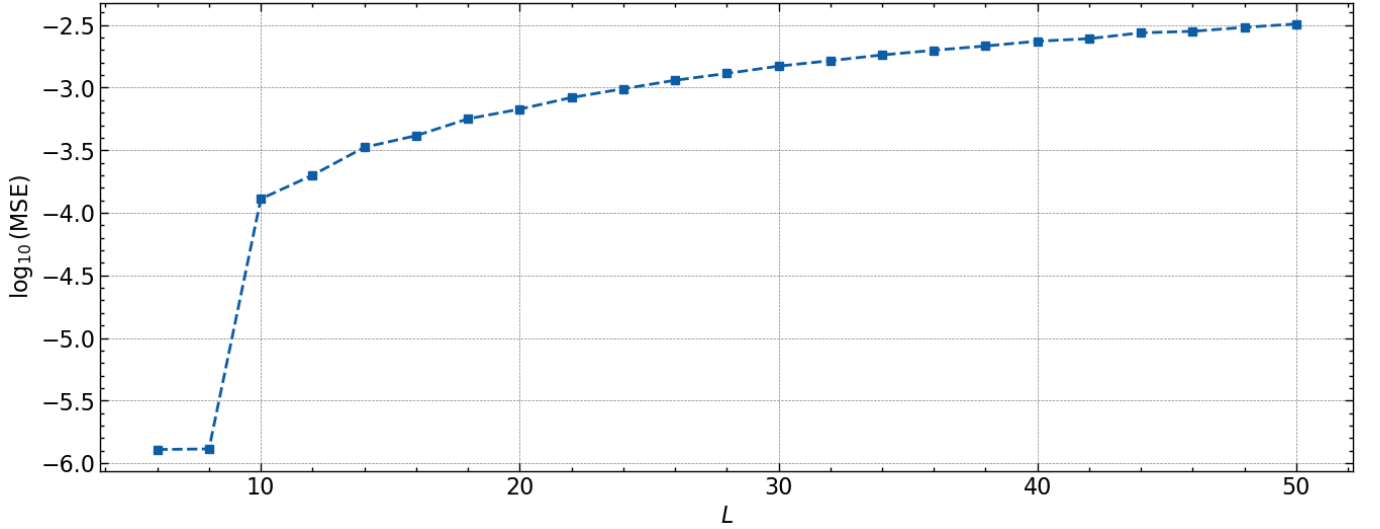


FIG. 13. Generalization test for the translationally-invariant HF calculation (see Eqs. (C1) to (C19)) using a self-attention NN trained only on $L = 6$ and $L = 8$, showing the MSE loss (defined in Eq. (A21)) as a function of the system size L .

L	Original	with NN	% Reduction
10	97.62	5.63	94.24
12	96.31	7.00	92.73
14	96.58	7.00	92.75
16	96.29	7.00	92.73
18	96.31	7.35	92.36
20	96.32	7.96	91.74
22	96.28	8.00	91.69
24	96.27	8.00	91.69
26	96.23	8.00	91.69
28	96.29	8.00	91.69
30	96.28	7.94	91.75
32	96.28	8.00	91.70
34	96.24	8.00	91.69
36	96.27	8.00	91.69
38	96.27	8.00	91.69
40	96.24	8.02	91.67
42	96.25	8.00	91.69
44	96.23	8.08	91.61
46	96.24	8.04	91.64
48	96.24	8.04	91.64
50	96.30	8.06	91.63

TABLE IV. Table showing results for the translationally-invariant HF calculation as described in Eqs. (C1) to (C19), using a self-attention NN trained on $L = 6$ and $L = 8$ and evaluated on $L = 10, 12, \dots, 50$. Here, “Original” refers to the average number of HF iterations with a random initial 1-RDM, while “with NN” refers to the average number of iterations when using the predicted final 1-RDM from the NN as the initial 1-RDM for HF. “% Reduction” refers to the percent difference between the two quantities.

Appendix D: Square-lattice Hubbard model

1. Model Set-Up

We study the spinful Hubbard model on a 2D square lattice [117, 118] with size $N \equiv L \times L$. In real space,

$$H = -t \sum_{\langle \mathbf{r}, \mathbf{r}' \rangle, \sigma} (c_{\mathbf{r}\sigma}^\dagger c_{\mathbf{r}'\sigma} + \text{h.c.}) + U \sum_{\mathbf{r}} n_{\mathbf{r}\uparrow} n_{\mathbf{r}\downarrow}, \quad (\text{D1})$$

with $c_{\mathbf{r}\sigma}$ the annihilation operator at site \mathbf{r} and spin $\sigma \in \{\uparrow, \downarrow\}$, and $n_{\mathbf{r}\sigma} = c_{\mathbf{r}\sigma}^\dagger c_{\mathbf{r}\sigma}$. With the lattice Fourier transform

$$c_{\mathbf{r}\sigma} = \frac{1}{\sqrt{L^2}} \sum_{\mathbf{k}} e^{i\mathbf{k}\cdot\mathbf{r}} c_{\mathbf{k}\sigma}, \quad c_{\mathbf{k}\sigma} = \frac{1}{\sqrt{L^2}} \sum_{\mathbf{r}} e^{-i\mathbf{k}\cdot\mathbf{r}} c_{\mathbf{r}\sigma}, \quad \mathbf{k} = (k_x, k_y) \in [0, 2\pi)^2. \quad (\text{D2})$$

The nearest-neighbor hopping $\boldsymbol{\delta} \in \{\pm\hat{x}, \pm\hat{y}\}$ gives

$$H_0 = -t \sum_{\langle \mathbf{r}, \mathbf{r}' \rangle, \sigma} (c_{\mathbf{r}\sigma}^\dagger c_{\mathbf{r}'\sigma} + \text{h.c.}) = -t \sum_{\mathbf{r}, \sigma} \sum_{\boldsymbol{\delta} \in \{\pm\hat{x}, \pm\hat{y}\}} c_{\mathbf{r}\sigma}^\dagger c_{\mathbf{r}+\boldsymbol{\delta}, \sigma} \quad (\text{D3})$$

$$= -\frac{t}{N} \sum_{\mathbf{r}, \sigma} \sum_{\boldsymbol{\delta}} \sum_{\mathbf{k}, \mathbf{k}'} e^{-i\mathbf{k}\cdot\mathbf{r}} c_{\mathbf{k}\sigma}^\dagger e^{i\mathbf{k}'\cdot(\mathbf{r}+\boldsymbol{\delta})} c_{\mathbf{k}'\sigma} \quad (\text{D4})$$

$$= -t \sum_{\mathbf{k}, \sigma} \left(\sum_{\boldsymbol{\delta}} e^{i\mathbf{k}\cdot\boldsymbol{\delta}} \right) c_{\mathbf{k}\sigma}^\dagger c_{\mathbf{k}\sigma} \quad \left(\text{here } \frac{1}{N} \sum_{\mathbf{r}} e^{i(\mathbf{k}'-\mathbf{k})\cdot\mathbf{r}} = \delta_{\mathbf{k}, \mathbf{k}'} \right) \quad (\text{D5})$$

$$= \sum_{\mathbf{k}, \sigma} \varepsilon(\mathbf{k}) c_{\mathbf{k}\sigma}^\dagger c_{\mathbf{k}\sigma}, \quad \varepsilon(\mathbf{k}) = -t \sum_{\boldsymbol{\delta}} e^{i\mathbf{k}\cdot\boldsymbol{\delta}} \quad (\text{D6})$$

$$= -t(e^{ik_x} + e^{-ik_x} + e^{ik_y} + e^{-ik_y}) = -2t(\cos k_x + \cos k_y). \quad (\text{D7})$$

Choosing $2t = 1$ yields

$$\varepsilon(\mathbf{k}) = -(\cos k_x + \cos k_y), \quad (\text{D8})$$

so the single-particle block reads

$$H_0(\mathbf{k}) = \varepsilon(\mathbf{k})\mathbb{I}_2, \quad (\text{D9})$$

with \mathbb{I}_2 the identity in spin space. The on-site repulsion is local in \mathbf{r} :

$$H_{\text{int}} = U \sum_{\mathbf{r}} n_{\mathbf{r}\uparrow} n_{\mathbf{r}\downarrow} = \frac{U}{L^2} \sum_{\mathbf{k}, \mathbf{k}', \mathbf{q}} c_{\mathbf{k}+\mathbf{q}, \uparrow}^\dagger c_{\mathbf{k}, \uparrow} c_{\mathbf{k}'-\mathbf{q}, \downarrow}^\dagger c_{\mathbf{k}', \downarrow}.$$

The spin-resolved 1-RDM (occupied-band projector) in momentum space is

$$[O_\sigma]_{\mathbf{k}\mathbf{k}'} = \langle c_{\mathbf{k}'\sigma}^\dagger c_{\mathbf{k}\sigma} \rangle, \quad \sigma \in \{\uparrow, \downarrow\}. \quad (\text{D10})$$

At temperature $T = 0$ and for collinear states O_σ is a projector onto the occupied subspace,

$$O_\sigma^\dagger = O_\sigma, \quad O_\sigma^2 = O_\sigma, \quad \text{Tr } O_\sigma = N_{\text{occ}, \sigma}. \quad (\text{D11})$$

We set the spin $U(1)$ symmetry not spontaneously broken, *i.e.*, $[O]_{\uparrow\downarrow} = [O]_{\downarrow\uparrow} = 0$. We further assume spin fillings to be

$$N_{\text{occ}, \uparrow} = N_{\text{occ}, \downarrow}, \quad (\text{D12})$$

but we do not impose translational symmetry. For the on-site Hubbard interaction, it may generate a mixing between \mathbf{k} and $\mathbf{k} + \mathbf{Q}$, if translational symmetry spontaneously breaks. At each iteration we diagonalize and refill the $N_{\text{occ}, \sigma}$ lowest eigenstates to update 1-RDM. This HF set-up provides true final 1-RDM labels (benchmarks to train and validate the ML model), and to quantify HF iteration savings at fixed discretization, filling, and U .

2. ML Results

Despite spontaneous translation breaking, the order parameters of Hubbard model can be simplified to be similar enough to the translation-invariant case to use the same techniques according to Sec. A 1 a.

Label the $L \times L$ BZ grid by integer coordinates Eq. (A46).

We investigated two approaches. Firstly, we trained a self-attention NN on the combined L^2 -long sequence. Additionally, for this model we also trained SIRENs separately on the central diagonal and off-diagonal elements, and then combined the outputs to form the new 1-RDM. For both models, the training data was generated via HF calculations (for systems with small L) that had a convergence criterion of 2×10^{-5} . The trained model was then used to predict a density matrix for larger L which was subsequently used as the initial guess for the density matrix in the HF algorithm, using the same convergence criterion.

The self-attention NN was trained only for $U = 1$ (due to limited data), while we also trained additional SIREN models for $U = 2$ and $U = 3$. In each case, the resultant reduction in the number of HF iterations required for convergence was noted, where the reduction is defined as the percent difference between the average number of HF iterations before and after using the NN outputs as the initial guess for the density matrix.

The training process for both NN architectures is detailed below.

a. Self-Attention NN

For each \mathbf{k} we transform 1-RDM into a real vector of length $2\xi^2$ and standardize them as described in Sec. A 1 b and Sec. A 1 a.

For the self-attention NN for the Hubbard model, we initialize W_{in} and W_{out} from a truncated normal distribution with $\sigma = 0.02$. Kaiming (He) normal initialization [123] is used for the learnable weight matrices in the feedforward

Hyperparameter	Value
Epochs	3201
N	3
N_{head}	4
D	64
D_{ff}	128
m	48
p	0.1

TABLE V. List of hyperparameters for training a self-attention NN on the Hubbard model. “Epochs” is the number of training iterations. N is the number of attention layers in the NN and D is the dimensionality (*i.e.* the “model width”) as defined in Sec. A 1 c. N_{head} is the number of attention heads in a single attention block and m is the total number of frequencies, as defined in Sec. A 1 d. D_{ff} is the size of the hidden layer in the FFN, as defined in Sec. A 1 e. p is the probability with which elements are set to 0 in the Dropout operation in Eq. (A37).

layers, while Xavier (Glorot) initialization [122] is used for each of the matrices $W_Q^{(h)}$, $W_K^{(h)}$, $W_V^{(h)}$, W_O in the attention heads. The matrix of frequencies W_r from Eq. (A23) is initialized with values drawn from a standard normal distribution. Furthermore, the weights γ for the LayerNorm operation from Eq. (A40), the vector of coefficients C (Eq. (A26)), the power p (Eq. (A27)), and the learnable scalar s (Eq. (A30)) are each initialized to be 1. All bias vectors are set to 0 initially. After initialization, these learnable parameters are updated by backpropagation to minimize the loss, as indicated in Sec. A 1 c.

In order to train the NN, we used a custom learning rate schedule consisting of a linear warmup phase followed by cosine annealing (without restarts) [121], which is a well-established method for training self-attention models with adaptive optimizers. This learning rate cycle is repeated twice: initially, we train for 500 epochs, and then for 5000 epochs. Each time, the warmup phase lasts for 20 epochs followed by cosine decay for the rest of the cycle. Thus, we train for a total of 5500 training epochs. Nevertheless, we found that the loss decreased to a minimum around 3200 epochs, which is the checkpoint used for evaluation. The self-attention NN was trained on 467 samples (*i.e.* input/output pairs) for $L = 8$ and 1001 samples for $L = 10$, and performance was observed to vary noticeably based on the random seed used (where “random seed” refers to the initializer for the pseudorandom number generator(s) of the computer), corroborating the findings in [132]. A full list of hyperparameters can be seen in Tab. V.

b. SIREN

As aforementioned, each set of “significant” points forms a tensor of shape $L \times L \times 2 \times 2$. To take full advantage of dimensionality reduction, we trained a separate SIREN for every index of the 2×2 matrix at each \mathbf{k} that had significantly nonzero elements. That is, each SIREN was trained on an $L \times L$ matrix (for the Hubbard model, each of the SIRENs was trained on $L = 8$), and the outputs were then combined to reconstruct the original shape. Of course, just like with the Richardson model, we extend the size of the matrix to $(L + 1) \times (L + 1)$ by “wrapping” around the first element of each dimension in order to satisfy normalization constraints, as described in Sec. A 2 b. Due to the large search space of possible hyperparameter configurations, we again used TPE [120] through the Optuna and RayTune libraries to optimize hyperparameters individually for each SIREN model trained in this way.

c. Results

After training, we evaluate acceleration by re-running HF initialized with the NN-predicted final 1-RDM and reporting the percent reduction in iteration count relative to HF started from a random 1-RDM under the same tolerance and settings. Results are shown in Tab. VI.

	L	10	12	14	16	18	20	22	24	26	28	30
Self-Attention NN, $U = 1$		N/A	66.19	73.51	76.63	80.63	83.62	84.93	82.55	81.55	81.70	79.89
SIREN, $U = 1$		60.79	64.34	73.25	73.15	73.27	77.48	88.70	75.72	77.21	78.81	79.25
SIREN, $U = 2$		82.94	83.27	83.16	83.84	83.41	92.59	86.27	85.84	86.33	86.36	92.78
SIREN, $U = 3$		81.25	81.64	82.30	82.11	82.61	83.00	82.79	82.96	82.97	83.18	83.24

TABLE VI. % Reduction across various system sizes ($10 \leq L \leq 30$) for the Hubbard model. For $U = 1$, results are shown using both the self-attention NN and the SIREN, while for $U = 2$ and $U = 3$ we only obtained results for the SIREN due to limited training data.